**UNIVERSITÀ DEGLI STUDI DI PADOVA**

DIPARTIMENTO DI INGEGNERIA INDUSTRIALE

CORSO DI LAUREA MAGISTRALE IN INGEGNERIA CHIMICA E DEI PROCESSI INDUSTRIALI

**Tesi di Laurea Magistrale in**
**Ingegneria Chimica e dei Processi Industriali**

# Draining of the primary cooling circuits in actively cooled reactor components: numerical simulations and verifications for the Electrostatic Residual Ion Dump of MITICA experiment

***Relatore:***

*Chiar.mo Prof. Piergiorgio Sonato*

***Correlatori:***

*Dott. Ing. Mauro Dalla Palma*

*Dott. Ing. Matteo Zaupa*

***Laureanda:***

*Federica Favorido*

ANNO ACCADEMICO 2018-2019

# Riassunto

Lo svuotamento è un processo importante per componenti raffreddati attivamente di reattori esposti agli effetti delle reazioni nucleari. I prodotti di corrosione attivati, generati dall'interazione dell'acqua con i metalli devono essere controllati attraverso l'evacuazione dell'acqua di raffreddamento e il confinamento del componente per evitare spargimento e contaminazione. Il processo deve essere applicato ai circuiti di raffreddamento primari e ai componenti raffreddati attivamente dell'esperimento di fusione nucleare ITER, includendo i componenti degli iniettori del fascio di neutri e quelli della neutral beam test facility (NBTF) in costruzione a Padova.

Lo scopo di questa tesi è focalizzato su un componente dell'NBTF, l'Electrostatic Residual Ion Dump (ERID) i cui circuiti di raffreddamento devono essere raffreddati prima di eseguire operazioni di manutenzione ed ispezione.

Azoto pressurizzato come gas inerte sarà usato per evacuare l'acqua dal circuito di raffreddamento e il processo è simulato utilizzando il codice RELAP5. La pressione massima ammissibile per il processo, viene fissata in accordo con la Pressure Equipment Directive a 5 bar(g) per restare nella categoria Sound Engineering Practice (basso livello di rischio e non marcata CE). Ogni elemento, partendo dal beam stopping element interagente con gli ioni residui fino al pannello completo dell'ERID è modellato e integrato nel circuito di raffreddamento; tutti i parametri caratterizzanti il processo di raffreddamento sono identificati: il tempo di evacuazione di 10-11 s in un range di pressione 5-1.5 bar con un parametro di efficienza dello svuotamento del 99%; le portate di gas e di acqua sono calcolate durante la simulazione transitoria riconoscendo instabilità di Rayleigh-Taylor che avvengono quando il fluido leggero è spinto da quello pesante.

Nell'ultima parte viene sviluppato un modello semplificato dei componenti dell'ERID per superare i limiti del software. La configurazione viene validata e permette dunque di analizzare con un numero ridotto di elementi: il modello semplificato produce un errore massimo sulla massa di acqua del 25% e non è in grado di simulare la dinamica con i regimi di flusso; tuttavia il parametro di efficienza dello svuotamento varia di solo l'1% per il modello semplificato. Tra tutte le pressioni applicate nel range 1.5-5 bar, viene selezionata la pressione di 3 bar per lo svuotamento perché il margine rispetta la PED e le fluttuazioni; con queste condizioni al contorno lo svuotamento totale avviene in 37 s con una efficienza del 99%.

Viene proposto uno schema del processo di svuotamento dell'ERID che include misure della pressione, portate e volume d'acqua. Sono identificati i limiti del processo di svuotamento in ottica di sviluppi futuri. Il riscaldamento e l'asciugatura dell'acqua residua sono raccomandati per soddisfare i requisiti di sicurezza.

# Abstract

Draining is an important process for actively cooled reactor components exposed to effects of nuclear reactions. Activated corrosion products formed by the water interaction with metals in cooling circuits shall be controlled through coolant evacuation and component confinement in order to avoid spreading and contamination. The process shall be applied to the primary cooling circuits and to the in-vessel actively cooled components of the nuclear fusion experiment ITER, including the components of the neutral beam injectors and those of the neutral beam test facility (NBTF) under construction in Padova.

The aim of this thesis is focused on a NBTF component, the Electrostatic Residual Ion Dump (ERID) whose cooling circuits must be drained before carrying out maintenance and inspection operations.

Pressurised nitrogen as inert gas will be used to blow out water from cooling circuits and the process is simulated using the RELAP5 code. The maximum allowable pressure for blowing out, in accordance with the Pressure Equipment Directive (PED), is fixed to 5 bar(g) in order to stay in the Sound Engineering Practice category (low hazard level without CE marking). Each element, starting from the beam stopping element interacting with the residual ions to the overall ERID panel is modelled and integrated in the cooling circuit; all parameters characterizing the draining process are identified: the evacuation time is 10-11 s in the pressure range 5-1.5 bar, with a draining efficiency parameter of 99%; the gas and the water flow rates are calculated during the transient simulation recognising Rayleigh-Taylor instabilities which occur when the light fluid (nitrogen) is pushing the heavy fluid (water).

In the last part a simplified overall model of the ERID components is developed to overcome the limits of the software. This configuration is validated and it allows to perform the analyses with a reduced number of elements: the simplified model produces a maximum water mass error of 25% as it is not able to simulate the system dynamics with flow regime transitions; nevertheless the draining efficiency parameter varies of only 2% for the simplified model. Among all the applied draining pressures in the range 1.5-5 bar, 3 bar is selected to perform the blowing out because the margin with respect to the PED limit is consistent with simulated fluctuations; with this boundary condition the overall draining time is 37 s with a draining efficiency parameter of 99%.

The draining implementation on the ERID is addressed proposing a circuit scheme that includes monitoring and control sections for pressure, flow rate, and water volume measurement. Limitations of draining tests are identified for possible future developments. Heating up and drying of the residual water are recommended to satisfy safety requirements.

# Table of contents

# Introduction

ITER (International Thermonuclear Experimental Reactor) is a major international experiment under construction in Cadarache (France), aiming to demonstrate the scientific and technical feasibility of fusion as an energy source. Seven members participate in the ITER project: China, the European Union, India, Japan, Russia, South Korea and the United States. It is based on the tokamak concept, an experimental machine designed to harness the energy of fusion [1]. By the end of the century, demand for energy will have tripled under the combined pressure of population growth, increased urbanization and expanded access to electricity in developing countries. A new large-scale, sustainable and carbon-free form of energy is needed. Fusion is an abundant energy because fusing atoms together in a controlled way releases nearly four million times more energy than a chemical reaction such as the burning of coal, oil or gas. Fusion fuels are widely available and nearly inexhaustible, in fact deuterium can be distilled from all forms of water. Fusion doesn't emit harmful toxins like carbon dioxide or other greenhouse gases in the atmosphere. Risk due to nuclear accident is not possible in a tokamak fusion device because it is difficult enough to reach and maintain the precise conditions necessary for fusion and if any disturbance occurs, the plasma cools within seconds and the reactions stop. The quantity of fuel present in the vessel at any time is enough for a few seconds only and there is no risk of chain reaction. ITER will be equipped with two Neutral Beam Injectors (NBI), each of them capable to inject into the plasma up to 16.5 MW, by accelerating negative hydrogen or deuterium ions up to energy of 1 MeV. For this purpose, a Neutral Beam Test Facility (NBTF), called PRIMA (Padova Research on ITER Megavolt Accelerator) has been realized in Padova (Italy) at Consorzio RFX (in the CNR area) in order to host two experiments: SPIDER (Source for Production of Ion of Deuterium Extracted from Radio frequency plasma), the full scale negative ion source and MITICA (Megavolt ITer Injector & Concept Advancement), the full scale injector prototype. The target of these two prototypes is to address and solve the main physics and engineering issues related to this system.

The aim of the thesis is focused on the Electrostatic Residual Ion Dump (ERID) which is a beam line component of MITICA. In fact, its cooling system must be drained and dried in order to carrying out maintenance and inspection operations due to operating environment contamination caused by activated corrosion products that may be formed during ordinary operations. Nitrogen at high pressure is used to blow out water from the circuit, the process is called forced draining. Each element of the ERID is analysed and the draining parameters are found in order to assess if the draining process is performed and also to build the overall model of the ERID. At the end, this model needs to be simplified due to storage problems of the software that was not able to process all elements of the model.

The structure of the thesis is as follow.

In the first chapter, a general overview of fusion and NBTF is given, particularly the description of the ERID is performed which draining response represents the aim of this work.
In the second chapter, a description of the importance of the draining process considering useful correlations is presented. In the last part, the flow regimes are explained because they determine the macroscopic behaviour of two phase flow during the draining process.
In the third chapter, all simulation models are presented. In the first part, the software used for the simulation is presented, considering its structure and equations. The application of the Pressure Equipment Directive is needed to find the maximum allowable pressure for the simulations considering pressure-related hazard categories. All simulation results are presented and discussed in the last part of the chapter.
In the fourth chapter, a simplification of the model is explained because the software was not able to perform the simulation due to the large number of system elements. ERID cooling circuit is simplified and the results of its draining process are given.

# Chapter 1
# Fusion and NBTF

Substantial advantages over other forms of innovative energy generation distinguish nuclear fusion, in terms of environmental protection, fuel availability and intrinsic safety. The production of energy from nuclear fusion could represent a cleaner way to supply the global increasing energy demand. This chapter gives a short overview on the basic issues of the controlled thermonuclear fusion and the ITER project, in particular on the Neutral Beam Test Facility under construction in Padova. Finally, a brief description of the MITICA Electrostatic Residual Ion Dump is given, which represents the most important part of the thesis.

## 1.1 Fusion

Fusion is the process which powers the sun and the other stars. It is called fusion because two or more light nuclei fuse together, at the extremely high pressure and temperature, to generate a relatively heavier nucleus in which there is some mass deficiency that is released as energy [2]. The quantity of energy released follows the Einstein's formula, $E = mc^2$, in which $E$ is the energy in joules, $m$ is the mass difference in kilograms, and $c$ is the speed of light ($3\times10^8$ meters per second). At the high temperatures experienced in the core of the sun (15 million Celsius degrees) any gas becomes plasma, the fourth state of matter. In order to replicate this process on earth, gases need to be heated at extremely high temperatures of about 150 million Celsius degrees whereby atoms become completely ionised. The easiest fusion reaction in fusion machines is between two hydrogen isotopes: deuterium, extracted from water and tritium, produced during the fusion reaction through the contact with lithium:

$$D + T \rightarrow {}^4He(3.5MeV) + n\ (14.1MeV) \tag{1.1}$$

When deuterium and tritium nuclei fuse, they form a helium nucleus, a neutron and energy. Neutral beam injection is considered one of the most effective methods for plasma heating and current drive in fusion experiment: beams of high energy neutral hydrogen or deuterium atoms are injected into the plasma, transferring their energy to the plasma via collisions with the plasma ions. In ITER, fusion will be achieved by a tokamak device (Figure 1.1), an experimental machine designed to harness the energy of fusion. The plasma particles are heated by different types of auxiliary heating methods. The helium nucleus carries an electric charge which will be subject to the magnetic fields of the tokamak and remain confined within the plasma, contributing to its continued heating. The neutrons will be absorbed by the surrounding walls of the tokamak, where their kinetic energy will be transferred to the walls as heat. In ITER, this heat will be captured by cooling water circulating in the vessel walls and eventually dispersed through cooling towers.

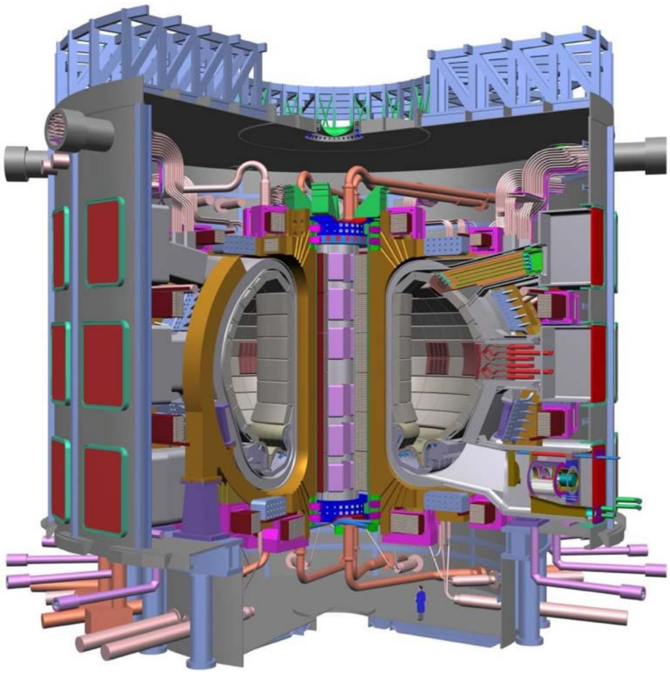

**Figure 1.1** *Cutaway of the ITER Tokamak*

## 1.2 Primary confinement for tritium and activated corrosion products

Nuclear reactors are designed with a multi-loop flow and heat transfer configuration to provide barriers for the containment of radioactive material. There are two major systems utilized to convert the heat generated from the nuclear reaction into electrical power. The primary system transfers the heat from the fuel (fission) or blanket (fusion) to the steam generator, where the secondary system begins. The steam formed in the steam generator is transferred by the secondary system to the main turbine generator, where it is converted into electricity. The primary function of the primary (or reactor coolant) system is to transfer the heat from the fuel/blanket to the steam generators. A second function of the primary system is to contain any nuclear products. A schematic of primary and secondary heat transfer systems for a fusion reactor is given in Figure 1.2.

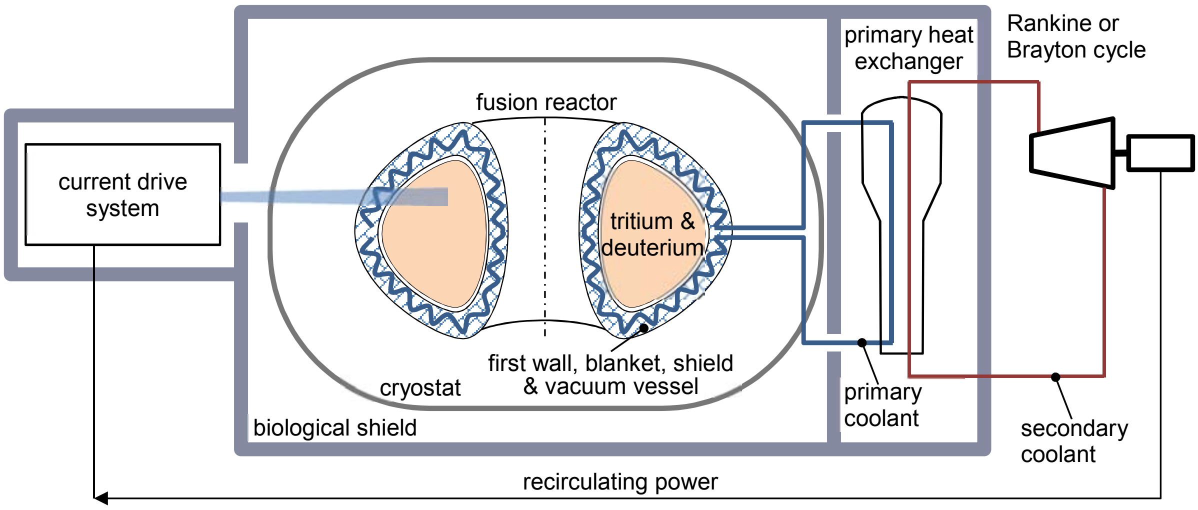


**Figure 1.2** *Schematic of a possible tokamak fusion power plant [3]*

It is a goal of ITER to demonstrate the safety and environmental potential of fusion and thereby provide a good precedent for the safety of future fusion power reactors. To accomplish this goal, ITER needs to address the full range of hazards and minimise exposure to these [4]. As in a Pressurised Water Reactor (PWR), both the reactor and the primary heat exchanger must be inside a biological shield, since the reactor is a powerful source of neutrons, and the coolant contain activation products as well as tritium. The primary coolant has to collect heat from several distinct components, which receive different power densities and radiation levels. Listing from the plasma outwards, they are the "first wall" (the surface facing the plasma), the blanket, the radiation shield (which protects the vacuum vessel), and the vacuum vessel. In addition the ions leaking from the plasma must be collected in a structure as a divertor. In principle a direct Brayton cycle is possible with a single coolant, but indirect cycles with primary and secondary coolants have received most attention, since the tritium concentration in the primary coolant will be high. ITER protects personnel and the public by using confinement barriers. Successive physical and functional barrier protect against spread and release of hazardous materials. Every radioactive inventory is contained in its vessel, process piping, component, etc. which serves as the first confinement barrier. This confinement barrier is designed to have high reliability to prevent releases. Another barrier is provided, usually close to the first one, to protect personnel and limit the spread of contamination from leaks and to mitigate the consequences in the event of failure of the first barrier to assist in meeting project release guidelines.

The primary confinement for the source term within the vacuum vessel is the vacuum vessel and its extension including the neutral beam (NB) injector vessels and confinement barriers in the radio-frequency (RF) heating systems and diagnostics. The tokamak cooling water system (TCWS) piping forms the primary confinement for tritium and activated corrosion products in the loops of its constituent primary heat transfer system (PHTs). Since experimental components inside the vacuum vessel are not assigned a safety function, the TCWS must also confine the in-vessel source term for events such as an in-vessel coolant spill. For the in-vessel and TCWS source terms, another barrier is available. Penetration confinement barriers, typically at the cryostat closure plate, in the RF heating systems and diagnostics form part of this barrier. Using the vacuum vessel and cryostat as confinement barriers takes advantage of the inherent magnetic fusion characteristic that high quality and high reliability vacuums are needed for fusion operation. The other confinement barriers are tailored to the nature of hazards in each compartment. The vacuum vessel and its extensions (including penetration barriers), the fuel cycle process piping, hot cells, etc. that form the primary enclosures for radioactive inventories, together with the building and filter systems, may be considered a minimum set of systems to meet project release guidelines.

## 1.3 PRIMA

The ITER NBTF, called PRIMA is hosted in Padova, Italy. It includes two experiments: SPIDER, the full size plasma source with low acceleration voltage (100 kV), and MITICA, the full size neutral beam injector at full beam power (18 MW), and all the experimental service plants and the control rooms necessary to the operation of the two devices. The buildings are built on a surface of approximately 17500 $m^2$, whereas the area covered by buildings is of approximately 7000 $m^2$. The realization of the ITER NBTF and the start of its experimental phase are important tasks of the fusion roadmap, since the target requirements of injecting to the plasma a beam of deuterium atoms with a power up to 16.5 MW, at 1 MeV of energy and with a pulse length up to 3600 s have never been reached together before [5].

### *1.3.1 MITICA*

MITICA (Figure 1.3) is the prototype of the injectors which will be realized and installed in ITER. Each injector has been designed in order to deliver about 16.5 MW neutral beam of deuterium/hydrogen particles obtained from a precursor beam of negative ions accelerated to 1MeV. The ion source is held at –1 MV, so the ions are accelerated up to ground potential by a system of five grids, called Accelerator, set at different growing potentials, by steps of 200kV, applied to each couple of grids. The composition of the ions source and the accelerator is called Beam Source. The other beamline components are: the neutraliser and electron dump (NED), realising four vertical beam channels where the collision of the negative ions with the cloud of hydrogen/deuterium gas leads not only the formation of neutral particles but also positive and negative ions due to different processes like stripping of the outer electron, double stripping and re-ionization; the Electrostatic Residual Ion Dump (ERID) which consists of five vertical dump walls which realizes four channels crossed by the particle beam. Inside the channels, an electric field deflects the partially positive and partially negative residual ions. The last component is the Calorimeter, constituted by two panels in a V shape, onto which the neutral beam impinges. In the high heat flux components, swirl tubes and actively cooled panels are adopted to remove the huge deposited power: ~5MW in Neutralizer, ≤ 19MW on ERID and 18MW on Calorimeter [6]. Large cryopumps are places on each side of the beam path and the beamline components inside the injector to reduce the pressure downstream of the neutralizer exit. The pressure downstream of the neutralizer must be low in order to minimize re-ionization of the neutral particles by collision with the background gas.

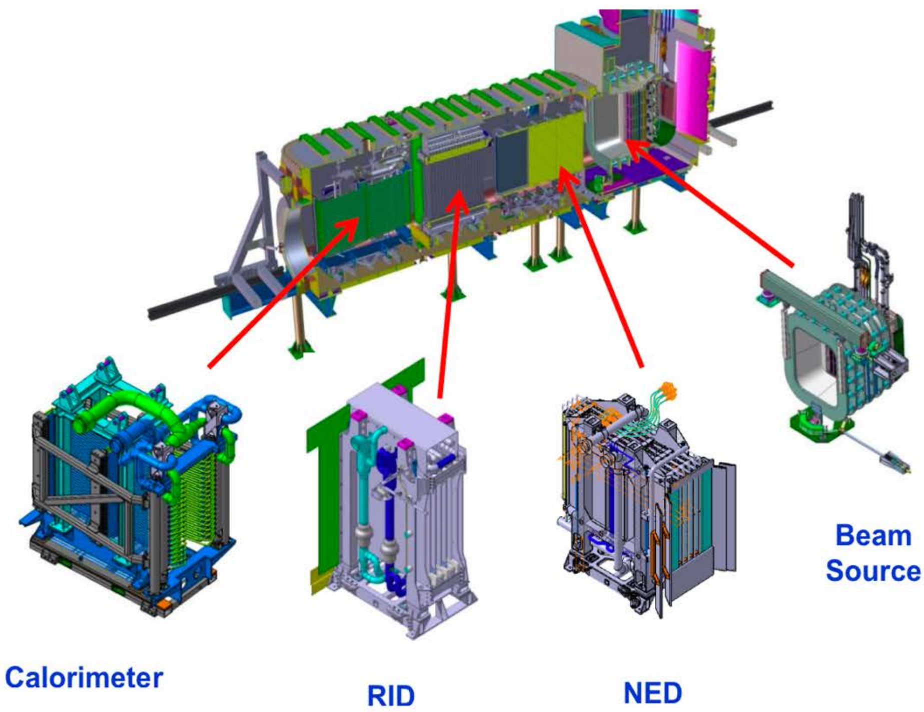


**Figure 1.3** *Schematic view of MITICA*

## 1.4 Electrostatic Residual Ion Dump

The MITICA Electrostatic Residual Ion Dump is made of five vertical panels, manifolds and headers for the water cooling supply, Figure 1.4 [7]. Panels are connected in parallel and, in particular, three of them (Panel 1, Panel 3, Panel 5) are electrically connected to the vessel ground and hydraulically fed from the top while the others (Panel 2, Panel 4) are electrically biased at 20 kV (± 5 kV @ 60 Hz) and hydraulically fed from the bottom. This cooling arrangement derives from the voltage holding at the cooling manifolds needed for the application of the biasing voltage and so for the realisation of the electrostatic field deflecting residual ions emerging from the neutraliser. Each panel is composed by 18 CuCrZr (Copper Chromium Zirconium) beam stopping elements (BSEs), that have a rectangular cross-section (22mmx100mm) with four internal channels of 14 mm in diameter (Figure 1.5). Inside the channels, AISI 316L twisted tapes with a pitch of 50 mm are inserted as turbulence promoter: water runs through two channels fed in parallel and the flow is reversed at the opposite end into two other channels. Different solutions in terms of twisted tape thickness have been proposed in order to find the final design for the ERID cooling system which allow to have a higher mass flow where the thermal power is expected to be higher. For this reason, 4 mm of thickness for all BSEs is set, except for the BSEs located in the middle walls for which 2 mm of tape thickness is necessary to increase the mass flow rate (9 BSEs from no. 7 to no. 15, see Figure 1.6) thus exhausting the higher thermal power expected in that regions. The ERID is fed with 100 kg/s of demineralised water supplied by the PRIMA cooling plant.

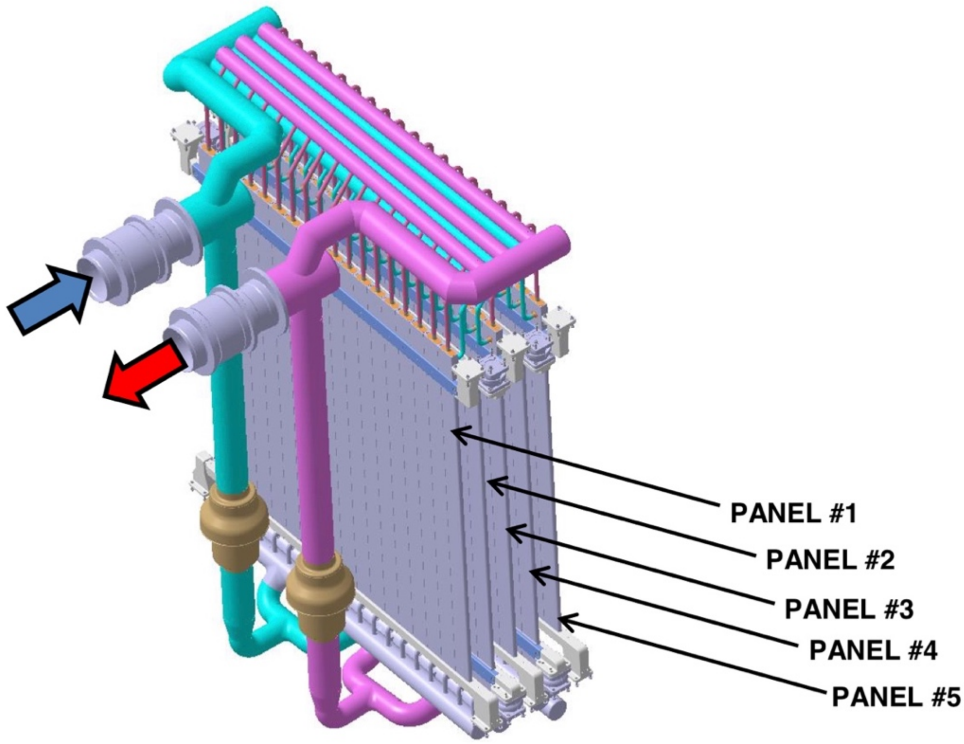


**Figure 1.4** E*RID 3D overview*

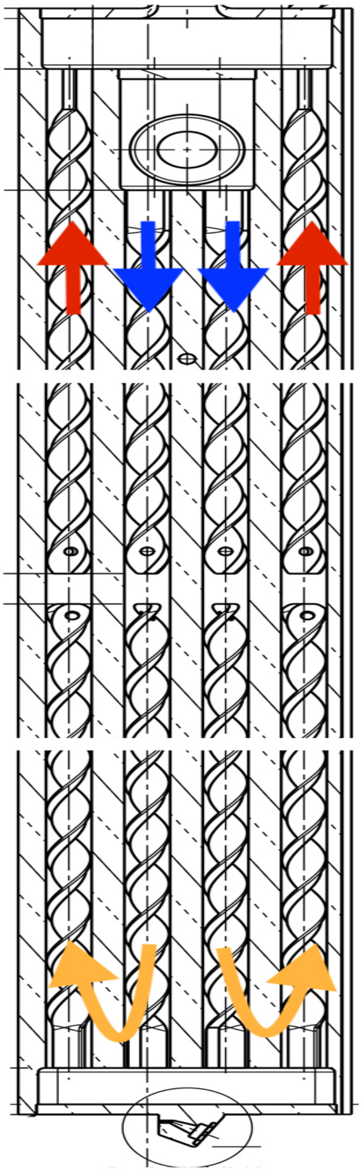

**Figure 1.5** *BSE schematic view with internal channels*

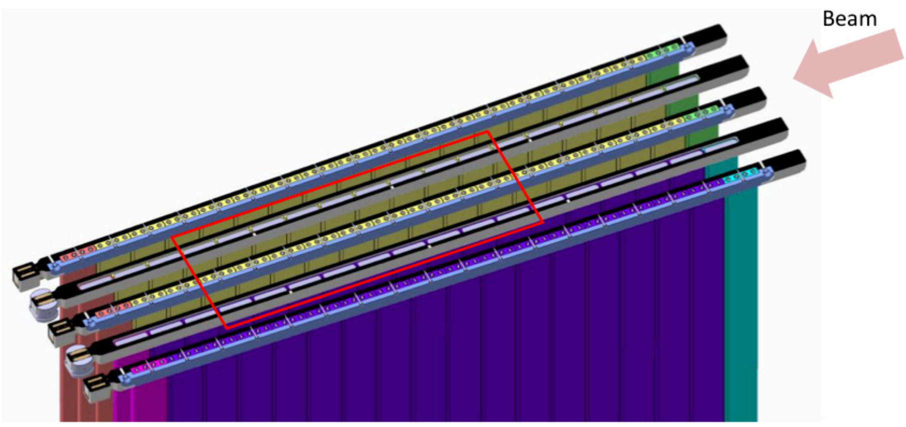


**Figure 1.6** *BSEs with different twisted tape thickness*

# Chapter 2
# Draining in fusion experiment

Draining is an important process before carrying out maintenance and inspection operations due to operating environment contamination caused by activated corrosion products that may be formed during ordinary operations in a fusion reactor. Draining process is usually followed by a drying process, by which hot nitrogen gas can be circulated through the system for an extended time to remove residual water by evaporation. After the completion of the drying operations, the system is cooled down to room temperature for maintenance temperature. This thesis is focused only on the draining process, in fact, this Second Chapter gives a short overview of the draining procedure and takes into account some analytical correlations useful to characterized the draining process and find the minimum required gas flow rate to blow out water from the in-vessel components. In the last part of the Chapter, a brief description of the flow regimes is given, which represent some phenomena that take place during the draining process.

## 2.1 Draining procedure

Draining is an important process for actively cooled reactor components operating in regions where fusion reactions occur. In the cooling loop of water-cooled fusion reactor, the corrosion is caused by the contact of water and metal materials. The dominant radioactive source term under normal operation are activated corrosion products (ACPs), which have an important impact on reactor inspection and maintenance [8]. When contacting with coolant, the internal surface of heat transfer tubes and pipes tends to be corroded to form oxide, which is more stable compared to the original metal state. Metallic ions from the base material continuously travel through the inner oxide layer and outer oxide layer, and are released into the coolant [9]. When the ions in the coolant are over-saturated, some ions will precipitate on the outer oxide layer to make it grow, or precipitate in the coolant to form particulates. The particulates continue to absorb ions and then land on the outer oxide layer by gravity to form deposit. While if the coolant is under-saturated, the outer oxide layer and the deposit may re-dissolved to be ions and then transferred in the coolant, besides, the shear force from the coolant leads to part of the outer oxide layer and the deposit directly eroded to be particulates and go with the coolant. When the corrosion products on the wall or in the coolant are under neutron radiation, they will be activated to be ACPs. Then, part of ACPs will circulate along the loop with the coolant and adhere to the internal surface of heat exchanger, pipe, valve, pump and filter, where the ACPs are continuously decaying and emitting gamma-rays even after shutdown of the reactor for a long time. The gamma radiation field created is hazardous to the staff working for reactor operation, inspection and maintenance, so an automatic draining system is necessary to perform these operations. There are two possible types of draining: the gravity draining, in which water is drained by gravity, and the forced draining, in which nitrogen is used to blow out water from the circuit. In the specific case, draining is applied to the ERID cooling circuits and since the inlet and the outlet are located at a higher quote than the component, only the forced draining is used to blow out water: pressurized nitrogen is blown through the system to remove as much of the water into the system. The two phase water-nitrogen mixture ejected from the cooling circuit will collected and drained in a separator where water is separated from the gas.

## 2.2 Analytical validation

A necessary condition needed for the blow out process to work is that the flowing gas must be able to exhaust the liquid out of the system. The interfacial friction between liquid and gas can overcome the gravity force on the liquid such that the gas can entrain all the liquid upwards. This is known as counter-current flow limitation (CCFL). For a given liquid rate there is a certain gas flow at which very large waves appear on the interface, the whole flow becomes chaotic, the gas pressure drop increases markedly and liquid is expelled from the top of the tube. This condition is known as flooding which is the result of a sudden and dramatic instability which increases the pressure gradient by an order of magnitude and it is described as the transition from counter-current to co-current flow. Under a simple geometry of a vertical tube, the Wallis correlation is a well-established empirical correlation that considers the inertial and gravitational forces in the equation. Counter current flow is maintained by buoyancy forces due to the density difference between gas and the liquid. Correlations for flooding in vertical tubes may be expressed in the general form [10]:

$$j_g^{*1/2} + m j_l^{*1/2} = C \tag{2.1}$$

where, $j_g^*$ and $j_l^*$ are dimensionless numbers or known as Wallis parameters in terms of dimensionless gas and liquid superficial velocities, *m* and *C* are constants which depend on the channel exit conditions. For turbulent flow *m* is equal to one, while the value of *C* is found to depend on the design of the ends of the tubes and the way in which the liquid and the gas are added and extracted. For tubes with sharp-edged flanges, $C = 0.725$, whereas a value between 0.88 and 1 can be used when end effect are minimized. These dimensionless groups can be defined as:

$$j_g^{*1/2} = j_g \rho_g^{1/2} \left[ g D_h (\rho_l - \rho_g) \right]^{-1/2} \tag{2.2}$$

$$j_l^{*1/2} = j_l \rho_l^{1/2} \left[ g D_h (\rho_l - \rho_g) \right]^{-1/2} \tag{2.3}$$

where, $j_g$ and $j_l$ are the gas and liquid superficial velocities [m/s], $\rho_g$ and $\rho_l$ are the gas and liquid densities [kg/m$^3$], $g$ is the gravitational acceleration [m/s$^2$] and $D_h$ is the hydraulic diameter [m]. The flooding limit can be expressed as minimum gas velocity required to prevent any liquid from flowing downwards, counter-current to the gas flow:

$$j_g^{*1/2} = C \tag{2.4}$$

Assuming that liquid density is much larger than gas density, Eq. 2.4 can be manipulated in an equation giving the minimum required gas mass flow rate $w_g$ [kg/s] [11]:

$$w_g = \left( \rho_g \rho_l g D_h \right)^{1/2} A C^2 \tag{2.5}$$

where $A$ is the flow area [m$^2$] and the other constants are defined above. Appling this correlation at different pressures, the minimum required gas mass flow can be estimated and it consists in a limit that must be exceeded to blow out water from the pipe.
Nitrogen density can be calculated by using the ideal gas law:

$$\rho_g = \frac{P}{RT} MW_g \tag{2.6}$$

where, $R$ is the gas constant [Pa m$^3$/ (mol K)], $T$ the temperature [K] and $MW_g$ is the nitrogen molecular weight [g/mol].
Assuming the same geometry and the same fluid, only the gas density changes because of the pressure change, so Eq. 2.5 can be rearranged obtaining a scaling law between the low and high-pressure experiments:

$$\frac{W_{g1}}{W_{g2}} = \left( \frac{P_1}{P_2} \right)^{1/2} \tag{2.7}$$

where, $P$ is the pressure of the experiment [Pa] and the indices 1 and 2 refer to the high and low pressure experiment, respectively, on the same geometry.
Another parameter useful to assess the draining performances of the cooling circuit investigated is the draining efficiency parameter $\varepsilon$, that can be defined as [12]:

$$\varepsilon = \frac{M_{l0} - M_l^{residual}}{M_{l0}} \tag{2.8}$$

where, $M_{l0}$ is the cooling circuit initial water amount [kg], while $M_l^{residual}$ is the cooling circuit residual water amount [kg]. In next chapters, a value for this parameter will be chosen to evaluate the draining performance.

## 2.3 Flow regimes

During the draining procedure, complex thermal-hydraulic phenomena arise since two components (water-nitrogen), two phase (liquid-gas) flow occurs inside a significant portion of the circuit, that progressively changes in time. Flow regimes determine the macroscopic behavior of two phase flow. Different regimes are classified by visual observation and it can be difficult to specify with a certainty, which regime a particular flow belongs to. Many different classifications exist in the literature but scientists don't agree on a unique set of flow regimes. Classification can be useful, since different flow regimes affect parameters in different manner, such as pressure drop, fluid properties, system configuration, size scale of the system, occurrence of phase change. Because of the geometrical difference, the flow regime can be divided into three main classes:

- Regimes for horizontal flow in pipes, where the heavier phase (water) tends to be located close to the bottom, because of gravity. In most cases the gas phase pushes the liquid phase along the flow direction.
- Regimes for vertical flow in pipes. The liquid phase tends to be on the pipe walls, forming a stable or an unstable film. Flow velocity can be different and flow regimes from differently for upward and downward flows.
- Regimes for sloped pipes, which are not as well known. Here the slope angle is important as well as the direction of the flow (upwards or downwards).

Vertical flow regimes are simpler than those in horizontal flow. This results from the symmetry in the flow induced by the gravitational force acting parallel to it.

The main vertical flow regimes are [13] (see Figure 2.1):

- Bubble flow: at very low liquid and gas velocities, the liquid phase is continuous, and the gas travels as dispersed bubble. As the liquid flow rate increases, the bubbles may increase in size via coalescence. Based on the presence of slippage between the two phases, bubble flow is further classified into bubbly and dispersed bubble flows. In bubbly flow, relatively fewer and larger bubbles move faster than the liquid phase because of slippage. In dispersed bubble flow, numerous tiny bubbles are transported by the liquid phase, causing no relative motion between two phases.
- Slug flow: as the velocity increases, the gas bubbles start coalescing, eventually forming large enough bubbles (Taylor bubbles) that occupy almost the entire cross sectional area. Taylors bubbles move uniformly upward and are separated by the slugs of continuous liquid that bridge the pipe and contain small gas bubbles. Typically, the liquid in the film around the Taylor bubbles may move downward at low velocities although the net flow of liquid can be upward. The gas bubble velocity is greater than that of the liquid.

- Churn (Transition) flow: if a change from a continuous liquid phase to a continuous gas phase occurs, the continuity of the liquid in the slug between successive Taylor bubbles is repeatedly destroyed by a high local gas concentration in the slug. This oscillatory flow of the liquid is typical of churn flow. It may not occur in small diameter pipes. The gas bubbles may join, and liquid may be entrained in the bubbles. In this flow regime, the falling film of the liquid surrounding the gas plugs cannot be observed.
- Annular flow: as the gas velocity increases even further, the transition occurs, and the gas phase becomes a continuous phase in the pipe core. The liquid phase moves upward partly as a thin film (adhering to the pipe wall) and partly in the form of dispersed droplets in the gas core.

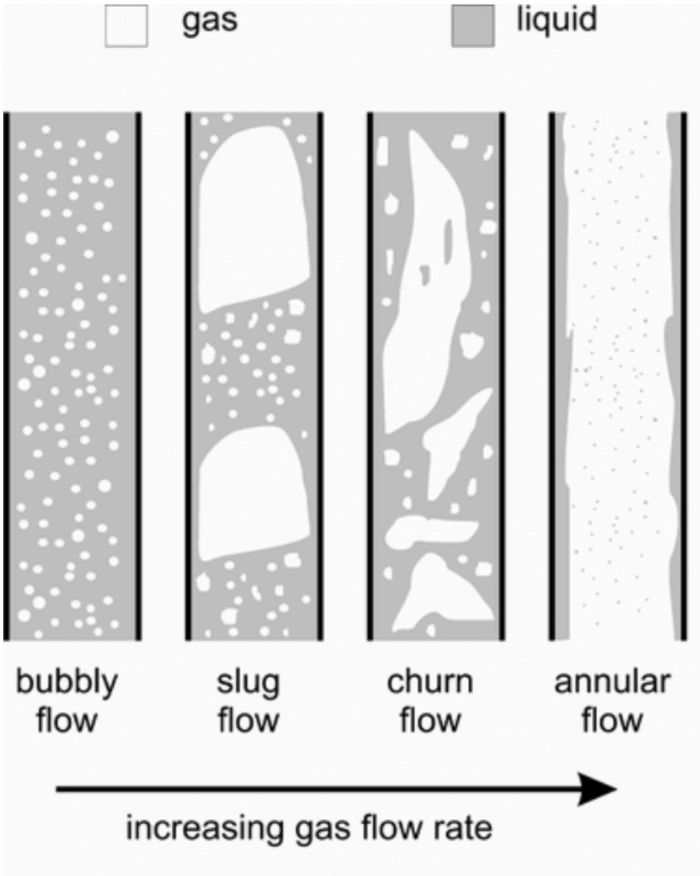


**Figure 2.1** *Flow regimes in vertical gas-liquid up-flows [14]*

Flow regimes observed in a horizontal pipe depend on gas and liquid velocities. Several classification are defined in literature [15] (see Figure 2.2):

- Dispersed bubble flow: at very low gas and high liquid rate, gas moves in the pipe as small bubbles. Gas bubbles do not have the same size. Due to lighter density, gas bubbles tend to move on the upper section of pipe.
- Stratified smooth flow: at low liquid and gas velocities in a horizontal pipe, gas and liquid separate and gas moves on the top and liquid on the bottom; the liquid-gas interface surface is smooth.
- Stratified wavy flow: increasing the gas injection from stratified smooth flow adds turbulence to liquid-gas interface-surface, causing a wavy interface.
- Slug flow: if gas further increases from stratified wavy flow, the wavy motion of interface increases till it reaches the upper side of the pipe and blocks the gas continuity in the system. In slug flow, the gas regime is not uniform in the pipe. Gas phase moves in separate pockets which are separated by columns (slugs) of the liquid phase.
- Annular flow: if gas injection rate further increases, gas moves as a core in the pipe surrounded by liquid. Due to gravity, liquid phase is thicker at the bottom.

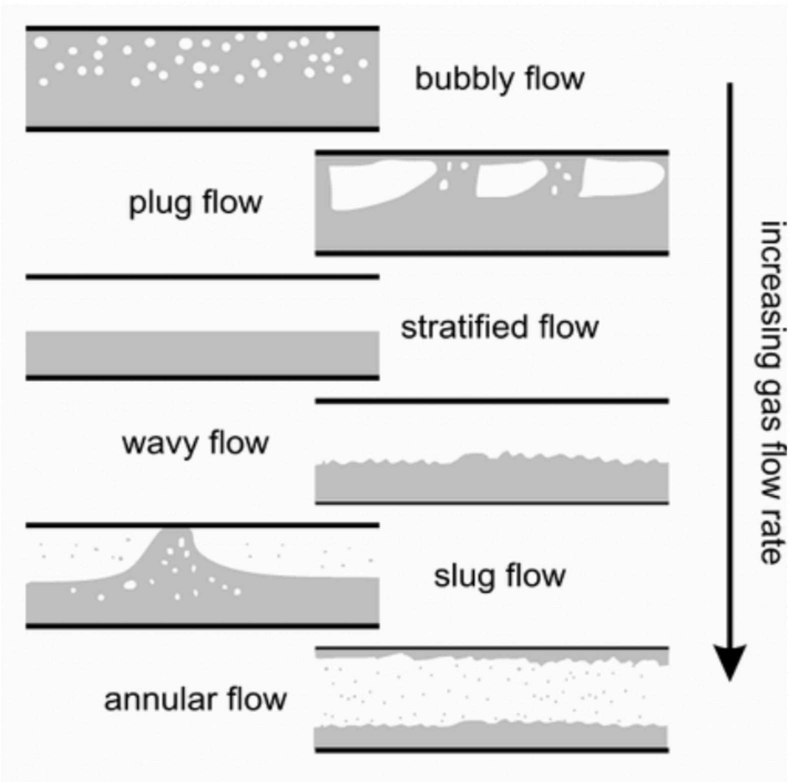


**Figure 2.2** *Flow regimes in horizontal gas-liquid flows [14]*

# Chapter 3
# Simulation Models

The draining process is analysed by using the RELAP5 software, which is described in the first part of this Chapter. Then, all simulation models, starting from the elementary components of the ERID which are the BSEs, to the overall system made of panels are analysed and all data and results are reported. Ranges for the boundary conditions of the model are identified considering practical operations (e.g. minimum over pressure and pressure steps of 0.5 bar) and limits corresponding to the hazard categories given by the Pressure Equipment Directive.

## 3.1 RELAP5 / Mod.3.3

The RELAP5 (Reactor Excursion and Leak Analysis Program) computer code is a light water reactor transient analysis code developed for the U.S. Nuclear Regulatory Commission (NRC) for use in rulemaking, licensing audit calculations, evaluation of operator guidelines, and as a basis for a nuclear plant analyser [16]. Specific applications of this capability have included simulations of transients in LWR (Light Water Reactor) systems, such as loss of coolant, anticipated transients without scram, and operational transients such as loss of feedwater, loss of offsite power, station blackout and turbine trip. RELAP5 is a highly generic code that, in addition to calculating the behaviour of a reactor coolant system during transient, can be used for simulation of a wide variety of hydraulic and thermal transients in both nuclear and non-nuclear systems involving mixtures of steam, water, non-condensable and solute.

### *3.1.1 Simulation approach*

RELAP used so called "cards" for the simulation of the models. Each card contains a special order: what the program has to do or under what conditions the program should run. For example, the card with the number 0000100 contains the name of the project and what kind of problem (steady state or transient) is simulated. With the help of this cards, every component of the system is modelled. Each new card implements a new part of the system. The modelling of a new component starts with the card XXX0000. This card implements the name of the new component and what kind of component is modelled. The XXX stands for the component number which is variable; a system of numbers would be an advantage because otherwise the overview of the simulated system is very quickly lost, if the system is too large. After naming the component, it is split into chosen number of cells for a more exact modelling. In fact, the code employs a control volume approach: components are subdivided into volumes connected by junctions. The typical components [17] used in this thesis are summarized:

- Time dependent volume (TMDPVOL): specify the boundary conditions for the model. In this specific case it represents the tank for the water or nitrogen depending if an hydraulic characterization or the draining process is studied. In the first case, water pressure and temperature are defined, while in the second case nitrogen pressure and temperature are defined.
- Pipe (PIPE): represents the pipeline in the system. PIPE can have 1-100 sub-control volumes, and each is connected by internal connection. Each sub-control volume is characterized with a series of parameters that represent its geometry, e.g. cross section, length in the direction of the flow, hydraulic diameter, roughness, angle. Average hydraulic properties are evaluated in the centre of the cell, which is the control volume for mass and energy quantities, except for velocities, which are evaluated in junctions.
- Time Dependent Junction (TMDPJUN): connects two components and specify the boundary conditions of the junctions.
- Single Junction (SNGLJUN): connects two components. To make the connection, the outlet and inlet of the control volumes that must be connected are required as input data. Junctions are characterized by the flow area and the form losses coefficients.
- Branch: consists of one system volume and zero to nine junctions.

In addition to the properties of each component, the temperature, the pressure and the boundary conditions of the fluid inside each cell have to be chosen. Before the start of the simulation, RELAP checks the code for mistakes, and will not start until every line is correct.

### *3.1.2 Relap equations*

RELAP5 uses a two-fluid, non-equilibrium, and non-homogeneous, hydrodynamic model for the transient simulation of the two-phase system behaviour. The hydrodynamic model of the code is a one-dimensional, transient, two-fluid model for flow of single-phase and two-phase steam-water mixture that can contain non-condensable components in the steam phase and/or a soluble component in the water phase [18]. Thus, simulations solve 1D-balance equations for liquid and vapor phases, which are formulated in terms of volume and time-averaged parameters of the flow. Phenomena that depend upon transverse gradients, such as friction and heat transfer, are formulated in terms of the bulk properties using empirical transfer coefficient formulations. The RELAP5 thermal-hydraulic model involves two phasic continuity equations, two phasic momentum equations and two phasic energy equations. In this model, each phase (liquid or gaseous) is considered separately and for each phase one of the conservation equations can be established. The nomenclature used hereinafter can be found in Nomenclature. The phasic continuity equations are:

$$\frac{\partial}{\partial t}\left(\alpha_g\rho_g\right)+\frac{1}{A}\frac{\partial}{\partial x}\left(\alpha_g\rho_g v_g A\right)=\Gamma_g \tag{3.1}$$

$$\frac{\partial}{\partial t}\left(\alpha_f\rho_f\right)+\frac{1}{A}\frac{\partial}{\partial x}\left(\alpha_f\rho_f v_f A\right)=\Gamma_f \tag{3.2}$$

Generally, the flow does not include mass sources or sinks, and overall continuity consideration yields the requirement that the liquid generation term be the negative of the vapor generation, that is,

$$\Gamma_f=-\Gamma_g \tag{3.3}$$

The interfacial mass transfer model assumes that total mass transfer can be portioned into mass transfer at the vapor/liquid interface in the bulk fluid ($\Gamma_{ig}$) and mass transfer at the vapor/liquid interface in the boundary layer near the walls ($\Gamma_w$), that is,

$$\Gamma_g=\Gamma_{ig}+\Gamma_w \tag{3.4}$$

The phasic conservation of momentum equations are used in an expanded form that is more convenient for development of the numerical scheme. The spatial variation of momentum terms is expressed in terms of $v_g^2$ and $v_f^2$. This form has the desirable feature that the momentum equation reduces the Bernoulli's equations for steady, incompressible, and frictionless flow. In RELAP5, momentum effects are secondary to mass and energy conservation in reactor safety analysis and a less exact formulation (compared to mass and energy conservation) is acceptable. The momentum equation for the vapor phase is

$$\begin{aligned}\alpha_g\rho_g A\frac{\partial v_g}{\partial t}+\frac{1}{2}\alpha_g\rho_g A\frac{\partial v_g^2}{\partial x}=&-\alpha_g A\frac{\partial P}{\partial x}+\alpha_g\rho_g B_x A-\left(\alpha_g\rho_g A\right)FWG\left(v_g\right)\\&+\Gamma_g A\left(v_{gI}-v_g\right)-\left(\alpha_g\rho_g A\right)FIG\left(v_g-v_f\right)\\&-D\alpha_g\alpha_f\rho_m A\left[\frac{\partial\left(v_g-v_f\right)}{\partial t}+v_f\frac{\partial v_g}{\partial t}-v_g\frac{\partial v_f}{\partial x}\right]\end{aligned} \tag{3.5}$$

And for the liquid phase is

$$\begin{aligned}\alpha_f\rho_f A\frac{\partial v_f}{\partial t}+\frac{1}{2}\alpha_f\rho_f A\frac{\partial v_f^2}{\partial x}=&-\alpha_f A\frac{\partial P}{\partial x}+\alpha_f\rho_f B_x A-\left(\alpha_f\rho_f A\right)FWF\left(v_f\right)\\&+\Gamma_g A\left(v_{fI}-v_f\right)-\left(\alpha_f\rho_f A\right)FIF\left(v_f-v_g\right)\\&-D\alpha_f\alpha_g\rho_m A\left[\frac{\partial\left(v_f-v_g\right)}{\partial t}+v_g\frac{\partial v_f}{\partial t}-v_f\frac{\partial v_g}{\partial x}\right]\end{aligned} \tag{3.6}$$

The derivation of these equations uses the following simplification:

- Reynolds stresses are neglected

- Equal phasic pressures
- The interfacial pressure is assumed equal to the phasic pressures
- The covariance terms are universally neglected
- Interfacial momentum storage is neglected
- Phasic viscous stresses are neglected
- The interface force terms consist of both pressure and viscous stresses
- The normal wall forces are assumed adequately modelled by the corresponding phasic velocity, and are subtracted from the momentum equations.

The force terms on the right and sides are, respectively, the pressure gradient, the body force, wall friction, momentum transfer due to interface mass transfer, interface frictional drug, and force due to virtual mass. The terms FWG and FWF are part of the wall frictional drug, which are linear in velocity, and are products of the friction coefficient, the frictional reference area per unit volume, and the magnitude of the fluid bulk velocity. The coefficients FIG and FIF are part of the interface frictional drag. The value of $D$ depends on flow regime (a value of $D$>1/2 has been shown to be appropriate for bubbly or dispersed flows, while $D$=0 may be appropriate for a separated or stratified flow).

The phasic thermal energy equations are:

$$\frac{\partial}{\partial t}\left(\alpha_g\rho_g U_g\right)+\frac{1}{A}\frac{\partial}{\partial x}\left(\alpha_g\rho_g U_g v_g A\right)=-P\frac{\partial\alpha_g}{\partial t}-\frac{P}{A}\frac{\partial}{\partial x}\left(\alpha_g v_g A\right) \\ +Q_{wg}+Q_{ig}+\Gamma_{ig}h_g^*+\Gamma_w h_g'+DISS_g \tag{3.7}$$

$$\frac{\partial}{\partial t}\left(\alpha_f\rho_f U_f\right)+\frac{1}{A}\frac{\partial}{\partial x}\left(\alpha_f\rho_f U_f v_f A\right)=-P\frac{\partial\alpha_f}{\partial t}-\frac{P}{A}\frac{\partial}{\partial x}\left(\alpha_f v_f A\right) \\ +Q_{wf}+Q_{if}+\Gamma_{ig}h_f^*+\Gamma_w h_f'+DISS_f \tag{3.8}$$

The derivation of these equations uses the following simplification:

- Reynolds heat flux is neglected
- Covariance terms are neglected
- Interfacial energy storage is neglected
- Internal phasic heat transfer is neglected

In the equations $Q_{wg}$ and $Q_{wf}$ are the phasic wall heat transfers rates per unit volume. These phasic wall heat transfer rates satisfy the equation

$$Q=Q_{wg}+Q_{wf} \tag{3.9}$$

where Q is the total wall heat transfer rate to the fluid per unit volume. Different enthalpies are inserted into the equations: $h_g^*$ and $h_f^*$ are the enthalpies associated with bulk interface mass transfer, defined in such a way that the interface energy jump conditions at the liquid-vapor interface are satisfied; $h'_g$ and $h'_f$ are the enthalpies associated with the wall (thermal boundary layer) interface mass transfer.

## 3.2 Pressure Equipment Directive

The Pressure Equipment Directive (PED) 2014/68/EU (formerly 97/23/EC) is a fundamental piece of European legislation relation to the safety of pressure equipment throughout Europe. The PED applies to the design, manufacture and conformity assessment of pressure equipment and assemblies in such a way to ensure its safety when put into service in accordance with the manufacturer's instructions, or in reasonably foreseeable conditions. The Directive is applied to the equipment with a maximum allowable pressure PS greater than 0.5 bar(g). Pressure equipment subject to a pressure of not more than 0.5 bar does not pose a significant risk due to pressure [19]. This Directive is considered for the beam stopping elements and for all the ERID assembly which are subjected to a pressure hazard after the entry of pressurized nitrogen and it is applied in order to find the maximum admissible pressure for the simulations. The Directive provides for a classification of pressure equipment in categories, according to the ascending level of hazards and also includes the classification of the fluid contained in the pressure equipment as dangerous or not. For the purpose of the Directive, the following definitions shall apply:

- "vessel" means a housing designed and built to contain fluids under pressure including its direct attachments up to the coupling point connecting it to other equipment; a vessel may be composed of more than one chamber;
- "piping" means piping components intended for the transport of fluids, when connected together for integration into a pressure system; piping includes in particular a pipe or system of pipes, tubing, fittings, expansion joints, hoses, or other pressure-bearing components as appropriate.

Thanks to this classification, also the type of fluid contained into that equipment can be classified in "group" depending on their dangerousness, but in this specific case nitrogen and water are not dangerous fluid. So, for vessel the following groups of fluids can be used:

- Gases, liquified gases, gases dissolved under pressure, vapours and also those liquids whose vapour pressure at the maximum allowable temperature is greater than 0.5 bar above normal atmospheric pressure, within the following limits: for fluids in Group 2, with a volume greater than 1 L and a product of PS and V is greater than 50 bar · L, or with a pressure PS greater than 1000bar.
- Liquids having a vapour pressure at the maximum allowable temperature of not more than 0.5 bar above normal atmospheric pressure within the following limits: for fluids

in Group 2 with a pressure PS greater than 10 bar and a product of PS and V greater than 10000 bar · L, or with a pressure PS greater than 1000 bar.

For piping, the following groups of fluids can be used:

- Gases, liquified gases, gases dissolved under pressure, vapours and those liquids whose vapour pressure at the maximum allowable temperature is greater than 0.5 bar above normal atmospheric pressure within the following limits: for fluids in Group 2 with a DN greater than 32 and a product of PS and DN greater than 1000 bar.
- Liquids having a vapour pressure at the maximum allowable temperature of not more than 0.5 bar above normal atmospheric pressure within the following limits: for fluids in Group 2 with a PS greater than 10 bar, a DN greater than 200 and a product of PS and DN greater than 5000 bar.

By using this classification, there are 9 separate conformity assessment tables, one for each of the possible combination of the equipment type, fluid state and fluid group. In this specific case, for the draining process, only the two tables of gases, one for vessel (Figure 3.1) and the other one for pipe (Figure 3.2) are reported and used for this purpose.

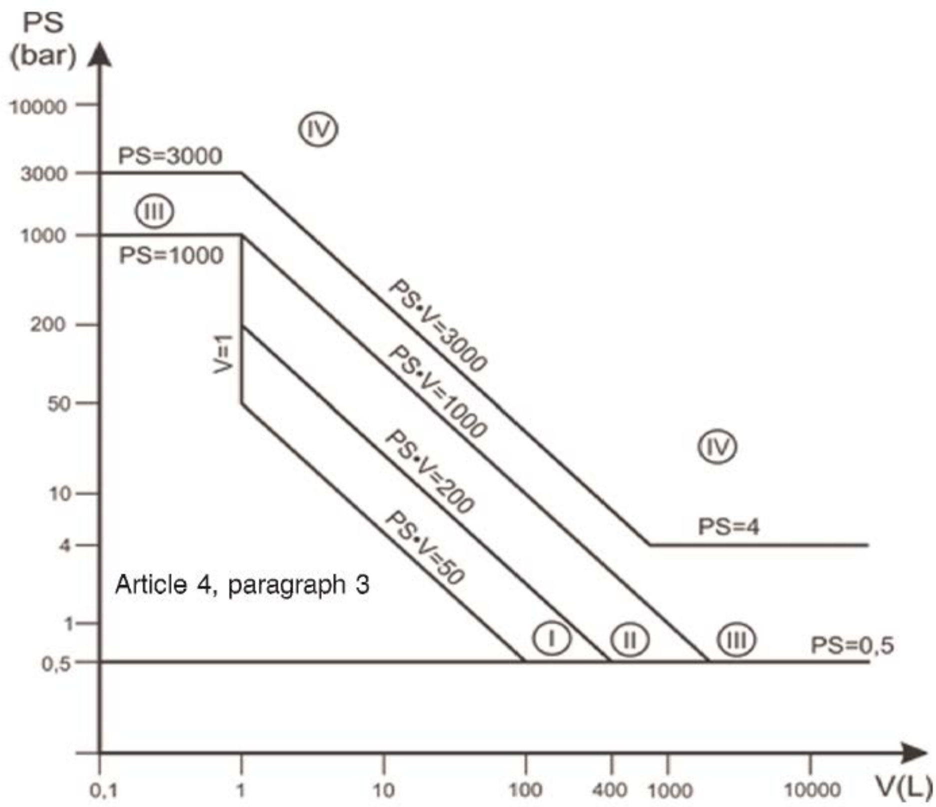


**Figure 3.1** *Areas of PED conformity assessment modules for gas group 2 inside vessel*

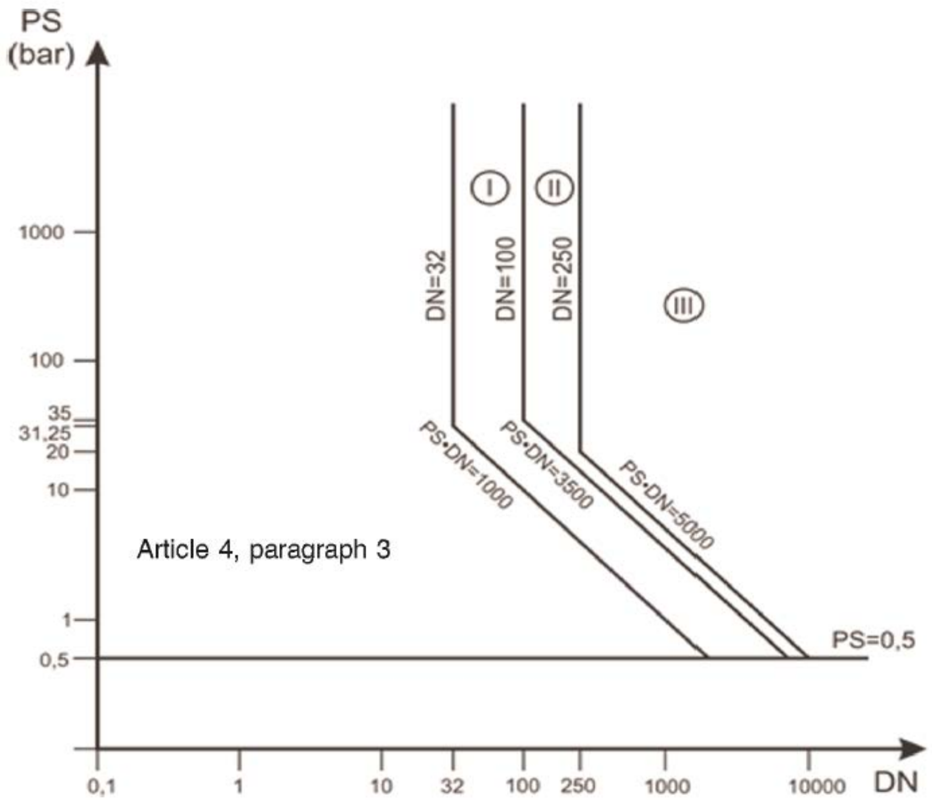


**Figure 3.2** *Areas of PED conformity assessment modules for gas group 2 inside piping*

The demarcation lines in the conformity assessment tables indicate the upper limit for each PED hazard category. In particular, the Directive sets five categories of equipment: SEP (Sound Engineering Practice) that is indicated with the name of the article, I, II, III and IV. CE marking only applies to categories I to IV, where SEP cannot be marked under PED and purely requires the manufacturer to use common sense. The higher the equipment PED category, the higher the level of hazard and therefore the more extensive the quality assurance requirements are. The PED category defines the required conformity assessment module.
For the draining operation the maximum allowable pressure PS for each active cooled element will be determined in the following section in order to fulfil PED specifications consistently with article 4, paragraph 3 of the Directive (design in accordance with the sound engineering practice); so considering the draining operation, the elements must not bear the CE marking.

### 3.2.1 PED classification for the ERID

The classification has been carried out considering each single BSE as single vessel in order to minimise the level of hazard [20]. The choice of a boundary enclosing only one BSE is consistent with the definition of vessel because the BSE inlet and outlet sections are evidently identified as coupling points connecting the panel to inlet and outlet tubes that are other equipment. The level of hazard of the BSE is reported in Table 3.1, where it is possible to see that the PED hazard category results SEP for a single BSE.

**Table 3.1** PED hazard category for BSE

| Vessel [-] | Gross internal volume [$m^3$] | PS [bar(g)] | Category [-] |
|---|---|---|---|
| Single BSE | 1.16 | 43 | SEP |

The cooling tubes are made of TP 316L. Classes of cooling elements are identified by grouping inlet tubes, outlet tube and manifolds (see Figure 3.3) consistently with the diameter.

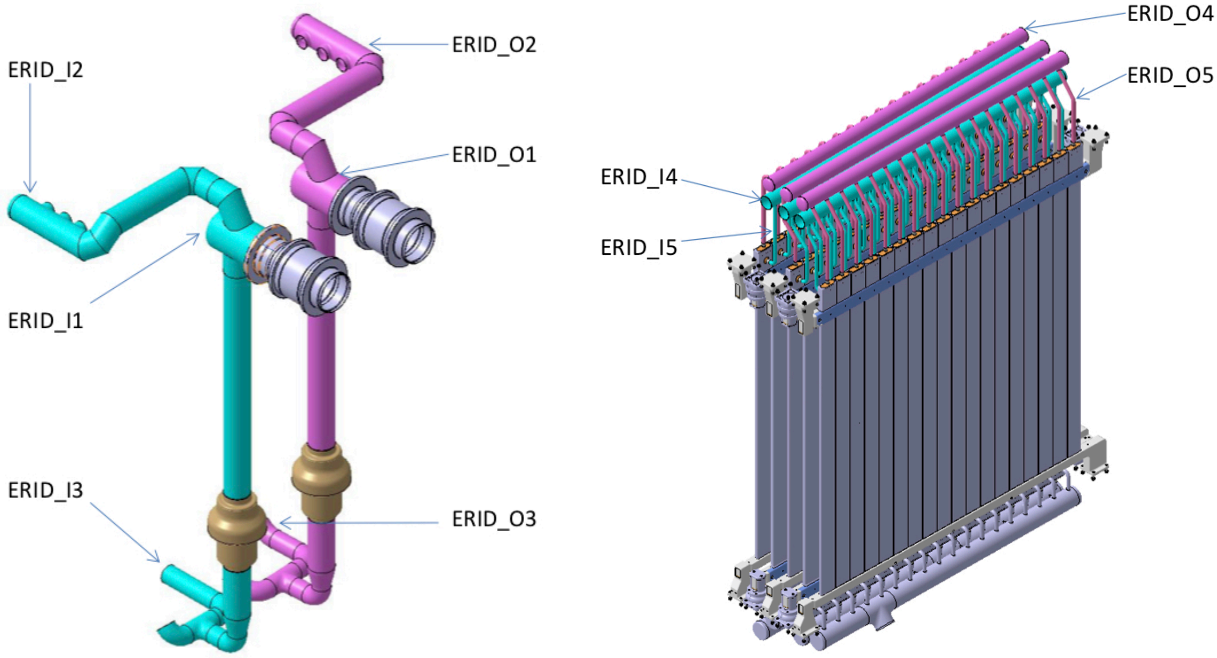


(a) (b)

**Figure 3.3** *Classes of cooling elements group consistently with diameter for the ERID: (a) headers; (b) tubes*

The detailed categories for each cooling tube is reported in Table 3.2.

**Table 3.2** *PED hazard categories for the cooling tubes*

| Piping label | Diameter [mm] | PS [bar(g)] | Category |
|---|---|---|---|
| ERID_I1 | 200 | 5 | SEP |
| ERID_I2 | 140 | 7.1 | SEP |
| ERID_I3 | 100 | 10 | SEP |
| ERID_I4 | 70 | 14 | SEP |
| ERID_I5 | 20 | any | SEP |
| ERID_O1 | 200 | 5 | SEP |
| ERID_O2 | 140 | 7.1 | SEP |
| ERID_O3 | 100 | 10 | SEP |
| ERID_O4 | 70 | 14 | SEP |
| ERID_O5 | 20 | any | SEP |

The PED hazard category for ERID cooling pipework results to be SEP, with a maximum allowable pressure $PS_{blowing}$=5bar(g). Considering both analysis, the results for the ERID cooling system can be summarized in Table 3.3.

**Table 3.3** *Summary of PED classification for the ERID*

| Element [-] | Maximum pressure [bar(g)] | PED classification |
|---|---|---|
| Piping | 5 | SEP |
| BSE | 43 | SEP |
| **ERID** | **5** | **SEP** |

The PED hazard category for the ERID results SEP with a maximum gas pressure for blowing out of $PS_{blowing}$=5 bar(g). Simulations for the BSEs and Panels will be performed by using a maximum nitrogen pressure of P = 5 bar(a), in order to stay below the limit and avoid some fluctuations.

## 3.3 Initial and Boundary Conditions

In the simulation of the draining process, it has been assumed that the system is initially full of water, depressurized (p=1 bar) and at ambient temperature (T=298K). To asses that the system is full of water, in the program, the static quality that represents the mass fraction of vapour phase at a particular cross section is assigned and it is defined as:

$$X = \frac{M_g}{M_g + M_f} \tag{3.10}$$

where, $M_g$ is the mass of the gaseous phase [kg] and $M_f$ is the mass of the liquid phase [kg], so a very small value of $X = 1.0 \times 10^{-9}$ is chosen to asses that the water mass is greater than the nitrogen mass and the component can be considered filled of water. The other conditions are related to nitrogen: the system is subjected to increase the inlet pressure, which purges the system and replaces the water with nitrogen. The inlet temperature of the gas is set to 298K. The mass inflow of nitrogen purely depends on the system resistance (wall and interface friction). The numerical simulations are conducted by varying the inlet nitrogen pressure from a lower value of P=1.5 bar to an upper value given by the Pressure Equipment Directive (PED).

## 3.4 Beam Stopping Element model

The beam stopping element is the simpler element of the ERID cooling system and as previously described two different types are necessary to respect the requirement of the cooling system. More precisely, twisted tapes are inserted as turbulence promoters in the four channels of the beam stopping elements and their thickness vary with respect to the cooling requirements, and consequently their water mass flow rate is different. The values of the water mass flow rate for both types of BSEs are reported in Table 3.4.

**Table 3.4** *BSEs water mass flow rate*

| Tape thickness [m] | $\dot{m}_{BSE}$ [kg/s] |
|---|---|
| 0.002 | 1.35 |
| 0.004 | 1.01 |

### 3.4.1 Swirl channels correlations

The hydraulic behaviour of the swirl channels have been characterised by using analytical formulas in order to find the pressure drop that are necessary to build the circuit in the software. The hydraulic diameter of these elements can be calculated as:

$$D_h = \frac{4A}{P_w} = D_i \frac{\pi D_i - 4\delta}{2D_i + \pi D_i - 2\delta} \tag{3.11}$$

where, $P_w$ is the wetted perimeter [m], $D_i$ is the inner diameter [m] and $\delta$ is the twisted tape thickness [m]. The values of the hydraulic diameter and the area for the BSEs are reported in Table 3.5.

**Table 3.5** *Data of the BSEs*

| Tape thickness [m] | $D_h$ [m] | A [m$^2$] |
|---|---|---|
| 0.002 | 0.00741 | 0.000126 |
| 0.004 | 0.00612 | 0.0000979 |

The Reynolds number, referred to the hydraulic diameter and swirl flow is defined as:

$$Re_{sw} = (1 + K_{sw}^2)^{0.5} \left(\frac{v_f \rho_b D_h}{\mu_b}\right) \tag{3.12}$$

where, $v_f$ is the axial component of the fluid velocity [m/s], $\rho_b$is the density of the bulk [kg/m$^3$], $\mu_b$ is the dynamic viscosity of the bulk [Pa s] and $K_{sw}$ is the twist ratio defined as:

$$K_{sw} = \frac{\pi D_h}{pitch} \tag{3.13}$$

where, the pitch is the distance between two homologous consecutive elements of the inserted twisted tape [m]. The non-linear Colebrook-White correlation for turbulent flow [21] modified in order to take in account the swirl flow, has been used for the friction factor $f_{sw}$calculation (in the Fanning form):

$$\frac{1}{\sqrt{4f_{sw}}} = -2\log_{10}\left(\frac{2.51}{Re_{sw}\sqrt{4f_{sw}}} + \frac{\varepsilon_r}{3.71}\right) \tag{3.14}$$

where, $\varepsilon_r = \varepsilon/D_h$ is the reduce roughness.
Finally, the pressure drop along the swirl channel is given by:

$$\Delta p_1 = 4f_{sw}\frac{L}{D_h}\rho_b(1 + K_{sw}^2)^{3/2}\frac{v_f^2}{2} \tag{3.15}$$

where, L is the tube length [m].

### 3.4.2 U-tube model

The model of the BSE has been developed starting from its two channels as a U-tube. The calculation of the Reynolds number and the twist ratio is necessary to find the friction factor, calculated thanks to a Matlab routine, that is then used to calculate the pressure drop according to Eq.3.15. The U-tube RELAP model is shown in Figure 3.4. The water flow rate ($\dot{m}_w$) for the U-tube model is half of the water flow rate of the BSE because half element is used.

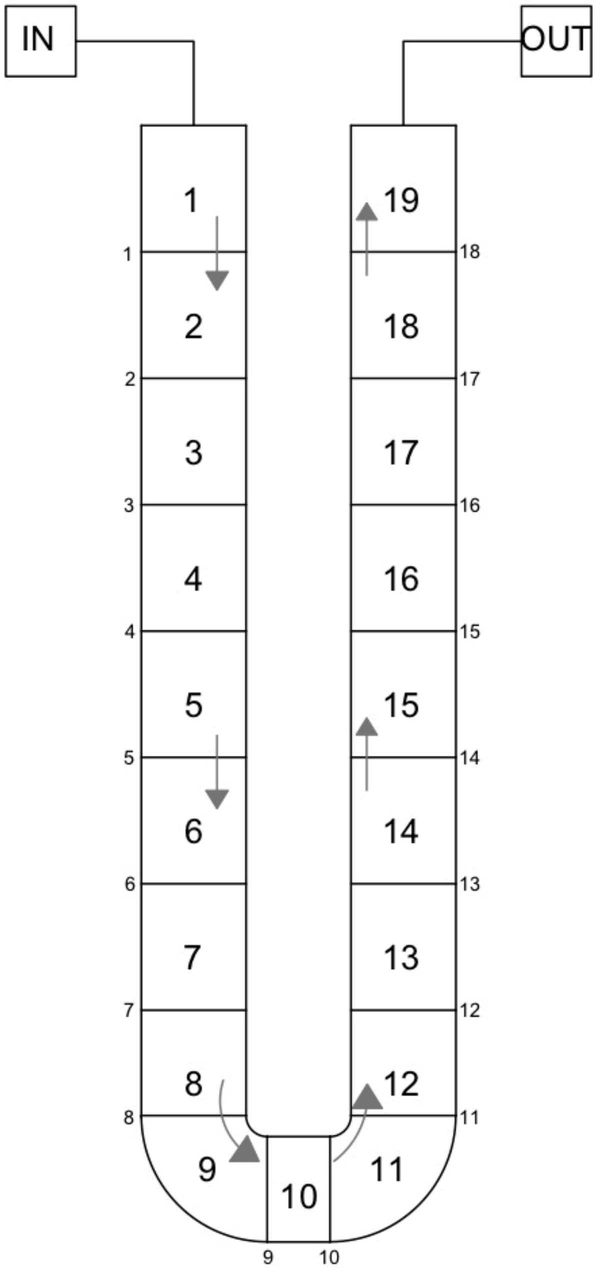


**Figure 3.4** *Relap U-tube model*

The inlet of the system is represented by a time dependent volume element in which nitrogen boundary conditions are defined. A single junction connects the inlet with the pipe that is made of 19 volumes with different length and inclination angles. Another single junction connects the outlet of the pipe with the tank that represents the outlet of the model. The total length of the system is $L$=3700mm; the length and the inclination angle of each volume are reported in Table 3.6.

**Table 3.6** *Data for the U-tube model*

| Volume number [-] | L [mm] | Incl. angle [°] |
|---|---|---|
| 1 | 204 | -90.0 |
| 2 | 204 | -90.0 |
| 3 | 204 | -90.0 |
| 4 | 204 | -90.0 |
| 5 | 204 | -90.0 |
| 6 | 204 | -90.0 |
| 7 | 204 | -90.0 |
| 8 | 204 | -90.0 |
| 9 | 204 | 0.0 |
| 10 | 24 | 0.0 |
| 11 | 204 | 0.0 |
| 12 | 204 | 90.0 |
| 13 | 204 | 90.0 |
| 14 | 204 | 90.0 |
| 15 | 204 | 90.0 |
| 16 | 204 | 90.0 |
| 17 | 204 | 90.0 |
| 18 | 204 | 90.0 |
| 19 | 204 | 90.0 |

RELAP can calculate itself the pressure drop of pipe with circular cross sections, but due to the particular geometry of the swirl channels localized pressure drop coefficients shall be applied. So, in order to have the right result and consequently the right model, the calculation of the pressure drop is made by inserting a loss coefficient in each junction (this is the reason why also the junctions of the pipe are highlighted in Figure 3.4) calculated as:

$$K = \frac{\Delta p_1}{\rho\left(\frac{v_f^2}{2}\right)} \tag{3.16}$$

This loss coefficient is then divided by the number of junctions minus two, because for junctions number 8 and number 10 a loss coefficient ($K_b$) due to a 90° bend is applied.

$$K_j = \frac{K}{N_j - 2} \tag{3.17}$$

The pressure drop of the bends can be calculated as:

$$\Delta p_2 = \frac{\rho v_f^2}{2} K_b \tag{3.18}$$

where, $K_b$=0.45 [22] for a 90° bend.
The total pressure drop can be calculated as:

$$\Delta p_{tot} = \Delta p_1 + \Delta p_2 \tag{3.19}$$

#### 3.4.2.1 U-tube with 2 mm of twisted tape

For 2 mm of twisted tape thickness, the previous equations are applied in order to find the localized loss coefficient that has to be inserted into the program. Results are reported in Table 3.7.

**Table 3.7** *Input data for U-tube with 2 mm of twisted tape*

| $f$ [-] | $\dot{m}_w$ [kg/s] | $D_h$ [m] | $v_f$ [m/s] | A [m$^2$] | $\Delta p_1$ [Pa] | $\Delta p_2$ [Pa] | $\Delta p_{tot}$ [Pa] | $K$ [-] | $K_j$ [-] |
|---|---|---|---|---|---|---|---|---|---|
| $6.0787 \times 10^{-3}$ | 0.675 | 0.00741 | 5.41 | 0.0001256 | 246775 | 13131 | 259906 | 16.91 | 1.057 |

#### 3.4.2.2 U-tube with 4 mm of twisted tape

For 4 mm of twisted tape thickness, the previous equations are applied in order to find the localized loss coefficient that has to be inserted into the program. Results are reported in Table 3.8.

**Table 3.8** *Input data for U-tube with 4 mm of twisted tape*

| $f$ [-] | $\dot{m}_w$ [kg/s] | $D_h$ [m] | $v_f$ [m/s] | A [m$^2$] | $\Delta p_1$ [Pa] | $\Delta p_2$ [Pa] | $\Delta p_{tot}$ [Pa] | $K$ [-] | $K_j$ [-] |
|---|---|---|---|---|---|---|---|---|---|
| $6.3136 \times 10^{-3}$ | 0.505 | 0.00612 | 5.21 | 0.00009786 | 253951 | 12178 | 266129 | 18.77 | 1.180 |

## 3.5 Draining of the BSEs

Thanks to the U-tube model, it's now possible to build the BSE model, that is shown in Figure 3.5. In this case, the inlet is connected to a branch that is necessary to divide the flow for the two channels of the BSE which are represented by two U-tubes. The two outlets are connected to a branch, and then water can be collected into the outlet tank.

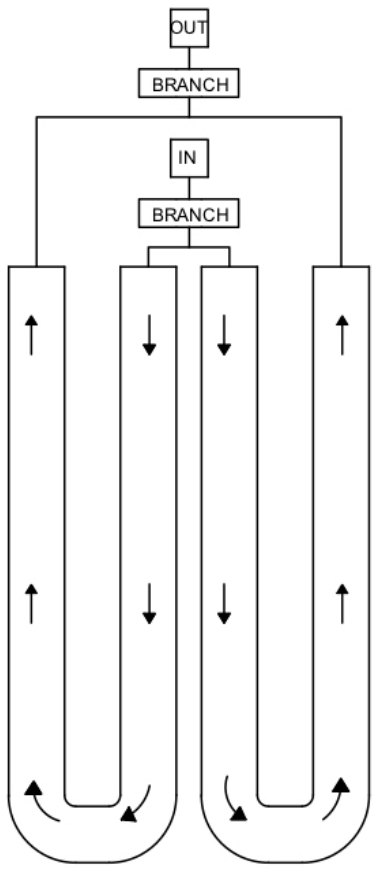


**Figure 3.5** *Relap BSE model*

### 3.5.1 Wallis correlation application

This model is necessary to compare the minimum nitrogen flow rate calculated thanks to the Wallis correlation and the simulated one. The data necessary to apply the Wallis correlation are reported in Table 3.9.

**Table 3.9** *Wallis correlation parameters [23] [24]*

| Parameter | Value |
|---|---|
| R [Pa $m^3$/ mol K] | 8.314 |
| $MW_g$ [g/mol] | 28.01 |
| Di [m] | 0.014 |
| T [K] | 298 |
| g [$m/s^2$] | 9.81 |
| C [-] | 1 |

For the 2 mm of twisted tape thickness the simulated nitrogen flow rate is shown in Figure 3.6.

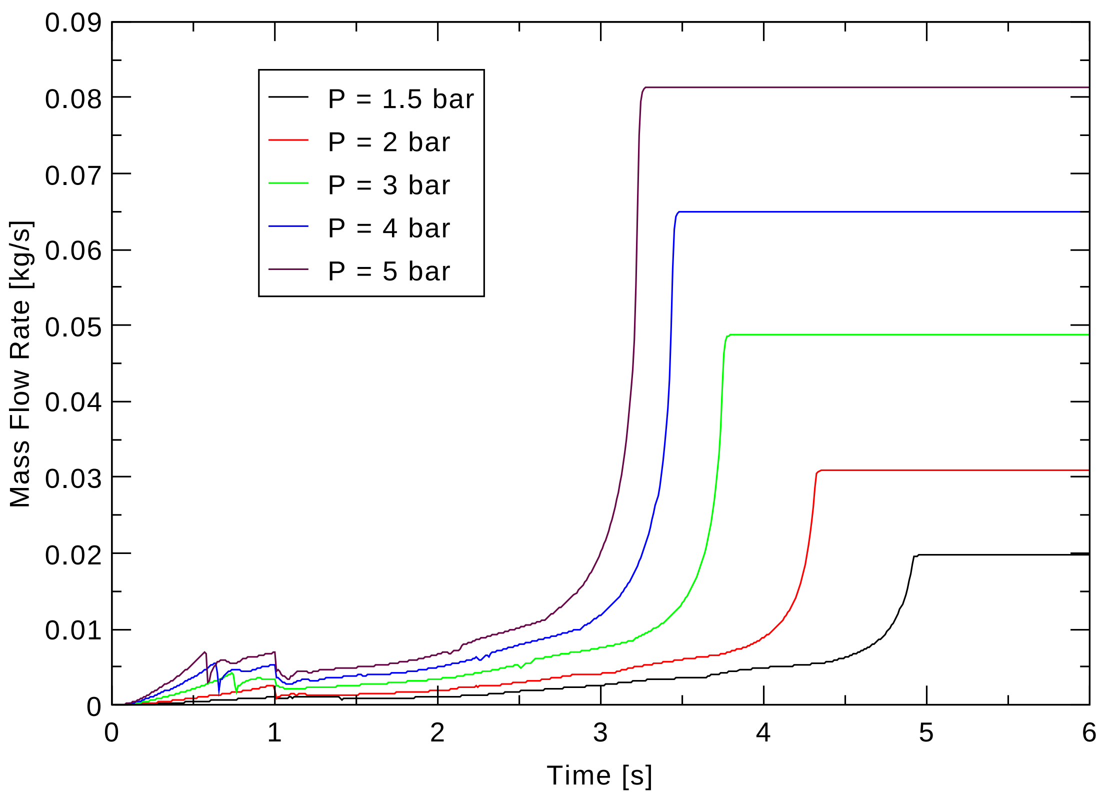


**Figure 3.6** *Minimum nitrogen flow rate for the BSE with 2 mm of tape thickness*

At the beginning, there are some instabilities because, precisely, the y-axis represents a combined flow rate between nitrogen and water. In fact, at the beginning, the mass flow rate is lower because the hydraulic resistance of the circuit that is filled of water is higher. In the last part of the plot, the flow rate is stable (horizontal line) because the system is empty and it represents the maximum flow rate for that pressure. The results of the calculated nitrogen flow rate coming from the Wallis correlation $w_g$ for different pressures is reported in Table 3.10.

**Table 3.10** *Nitrogen flow rate needed for 2 mm of tape thicnkess*

| P<br>[bar] | $w_g$<br>[kg/s] |
|---|---|
| 1.5 | 0.001395 |
| 2 | 0.001611 |
| 3 | 0.001973 |
| 4 | 0.002278 |
| 5 | 0.002547 |

In order to have the draining process the simulated mass flow rate must be higher than the calculated one. As it is possible to see from the figure, this condition is respected and the draining process can be evaluated for the total system.
For the 4 mm of twisted tape thickness the simulated nitrogen flow rate is shown in Figure 3.7.

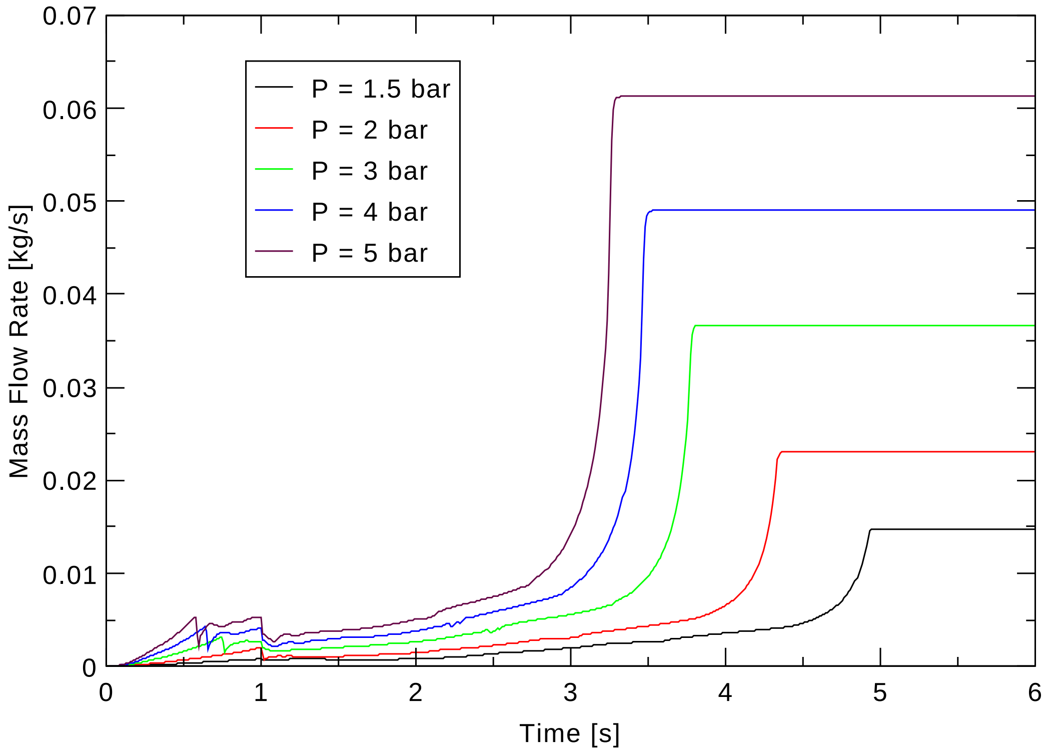


**Figure 3.7** *Minimum nitrogen flow rate for the BSE with 4 mm of tape thickness*

Also in this case there are some instabilities and the results are summarized in Table 3.11.

**Table 3.11** *Nitrogen flow rate needed for 4 mm of tape thickness*

| P [bar] | $w_g$ [kg/s] |
|---|---|
| 1.5 | 0.0009859 |
| 2 | 0.001130 |
| 3 | 0.001394 |
| 4 | 0.001610 |
| 5 | 0.001800 |

Also in this case the simulated flow rate is higher than the calculated one, and the draining process can be applied. The flow rate in this case is lower than that of the 2 mm of tape thickness because the amount of water that has to be discharged is lower.

The BSEs can also be divided in other two categories: the BSEs fed from the top and the BSEs fed from the bottom. The difference stays in the dimension of the pipes that connect the inlets and the outlets of the BSEs. For the simulations a value of $\varepsilon$=99 % for efficiency parameter is fixed to consider the draining process completed (Eq. 2.8 in Chapter 2).

### 3.5.2 BSE model fed from the top

The schematic view of the BSE is shown in Figure 3.8. In this case, two junctions are added in order to connect the inlet tank with the inlet pipe, and the outlet pipe with the outlet tank.

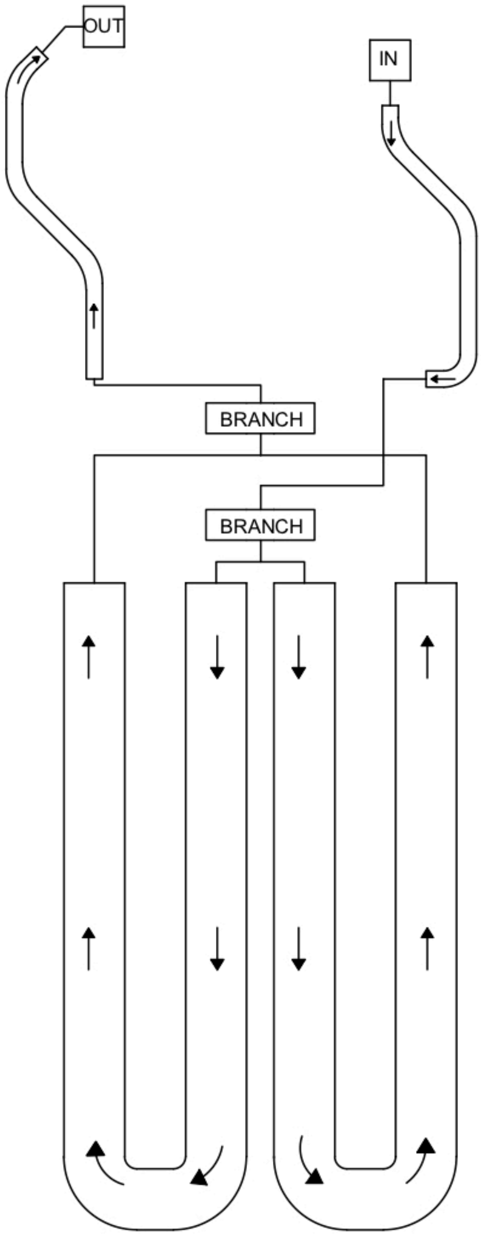


**Figure 3.8** *BSE model fed from the top*

The inlet pipe has a diameter of D=20mm and a total length L=395.7 mm, which is very small compared with the length of the BSE. The model of the pipe consists of 17 volumes, which are not represented in the figure to have a clear view of the overall system, and the pressure drop in this case is calculated by the program itself because this pipe is not made of a particular geometry. Only three loss coefficients related to three bends are inserted, in particular two of them are the loss coefficients for the 45° bend ($K_b$=0.2) and the other one is related to the 90°bend. The length and the inclination angle of each volume is reported in Table 3.12.

**Table 3.12** *Data for the inlet pipe of the BSE fed from the top*

| Volume number [-] | L [mm] | Incl. angle [°] |
|---|---|---|
| 1 | 24.237 | -90.0 |
| 2 | 24.237 | -90.0 |
| 3 | 22.961 | -45.0 |
| 4 | 23.031 | -45.0 |
| 5 | 23.031 | -45.0 |
| 6 | 23.031 | -45.0 |
| 7 | 23.031 | -45.0 |
| 8 | 23.031 | -45.0 |
| 9 | 22.961 | -90.0 |
| 10 | 23.31 | -90.0 |
| 11 | 23.31 | -90.0 |
| 12 | 23.31 | -90.0 |
| 13 | 23.31 | -90.0 |
| 14 | 23.31 | -90.0 |
| 15 | 23.31 | -90.0 |
| 16 | 23.31 | -90.0 |
| 17 | 23 | 0.0 |

The outlet pipe has a diameter of D = 20 mm and a total length of L = 441.8 mm, the length and the inclination angle of each volume is reported in Table 3.13. Also in this case, pressure drop is computed by the software.

**Table 3.13** *Data for the outlet pipe of the BSE fed from the top*

| Volume number<br>[-] | L<br>[mm] | Incl. angle<br>[°] |
|---|---|---|
| 1 | 27.01 | 90.0 |
| 2 | 27.01 | 90.0 |
| 3 | 27.01 | 90.0 |
| 4 | 27.01 | 90.0 |
| 5 | 27.01 | 90.0 |
| 6 | 22.961 | 45.0 |
| 7 | 22.54 | 45.0 |
| 8 | 22.54 | 45.0 |
| 9 | 22.54 | 45.0 |
| 10 | 22.54 | 45.0 |
| 11 | 22.961 | 45.0 |
| 12 | 23.50 | 90.0 |
| 13 | 23.50 | 90.0 |
| 14 | 23.50 | 90.0 |
| 15 | 23.50 | 90.0 |
| 16 | 23.50 | 90.0 |
| 17 | 22.961 | 45.0 |
| 18 | 30.189 | 45.0 |

#### 3.5.2.1 BSE with 2 mm of twisted tape fed from the top

The simulations are performed to find the characteristic parameters for the water blow out from the component. The volume of water in the BSE is V=0.001195 m$^3$, and the mass is $M_{l0}$=1.19 kg. The time needed at different nitrogen inlet pressure to discharge water from the circuit is shown in Figure 3.9. It's possible to see that increasing the nitrogen pressure, the water draining is much faster and the time needed is lower. The draining process is successfully achieved because the residual water is almost zero and it is less than 0.0119 which represent the 1% of the total water mass.

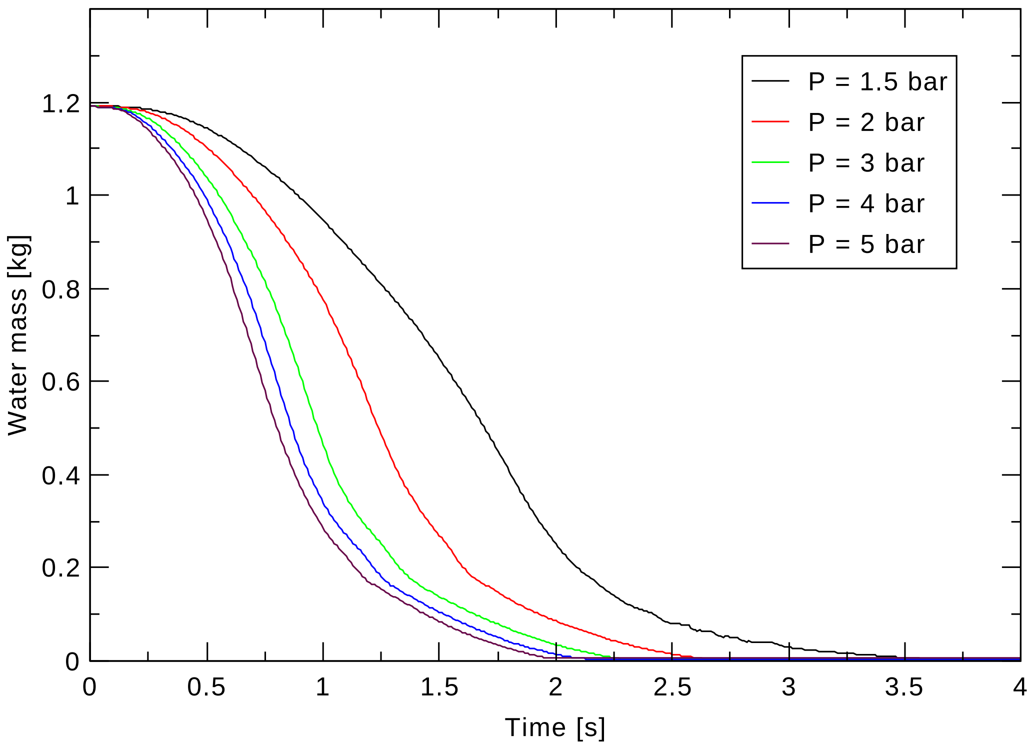


**Figure 3.9** *Time variation of water mass of the BSE with 2 mm of tape thickness fed from the top*

The liquid void fraction (see Figure 3.10) is evaluated in the more unfavorable volume of the BSE, which is the bend. It is possible to see that the water discharged is total.

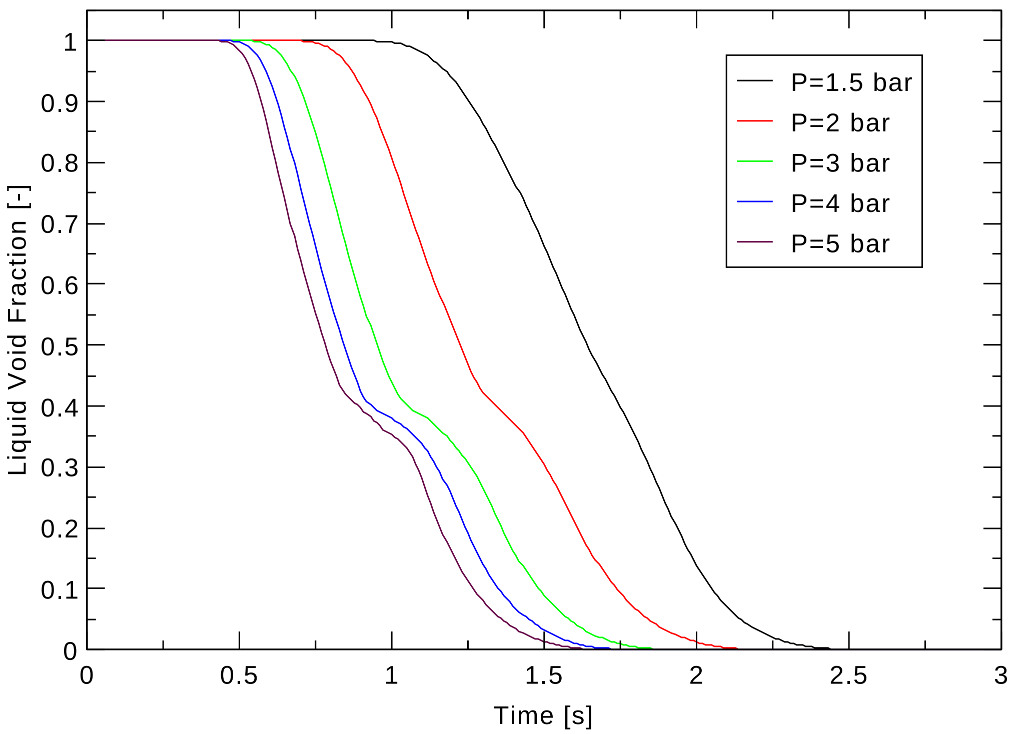


**Figure 3.10** *Time variation of the liquid void fraction of the BSE with 2 mm of tape thickness fed from the top*

The mass flow rate needed to blow out water from the circuit is shown in Figure 3.11, where it is possible to see that also in this case, in the first part of the graph there is a pick and a sort of flow rate instability that dampens after few seconds. In fact, at the beginning instabilities are present because nitrogen pushes water and then when the circuit is empty the nitrogen flow rate can be read from the graph (the horizontal line after the instabilities). Values of the calculated instabilities are of the same order of magnitude of the final flow rate, then pressure fluctuations and vibrations are expected. This evidence is controlled with linear increase of the blow out pressure at the beginning of the process, as discussed in Chapter 4.

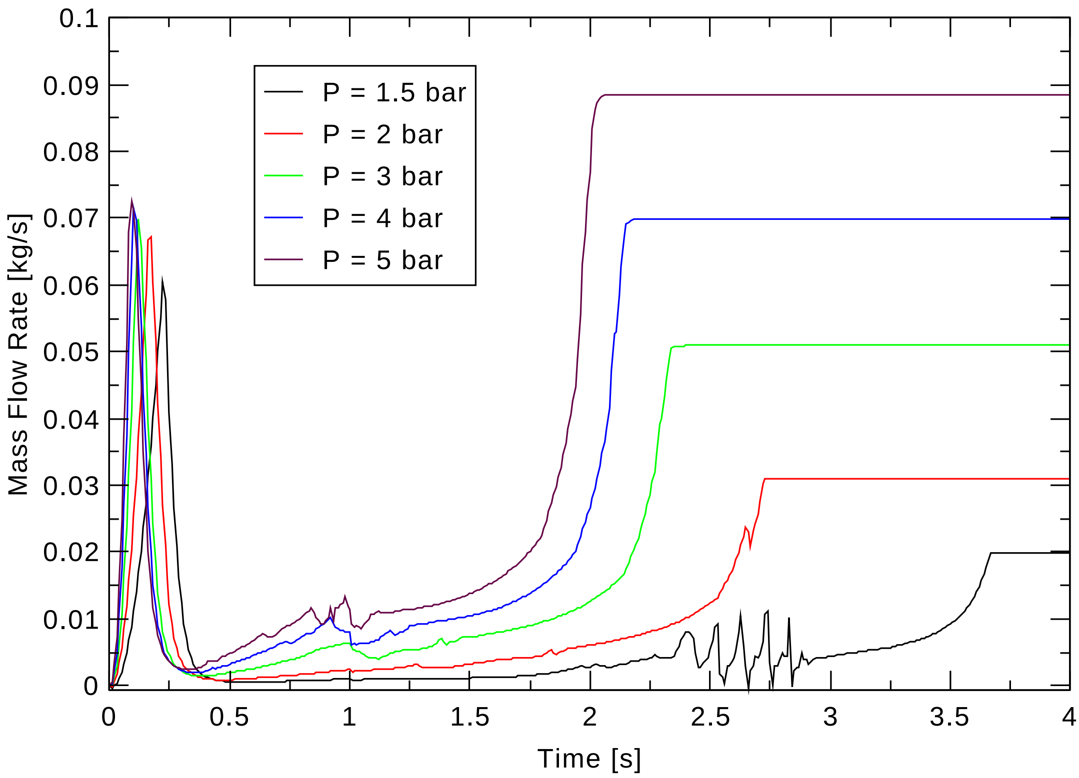


**Figure 3.11** *Time variation of inlet mass flow rate of the BSE with 2 mm of tape thickness fed from the top*

Nitrogen flow rate increases with pressure. The outlet mass flow rate is shown in Figure 3.12. At the beginning there is a sharp increase of outlet mass flow rate, and then the trend becomes quasi-steady-state.

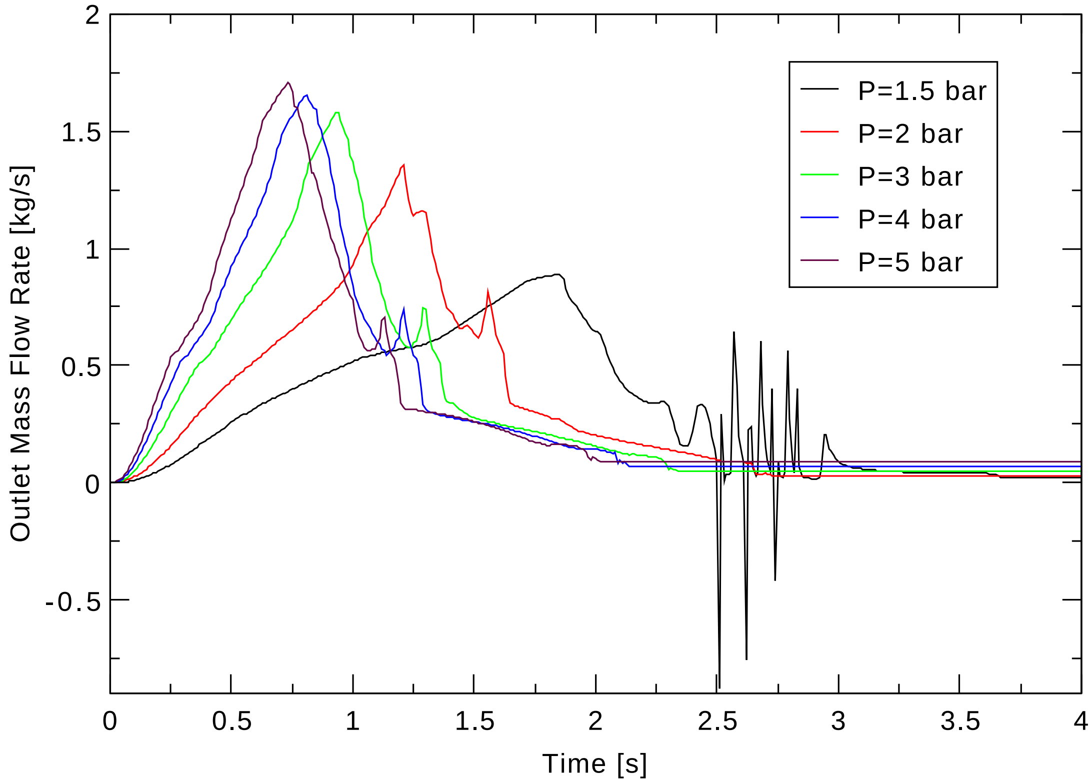


**Figure 3.12** *Time variation of outlet flow rate of the BSE with 2 mm of tape thickness fed from the top*

In Table 3.14 a summary of the results is given.

**Table 3.14** *Results for the BSE with 2 mm of tape thickness fed from the top*

| $P$ [bar] | $t$ [s] | $\dot{m}_{N_2}$ [kg/s] |
|---|---|---|
| 1.5 | 3.38 | 0.01985 |
| 2 | 2.52 | 0.03100 |
| 3 | 2.22 | 0.05093 |
| 4 | 2.04 | 0.06988 |
| 5 | 1.94 | 0.08843 |

### 3.5.2.2 BSE with 4 mm of twisted tape fed from the top

The volume of water in the BSE is V=0.0009870 m$^3$ and the water mass is $M_{l0}$=0.984 kg. The time needed to blow out water from the circuit is shown in Figure 3.13. The draining process is successfully achieved because the residual water mass is less than 0.00984 kg which represents the 1% of the total water mass.

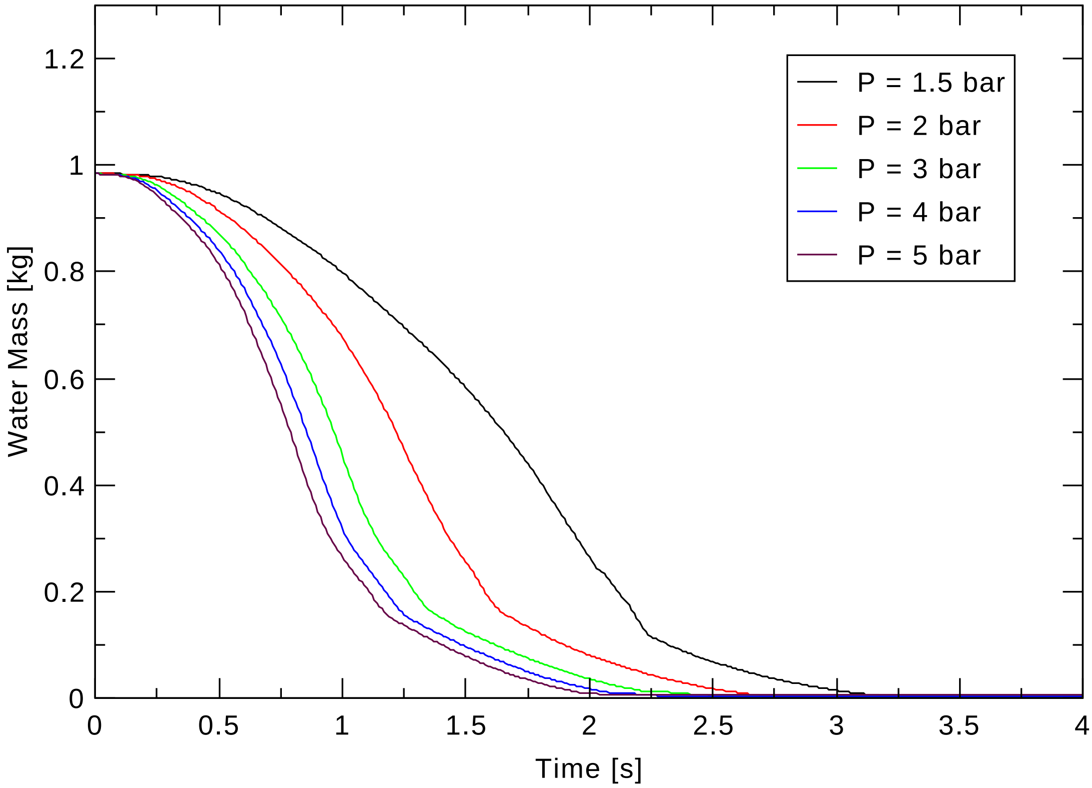


**Figure 3.13** *Time variation of water mass of the BSE with 4 mm of tape thickness fed from the top*

The liquid void fraction (see Figure 3.14) is evaluated in the more unfavorable volume of the BSE, which is the bend. It is possible to see that the water discharged is total. The mass flow rate needed to blow out water is shown in Figure 3.15. Also in this case, after the instabilities the nitrogen mass flow rate can be read from the graph.

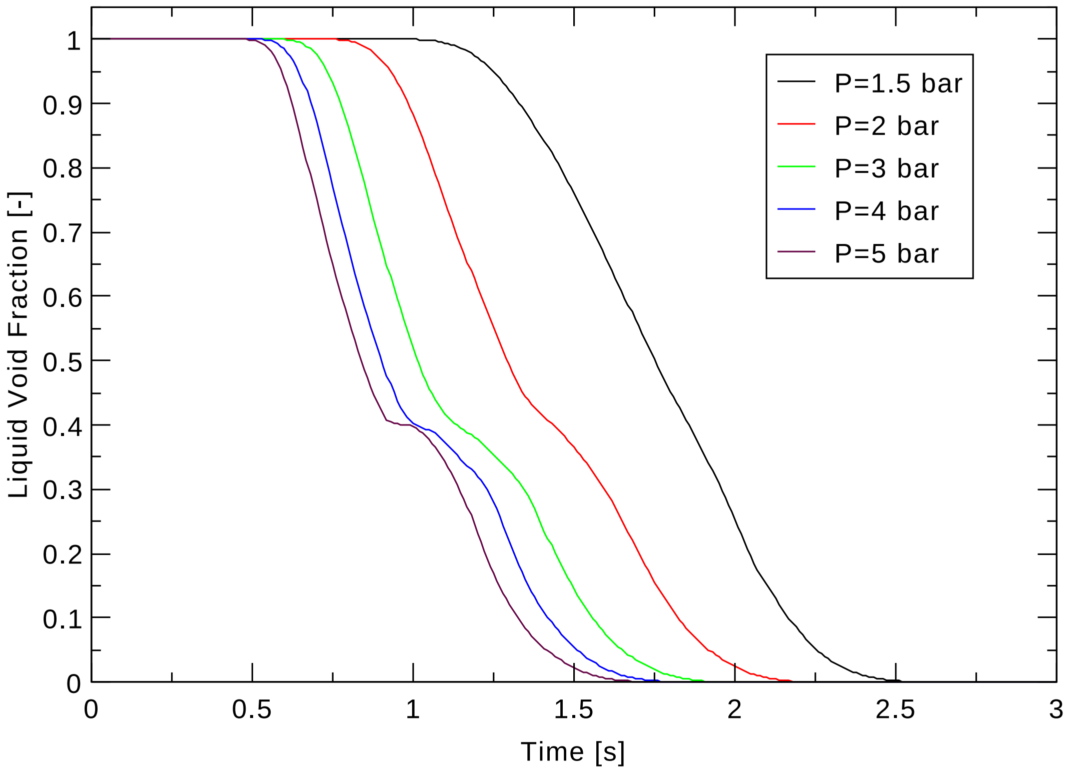


**Figure 3.14** *Time variation of the liquid void fraction of the BSE with 4 mm of tape thickness fed from the top*

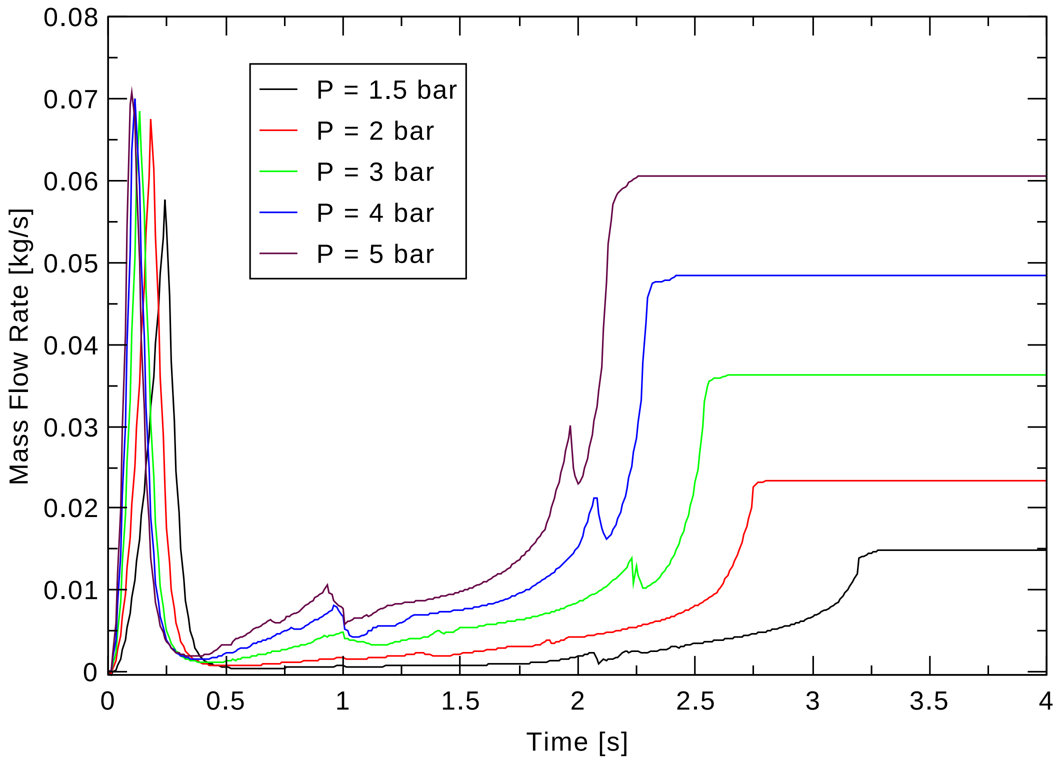


**Figure 3.15** *Time variation of inlet mass flow rate of the BSE with 4 mm of tape thickness fed from the top*

The outlet mass flow rate is shown in Figure 3.16.

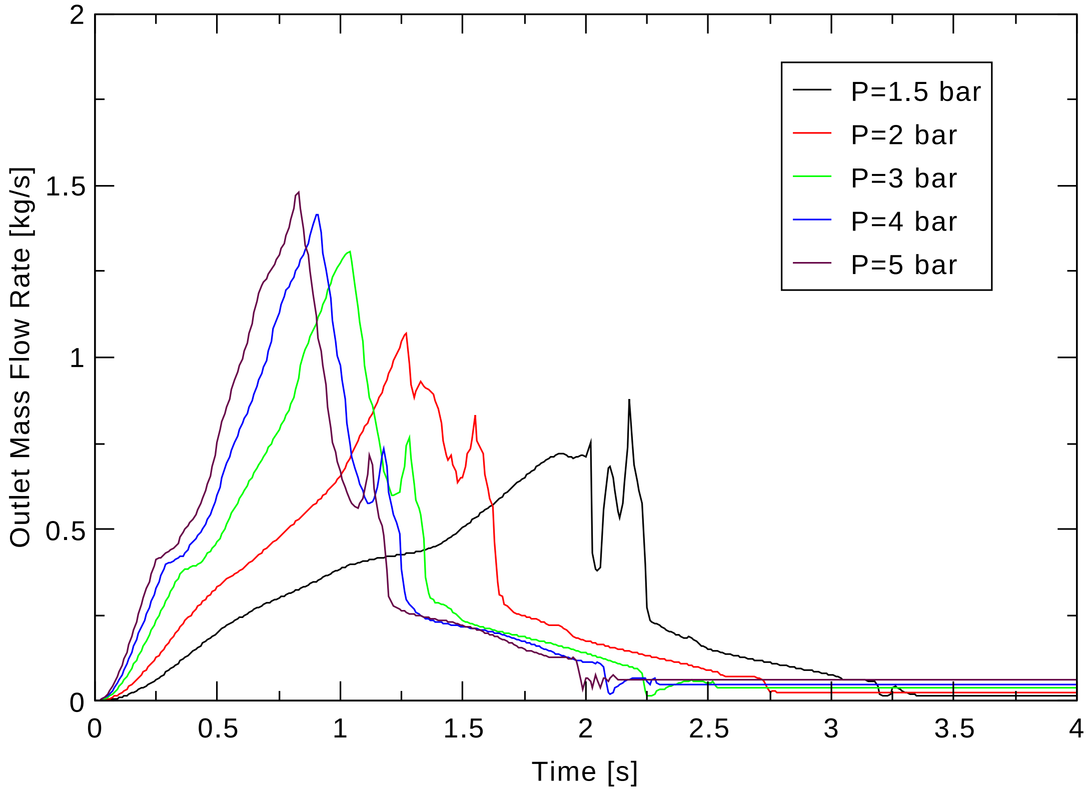


**Figure 3.16** *Time variation of outlet flow rate of the BSE with 4 mm of tape thickness fed from the top*

The summary of the time needed to blow out water and the nitrogen mass flow rate for different pressures are summarized in Table 3.15.

**Table 3.15** *Results for the BSE with 4 mm of tape thickness fed from the top*

| $P$ [bar] | $t$ [s] | $\dot{m}_{N_2}$ [kg/s] |
|---|---|---|
| 1.5 | 3.07 | 0.01496 |
| 2 | 2.59 | 0.02333 |
| 3 | 2.34 | 0.03645 |
| 4 | 2.13 | 0.04851 |
| 5 | 1.95 | 0.06066 |

### 3.5.3 BSE fed from the bottom

The model of the BSE fed from the bottom is given in Figure 3.17, where in this case the U-tubes are turned upside-down.

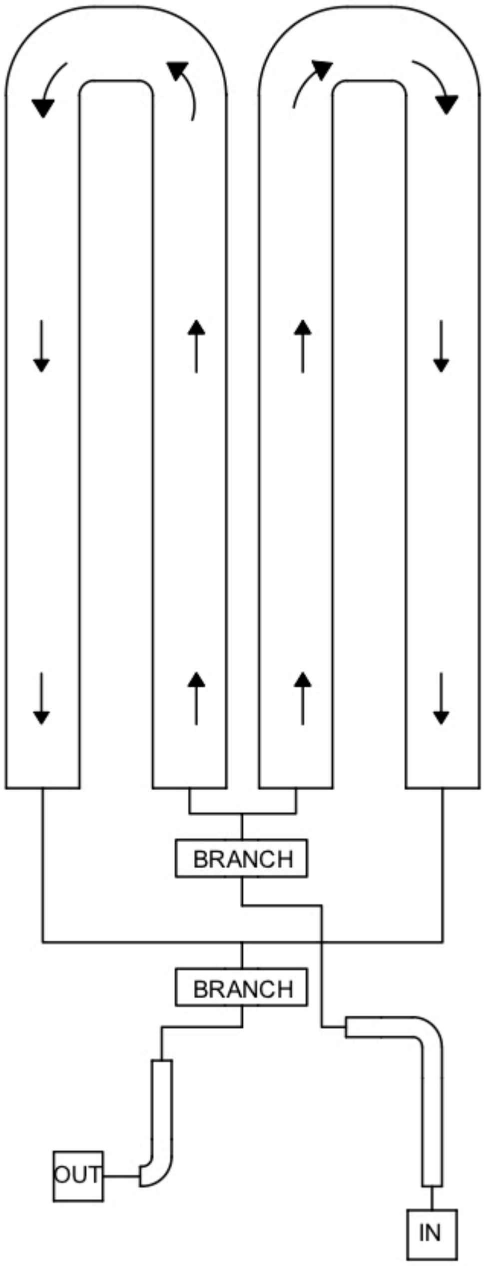


**Figure 3.17** *BSE model fed from the bottom*

The inlet pipe has a diameter of D=20mm and a total length L=198.4 mm. The model of the pipe consists of 9 volumes, which are not represented in the figure to have a clear view of the overall system, and also in this case the pressure drop is calculated by the program itself. The loss coefficient related to the 90° bend is inserted. The length and the inclination angle of each volume is reported in Table 3.16.

**Table 3.16** *Data for the inlet pipe of the BSE fed from the bottom*

| Volume number [-] | L [mm] | Incl. angle [°] |
|---|---|---|
| 1 | 24 | 90.0 |
| 2 | 24 | 90.0 |
| 3 | 24 | 90.0 |
| 4 | 24 | 90.0 |
| 5 | 24 | 90.0 |
| 6 | 42.4 | 90.0 |
| 7 | 12 | 0.0 |
| 8 | 12 | 0.0 |
| 9 | 12 | 0.0 |

The outlet pipe has a diameter of D = 20 mm and a total length of L = 120.7 mm, the length and the inclination angle of each volume is reported in Table 3.17. Also in this case, pressure drop are computed by the software.

**Table 3.17** *Data for the outlet pipe of the BSE fed from the bottom*

| Volume number [-] | L [mm] | Incl. angle [°] |
|---|---|---|
| 1 | 20.3 | -90.0 |
| 2 | 20.3 | -90.0 |
| 3 | 20.3 | -90.0 |
| 4 | 20.3 | -90.0 |
| 5 | 28.3 | -90.0 |
| 6 | 11.2 | 0.0 |

### 3.5.3.1 BSE with 2 mm of twisted tape fed from the bottom

The volume of water in this BSE is V=0.001032 $m^3$ and the water mass is $M_{l0}$=1.029 kg. The time needed for the water blow out from the circuit is shown in Figure 3.18. The draining process is successfully achieved because the residual water mass is less than 0.01029 kg which is the 1% of the total water mass.

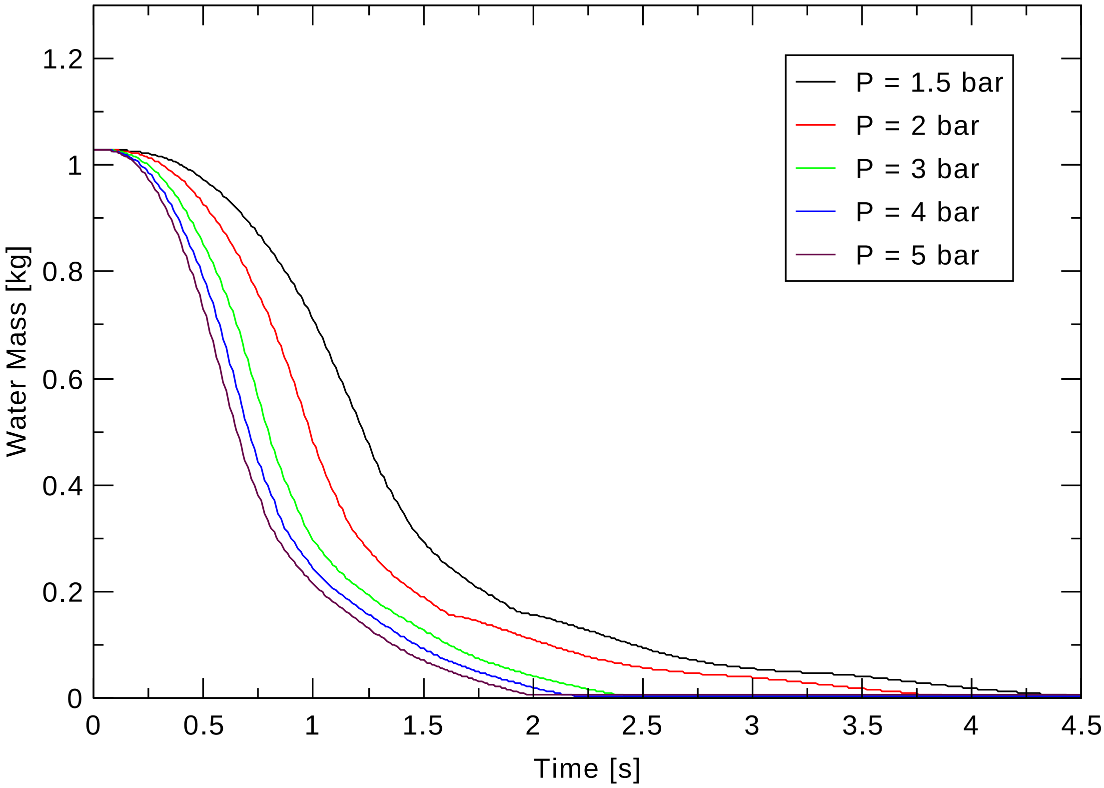


**Figure 3.18** *Time variation of water mass of the BSE with 2 mm of tape thickness fed from the bottom*

The liquid void fraction (see Figure 3.19) is evaluated in the more unfavorable volume of the BSE, which is the bend. It is possible to see that the water discharged is total.

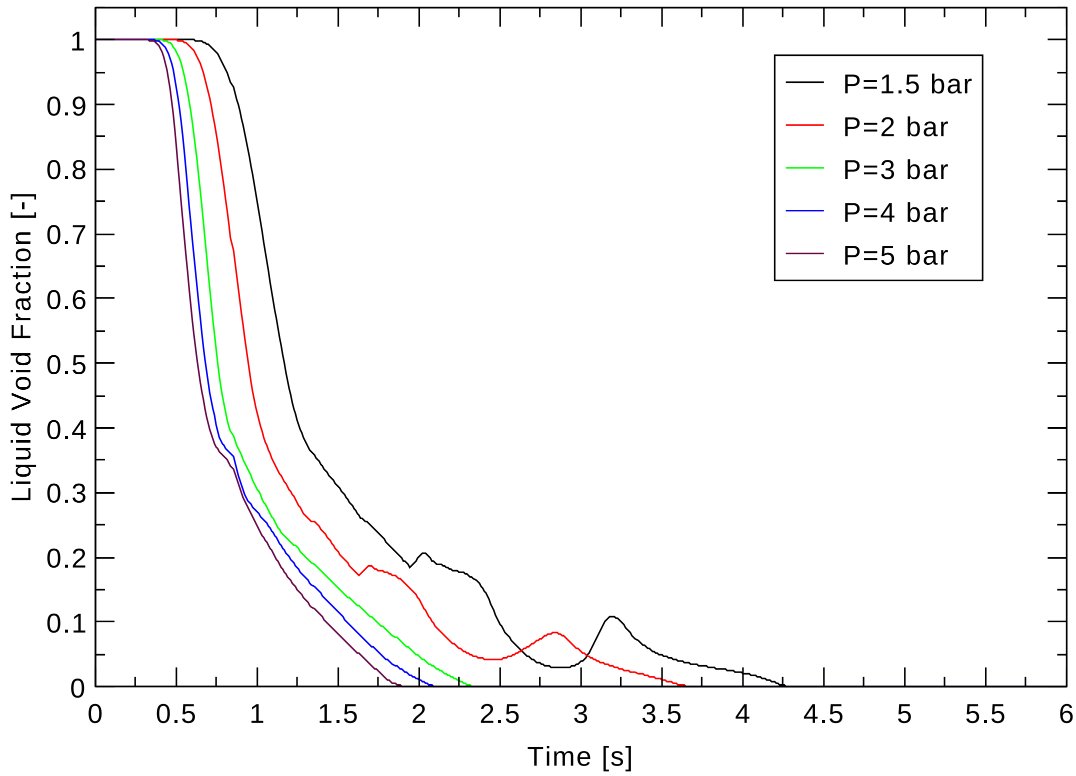


**Figure 3.19** *Time variation of the liquid void fraction of the BSE with 2 mm of tape thickness fed from the bottom*

The water mass flow rate needed to blow out water from the system is shown in Figure 3.20.

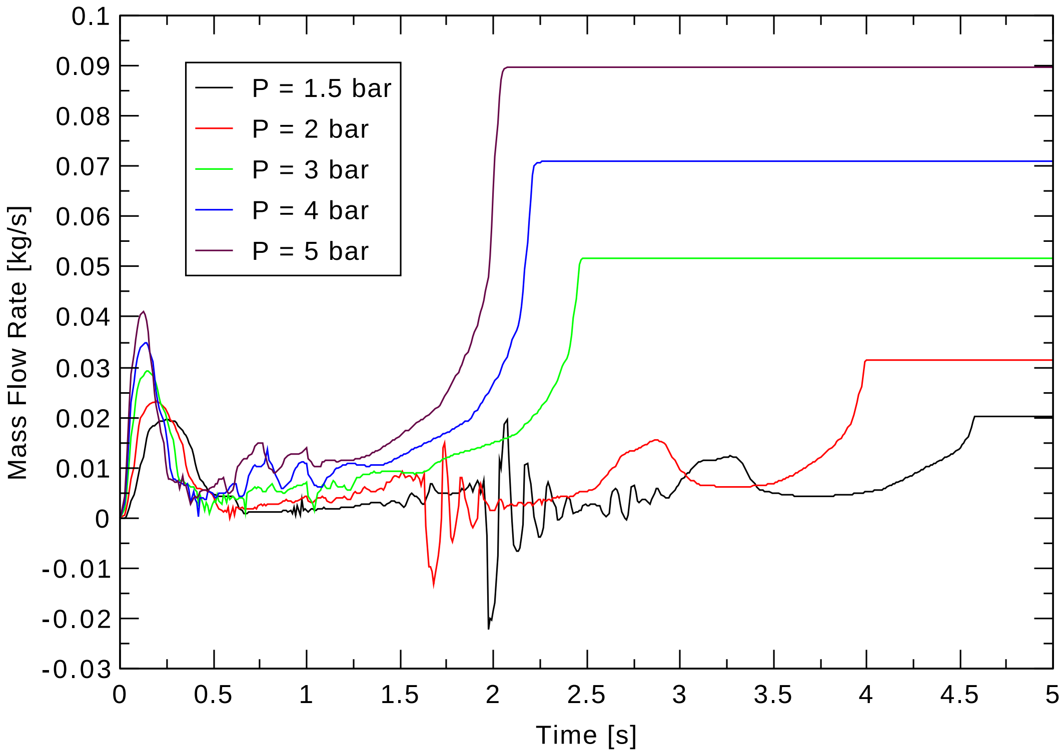


**Figure 3.20** *Time variation of inlet mass flow rate of the BSE with 2 mm of tape thickness fed from the bottom*

The outlet mass flow rate is shown in Figure 3.21.

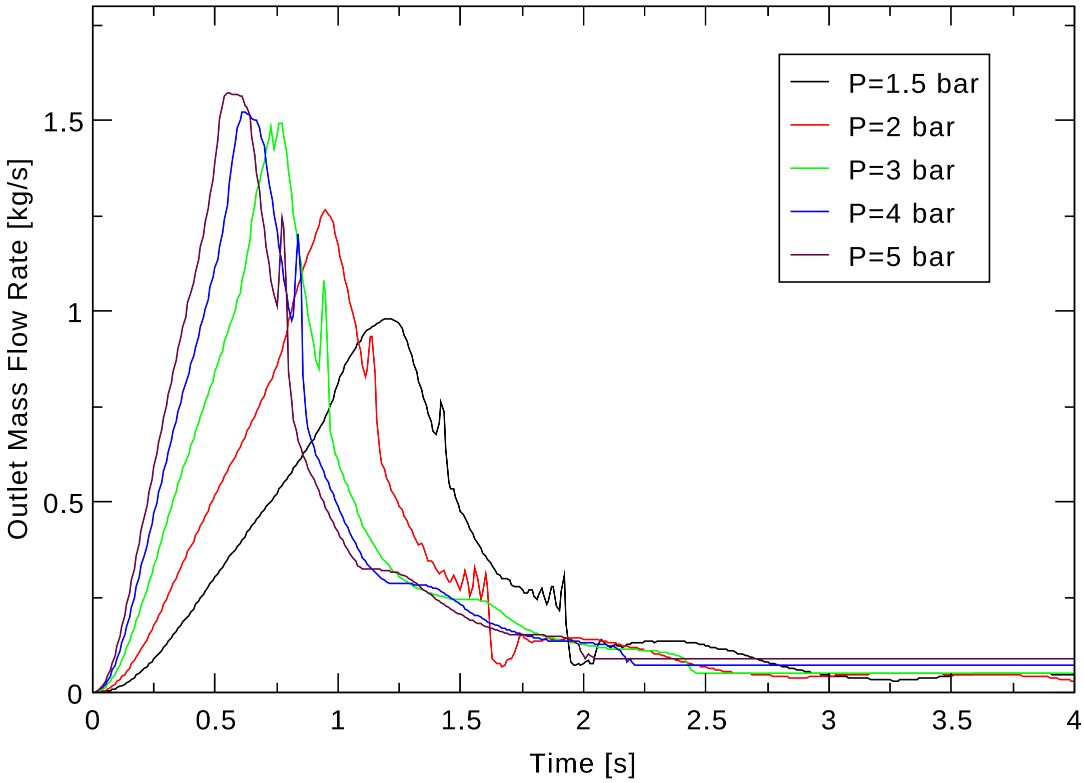


**Figure 3.21** *Time variation of outlet flow rate of the BSE with 2 mm of tape thickness fed from the bottom*

The summary of the results are reported in Table 3.18.

**Table 3.18** *Results for the BSE with 2 mm of tape thickness fed from the bottom*

| $P$ [bar] | $t$ [s] | $\dot{m}_{N_2}$ [kg/s] |
|---|---|---|
| 1.5 | 4.21 | 0.02020 |
| 2 | 3.70 | 0.03148 |
| 3 | 2.33 | 0.05169 |
| 4 | 2.09 | 0.07091 |
| 5 | 1.94 | 0.08974 |

### 3.5.3.2 BSE with 4 mm of twisted tape fed from the bottom

The volume of water in this BSE is V=0.000824 m$^3$ and the water mass is $M_{l0}$=0.822 kg. The time needed to blow out water from the circuit is shown in Figure 3.22. The draining process is successfully achieved because the residual water mass is less than 0.00822kg, which is the 1% of the total water mass.

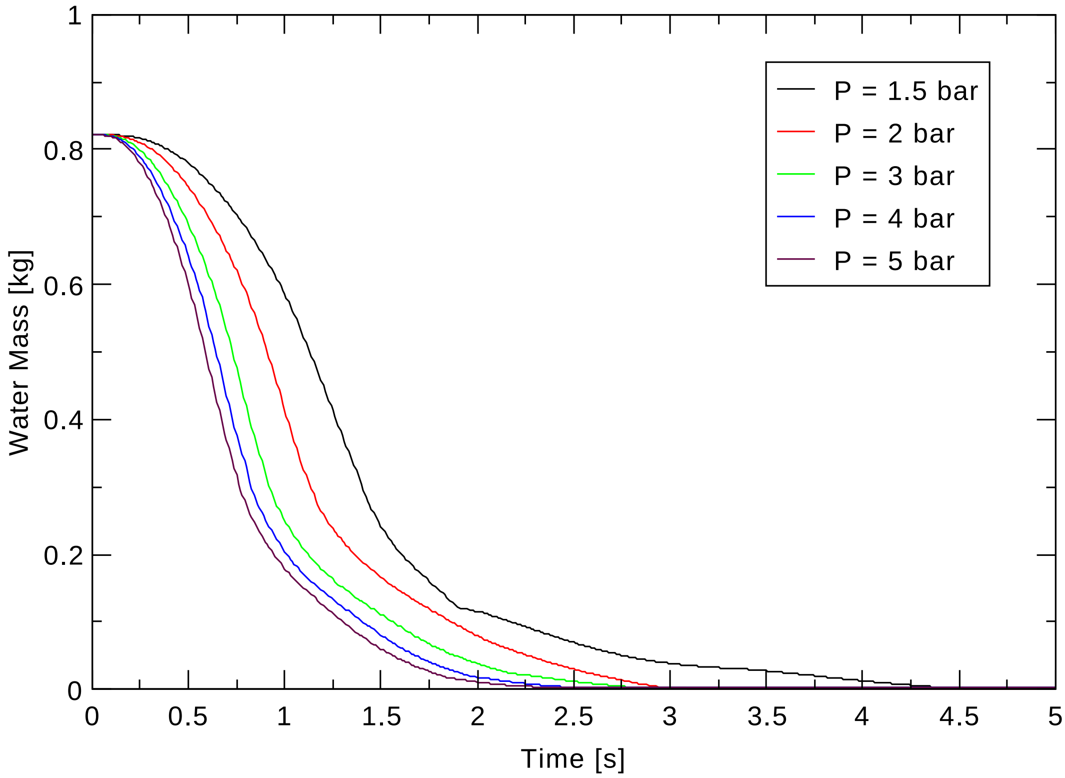


**Figure 3.22** *Time variation of water mass of the BSE with 4 mm of tape thickness fed from the bottom*

The liquid void fraction (see Figure 3.23) is evaluated in the more unfavorable volume of the BSE, which is the bend. It is possible to see that the water discharged is total. The water mass flow rate needed to blow out water from the system is shown in Figure 3.24.

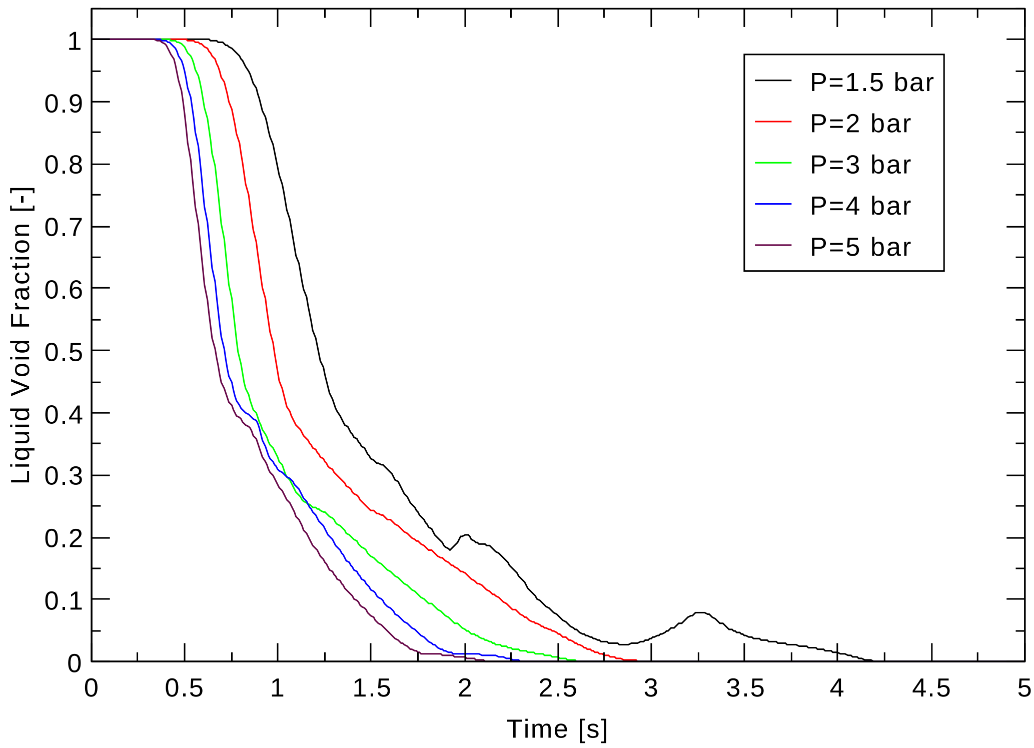


**Figure 3.23** *Time variation of the liquid void fraction of the BSE with 4 mm of tape thickness fed from the bottom*

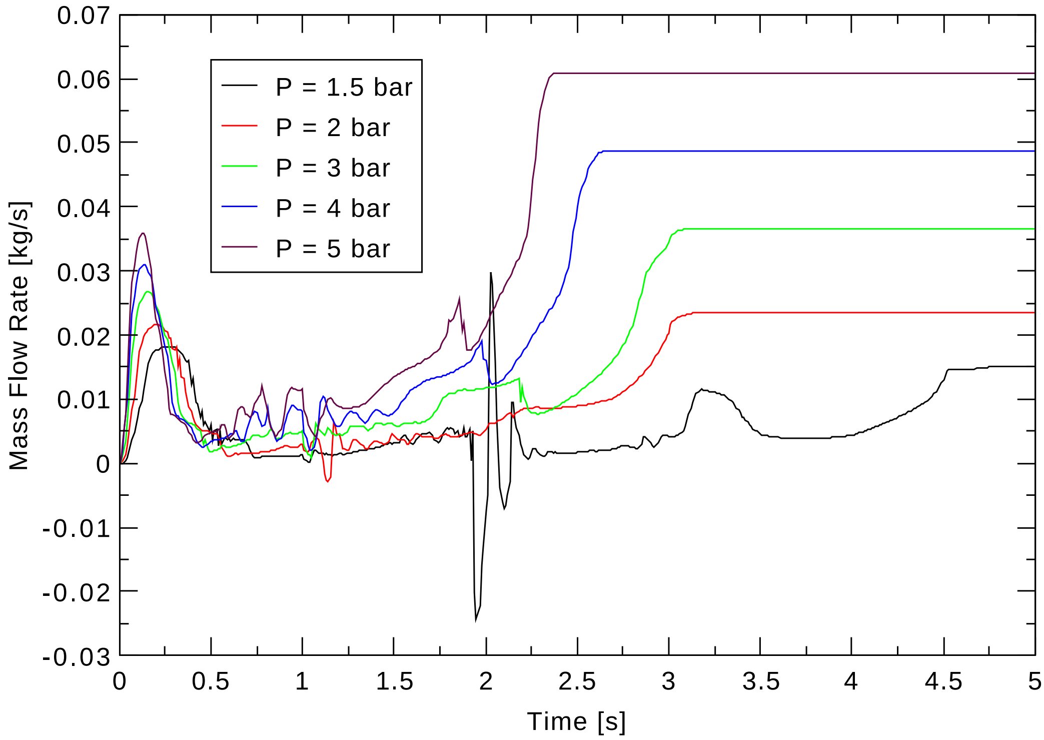


**Figure 3.24** *Time variation of inlet mass flow rate of the BSE with 4 mm of tape thickness fed from the bottom*

The outlet mass flow rate is shown in Figure 3.25.

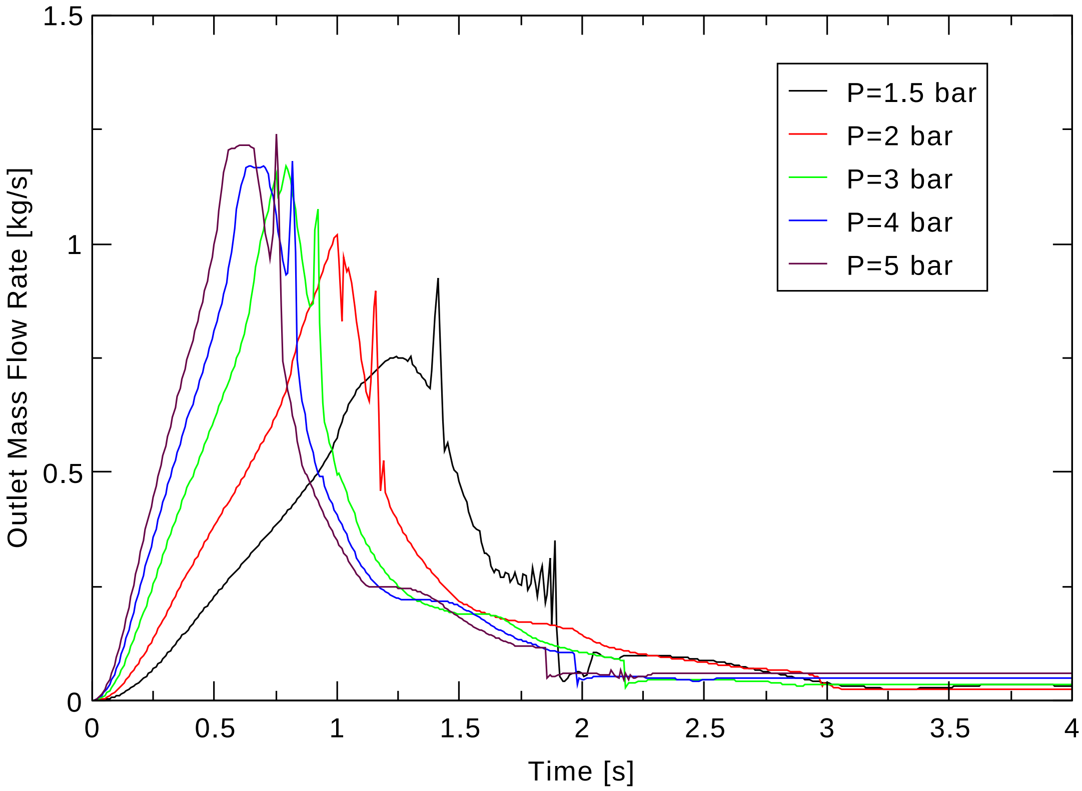


**Figure 3.25** *Time variation of outlet mass flow rate of the BSE with 4 mm of tape thickness fed from the bottom*

The summary of the results are reported in Table 3.19.

**Table 3.19** *Results for the BSE with 4 mm of tape thickness fed from the bottom*

| $P$ [bar] | $t$ [s] | $\dot{m}_{N_2}$ [kg/s] |
|---|---|---|
| 1.5 | 4.16 | 0.01508 |
| 2 | 2.87 | 0.02354 |
| 3 | 2.63 | 0.03648 |
| 4 | 3.61 | 0.04868 |
| 5 | 2.16 | 0.06088 |

## 3.6 Draining of the Panels

The simulations of the BSEs are necessary to build the model of the panels. Five panels constitute the ERID and as mentioned in the previous Chapters, there are two different types in terms of feed position (see Figure 3.26) and also types of beam stopping elements.

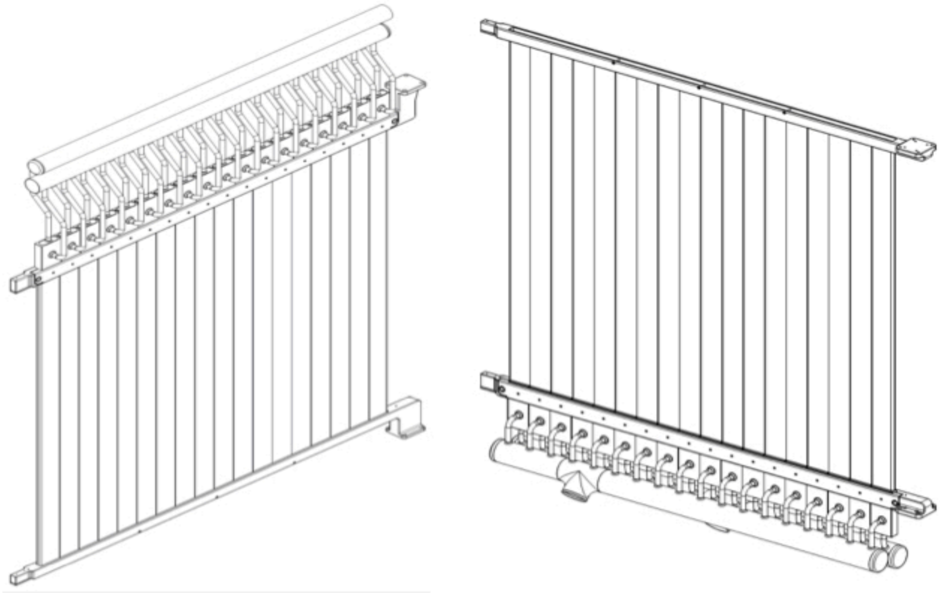

(a) (b)

**Figure 3.26** *Schematic view of the Panels: (a) Panel fed from the top; (b) Panel fed from the bottom*

Water for the cooling or nitrogen for the blow out are fed through two manifolds. Manifolds have a total length of 1.804 m and a diameter of 70.9 mm. Manifolds model is made of pipes with two volumes, and branches that connect two pipes and the beam stopping elements.
For the BSEs the previous models are used in the simulations, they are connected to the branches of the manifolds. Simulations are performed by using the same approach of the beam stopping elements, so by varying the nitrogen pressure and find the draining parameters. In this case, due to the greater amount of water a value of $\varepsilon$ = 98% is fixed.

### *3.6.1 Panel 1 & Panel 5*

According to Figure 1.3, Panel 1 and Panel 5 are located on the external part of the Residual Ion Dump and they are fed from the top. All beam stopping elements have the twisted tape thickness of 4 mm and a schematic view of the model built in RELAP is shown in Figure 3.27, where the volumes in the pipes are not indicated to have a more clear view of the scheme. The total water volume of the panel is V=0.0319646 $m^3$ and its mass is $M_{l0}$=31.87 kg.

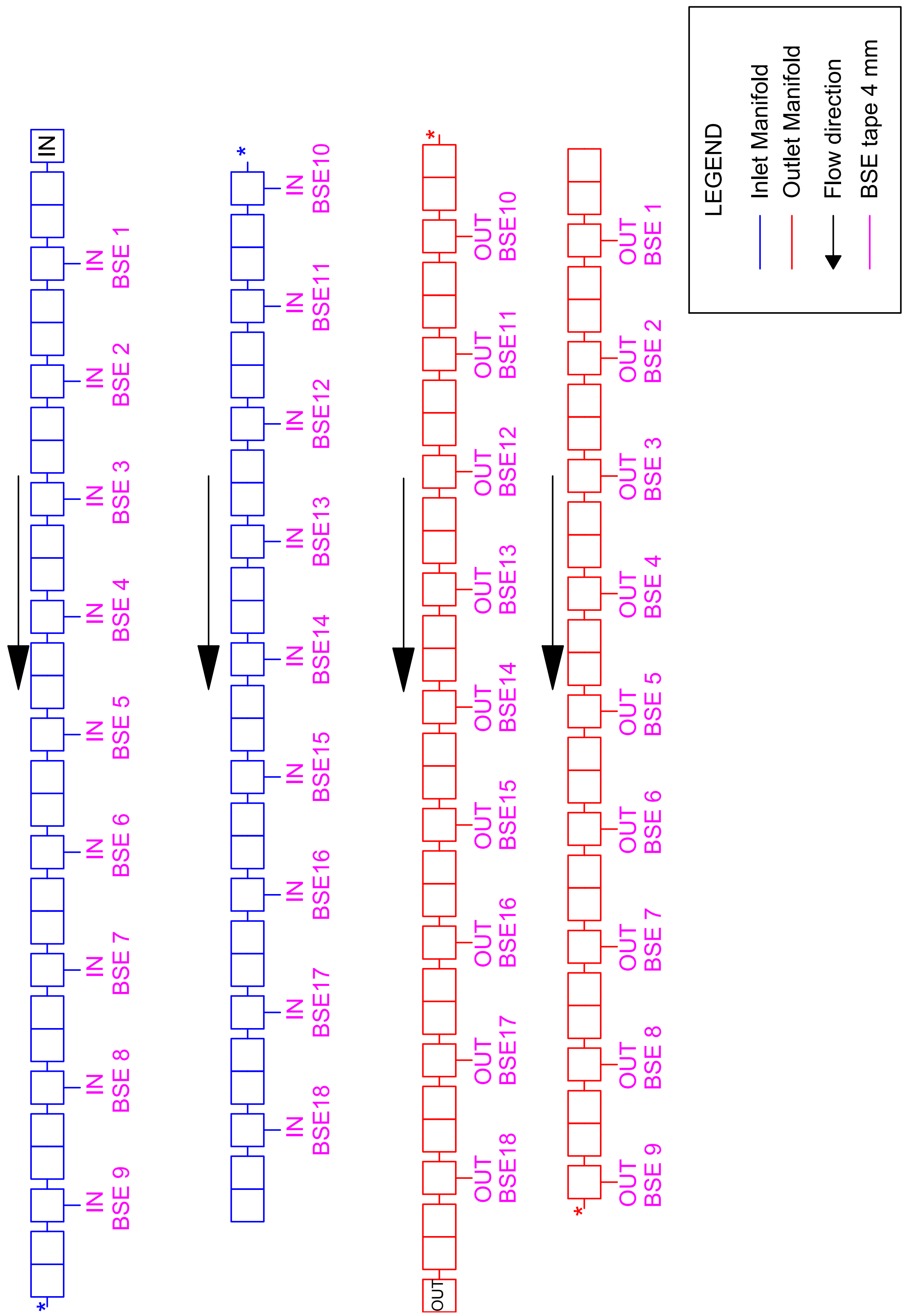


**Figure 3.27** *Panel 1 & Panel 5 model*

The time needed to blow out water from the circuit is shown in Figure 3.28. The draining process respects the requirement, because the residual water amount is less than 0.6374 kg, which represents the 2% of the total mass.

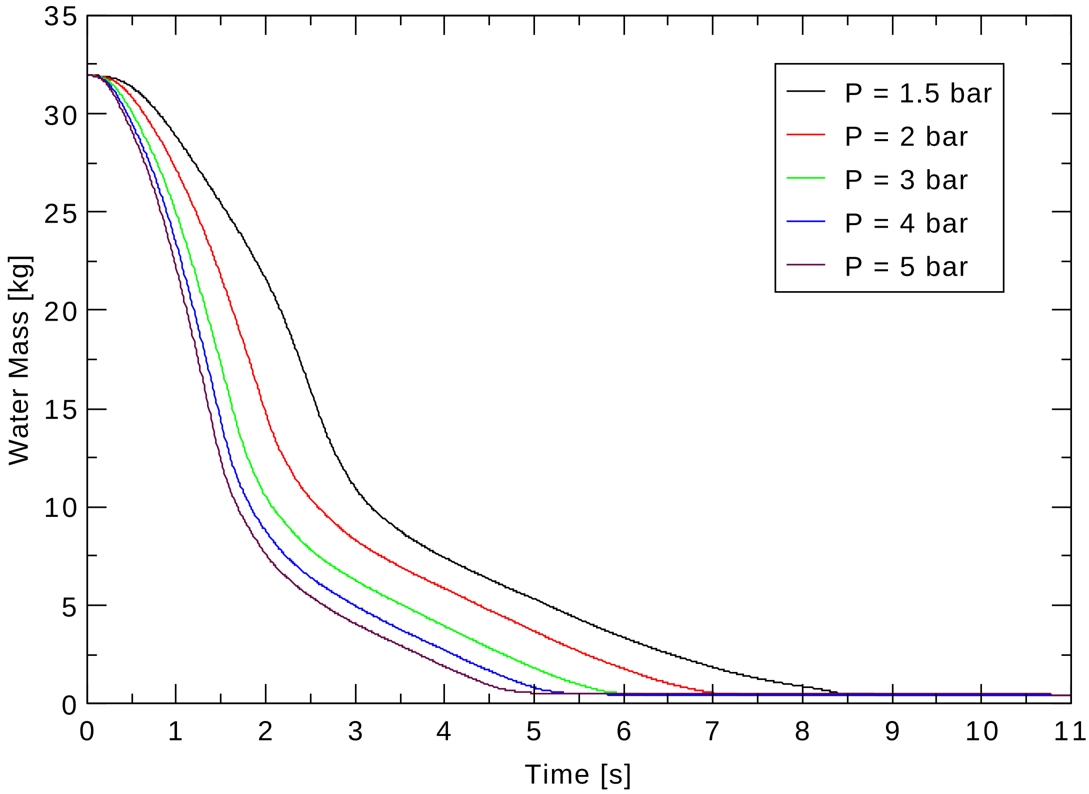


**Figure 3.28** *Time variation of water mass of Panel 1 & Panel 5*

The liquid void fraction is evaluated for the more unfavorable volume, which is the bend, of the farther BSE with respect to the inlet. The Figure 3.29 shows that the discharged water is almost total. The trend of the nitrogen flow rate needed to blow out water from the circuit is shown in Figure 3.30.

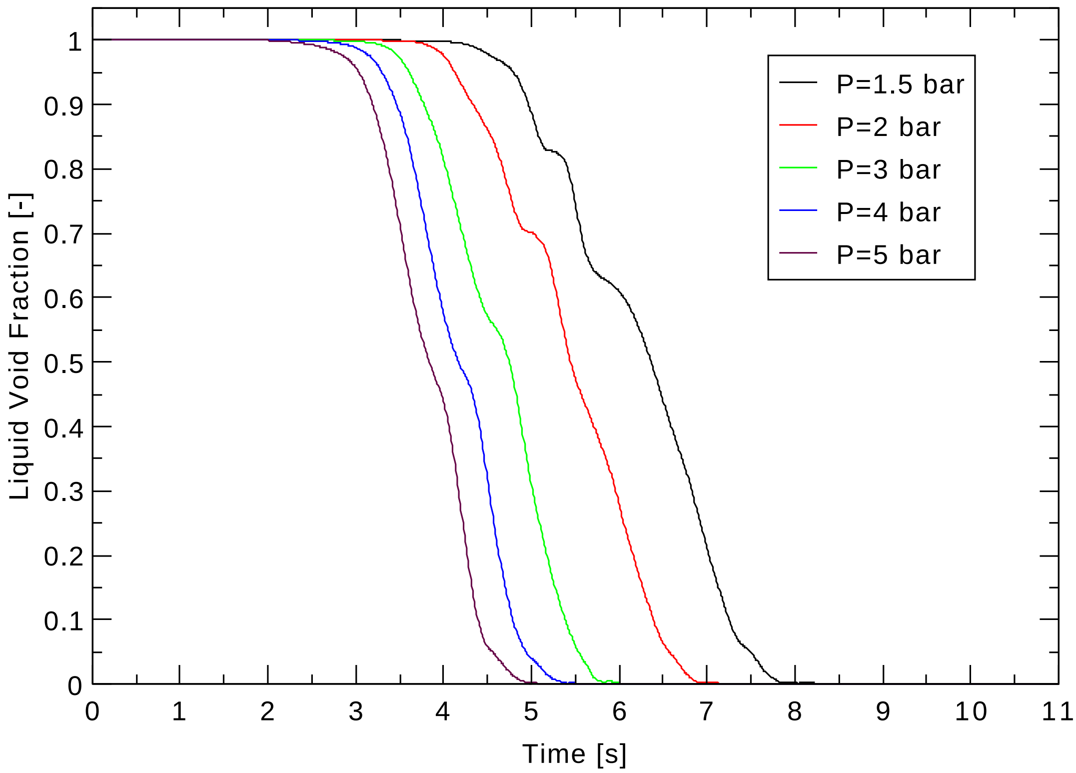


**Figure 3.29** *Time variation of the liquid void fraction of Panel 1 & Panel 5*

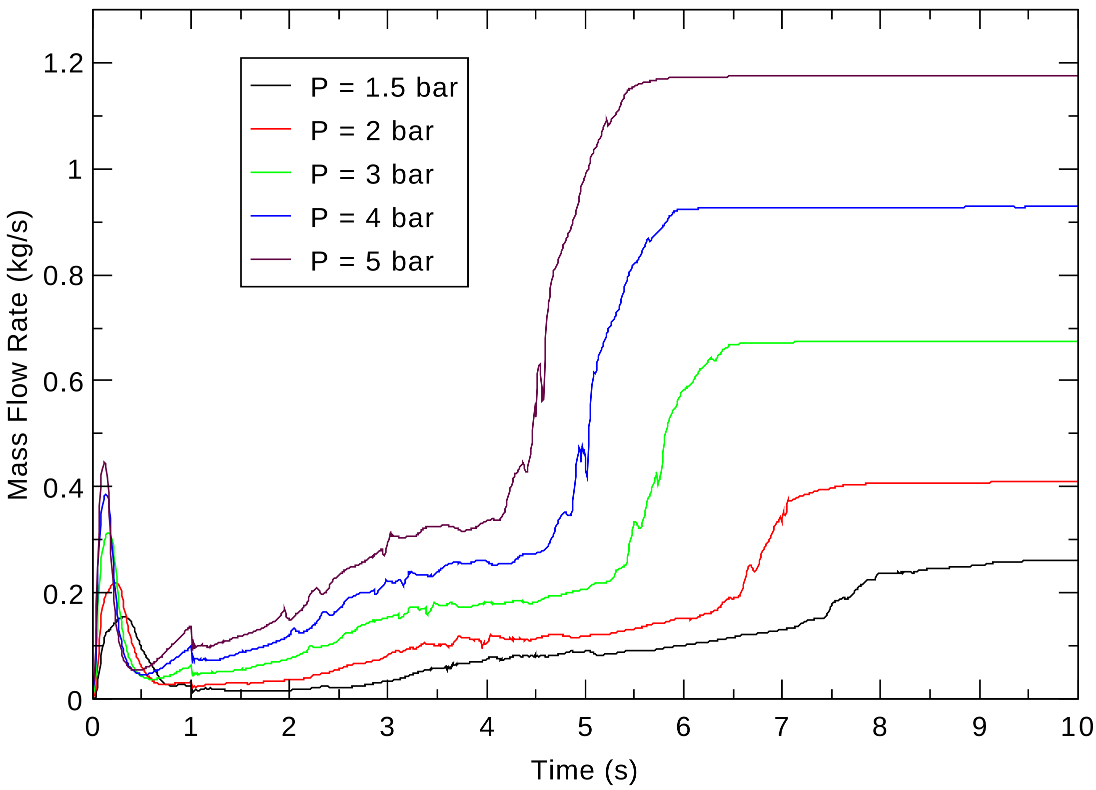


**Figure 3.30** *Time variation of inlet mass flow rate of Panel 1 & Panel 5*

The outlet mass flow rate is shown in Figure 3.31.

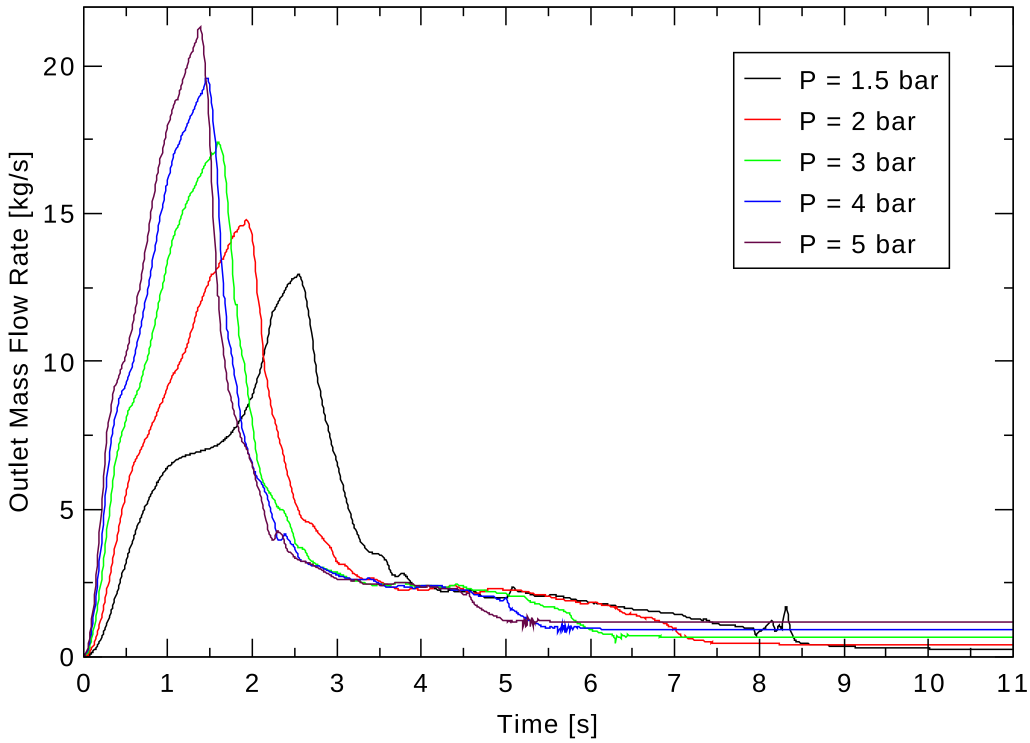


**Figure 3.31** *Time variation of outlet mass flow rate of Panel 1 & Panel 5*

In Table 3.20 a summary of the results is given.

**Table 3.20** *Results for Panel 1 & Panel 5*

| $P$ [bar] | $t$ [s] | $\dot{m}_{N_2}$ [kg/s] |
|---|---|---|
| 1.5 | 8.71 | 0.2615 |
| 2 | 7.24 | 0.4095 |
| 3 | 6.27 | 0.6749 |
| 4 | 5.50 | 0.9278 |
| 5 | 5.08 | 1.175 |

### *3.6.2 Panel 3*

Panel 3 is located on the center of the Residual Ion Dump and it is fed from the top but it is made of different beam stopping elements. In fact, starting from the feed, there are six BSEs with 4 mm of twisted tape thickness, nine BSEs with 2 mm of twisted tape thickness and finally three BSEs with 4 mm of twisted tape thickness (see Figure 3.32). The total water volume of the panel is V=0.0338896 m$^3$ and the water mass is $M_{l0}$=33.79 kg.

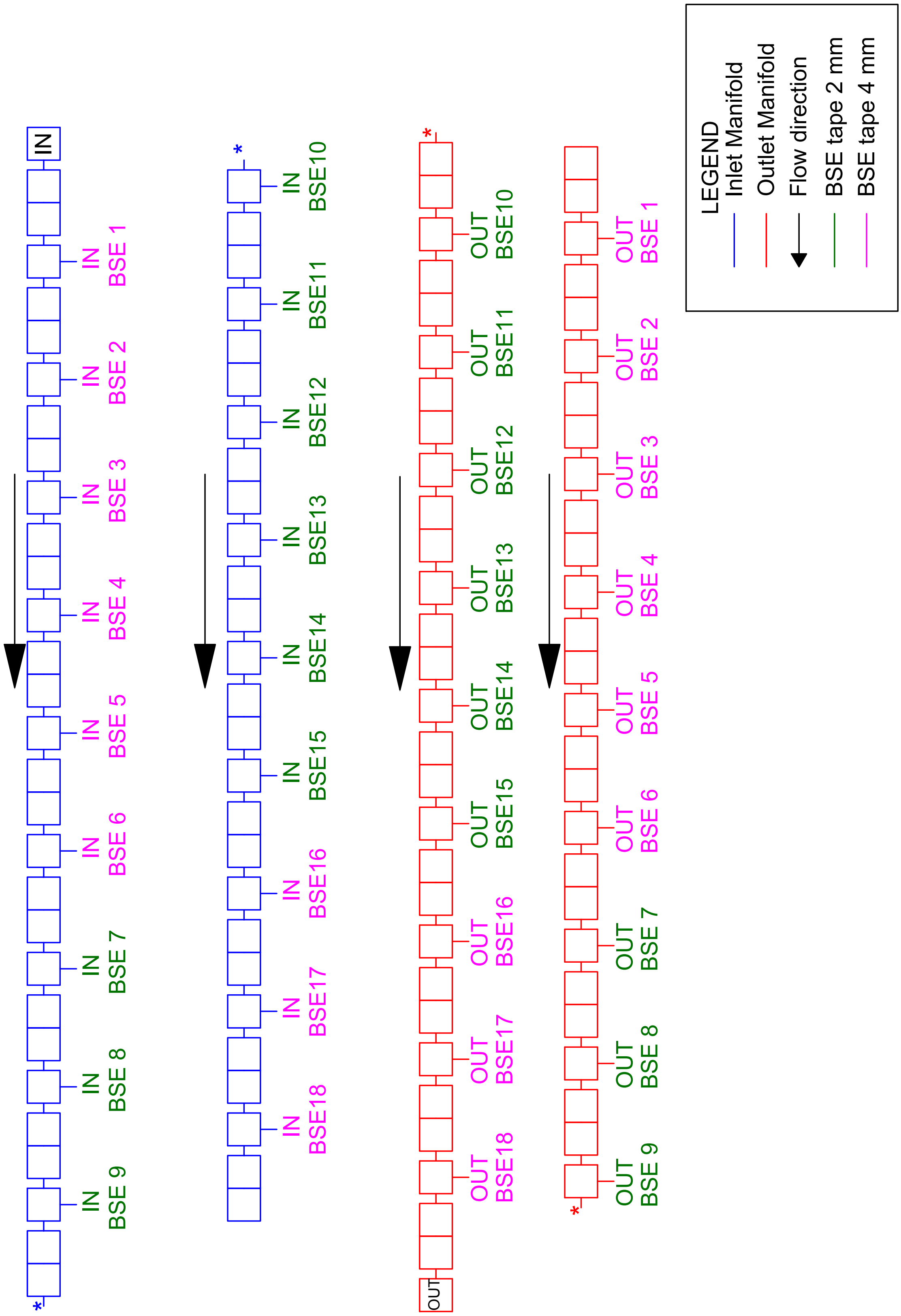


**Figure 3.32** *Panel 3 model*

The time needed to blow out water from the circuit is shown in Figure 3.33. The draining process respects the requirement, because the residual water amount is less than 0.6758 kg, which represents the 2% of the total mass.

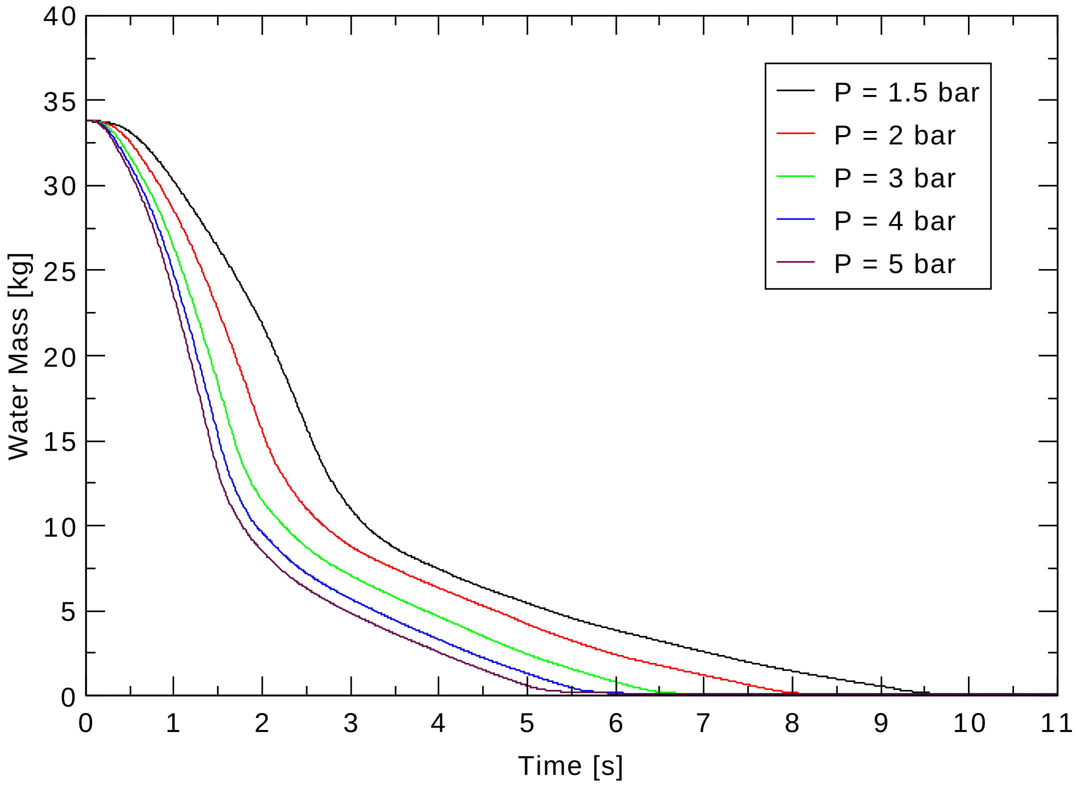


**Figure 3.33** *Time variation of water mass of Panel 3*

The liquid void fraction is evaluated for the more unfavorable volume, which is the bend, of the farther BSE with respect to the inlet. The Figure 3.34 shows that the discharged water is almost total. The trend of the nitrogen flow rate needed to blow out water from the circuit is shown in Figure 3.35.

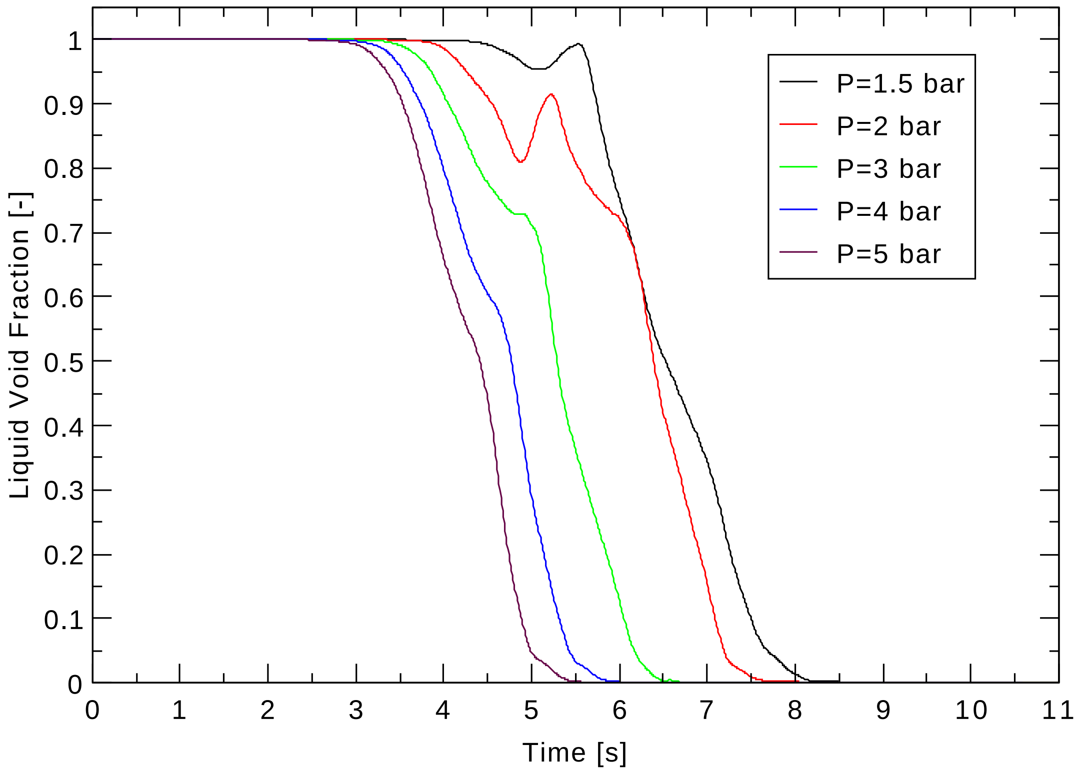


**Figure 3.34** *Time variation of the liquid void fraction of Panel 3*

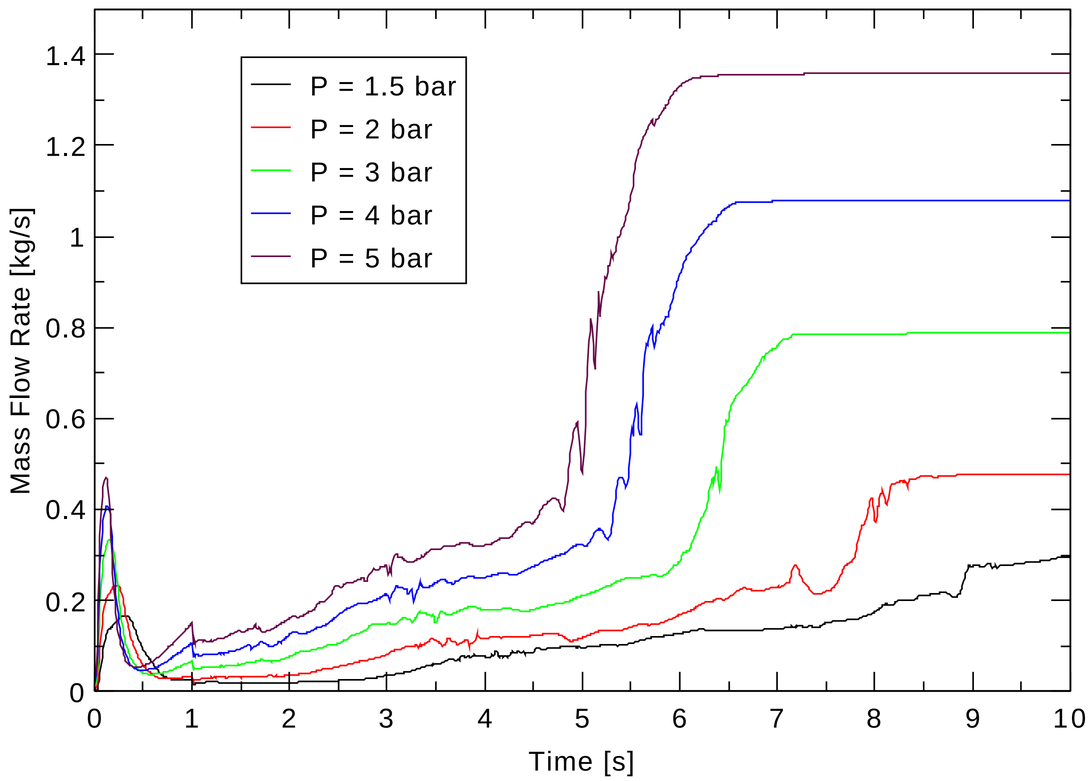


**Figure 3.35** *Time variation of inlet mass flow rate of Panel 3*

The outlet mass flow rate is shown in Figure 3.36.

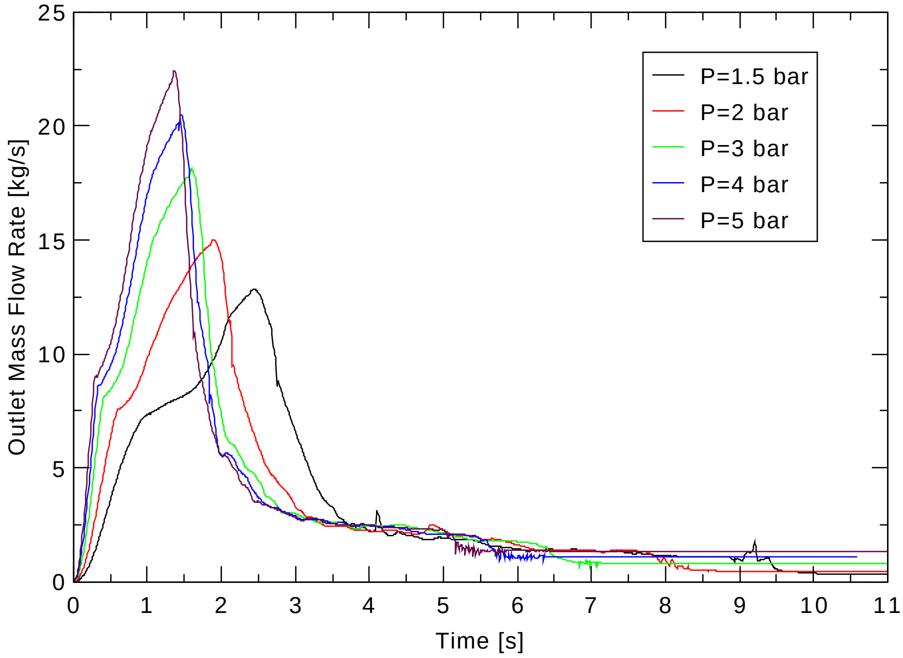


**Figure 3.36** *Time variation of outlet mass flow rate of Panel 3*

Table 3.21 reports a summary of the results.

**Table 3.21** *Results for Panel 3*

| $P$ [bar] | $t$ [s] | $\dot{m}_{N_2}$ [kg/s] |
|---|---|---|
| 1.5 | 9.5 | 0.3053 |
| 2 | 8.07 | 0.4777 |
| 3 | 6.71 | 0.7877 |
| 4 | 6.10 | 1.079 |
| 5 | 5.83 | 1.359 |

### *3.6.3 Panel 2 & Panel 4*

These two panels are located between Panel 3 and the two external panels. The main difference between these two panels and the others is the feed position, because in this case panel is fed from the bottom and the inlet of the feed is not located in the inlet of the manifolds but in a more central position as shown in Figure 3.37. The total water volume is V=0.031084m$^3$ and the water mass is $M_{l0}$=30.99 kg.

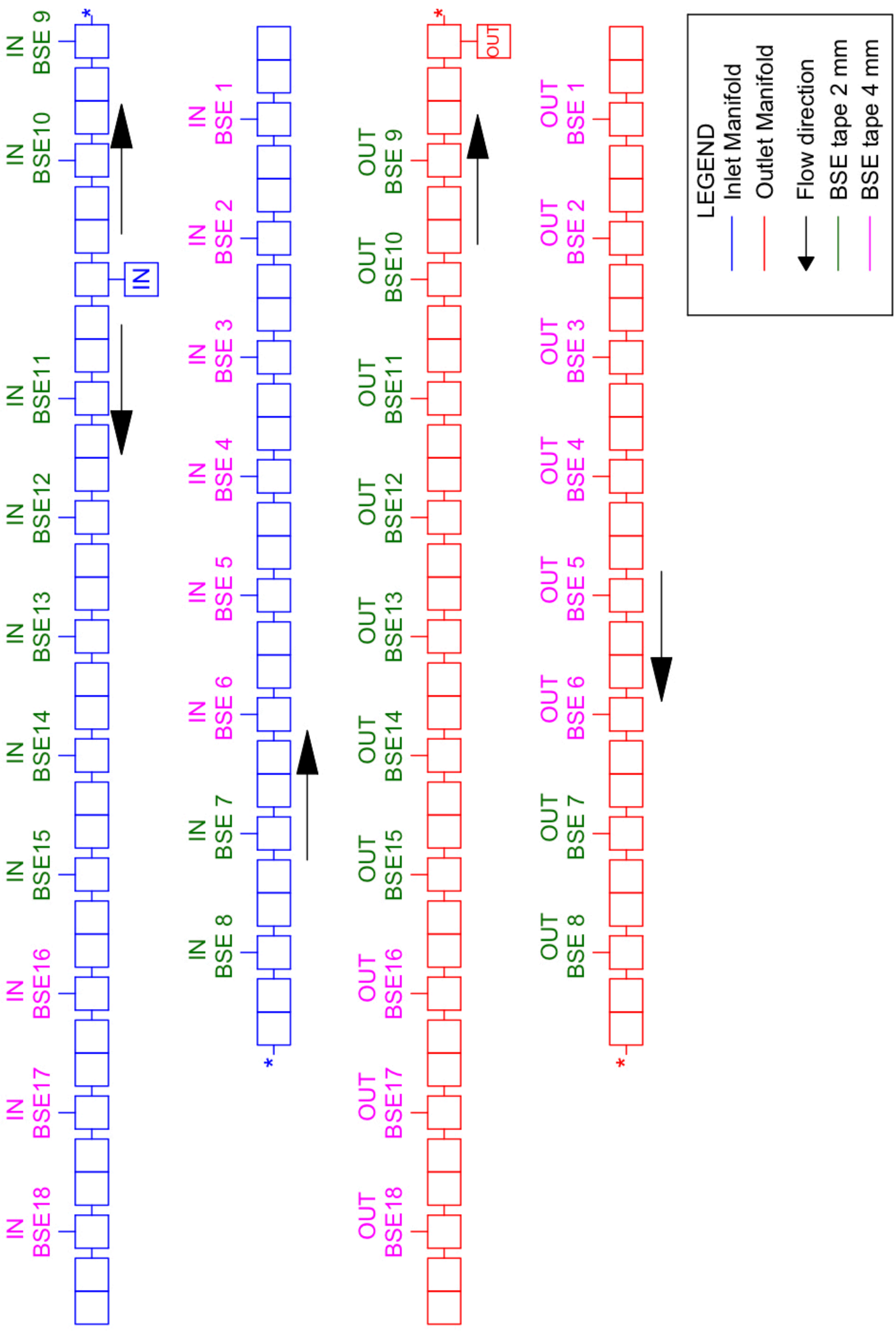


**Figure 3.37** *Panel 2 & Panel 4 model*

The time needed to blow out water from the circuit is shown in Figure 3.38. The draining process respects the requirement, because the residual water amount is less than 0.6198 kg, which represents the 2% of the total mass.

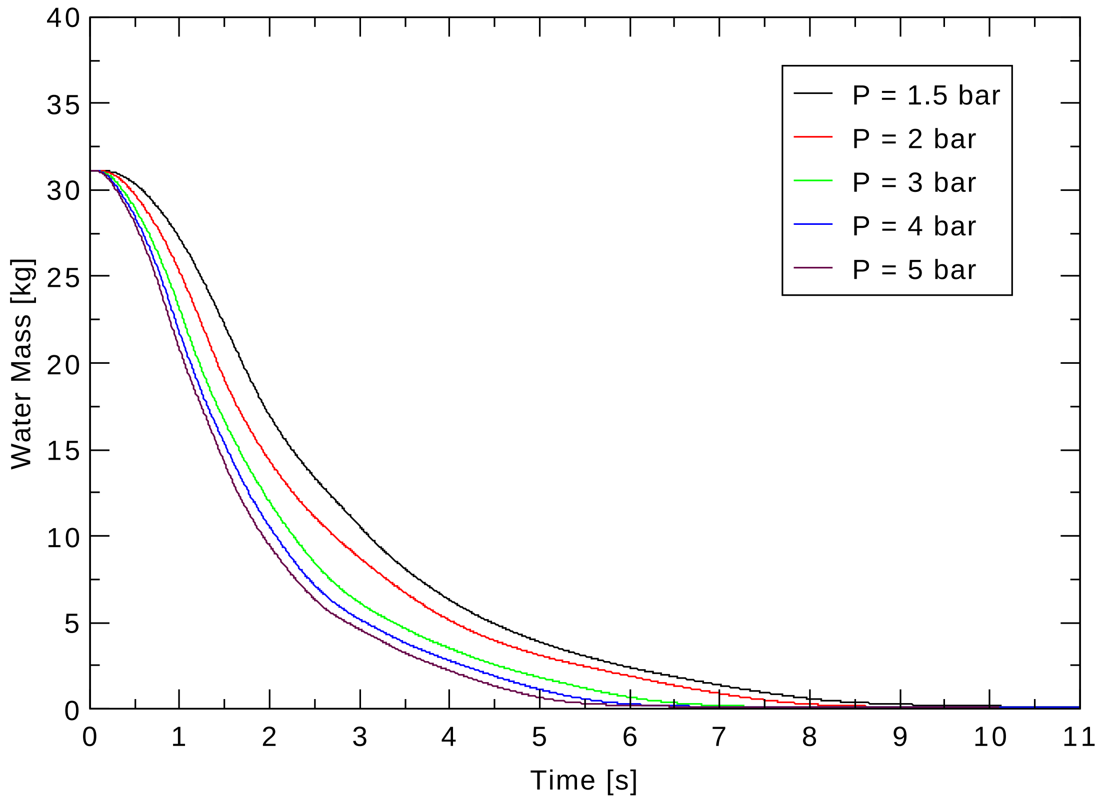


**Figure 3.38** *Time variation of water mass of Panel 2 & Panel 4*

The liquid void fraction is evaluated for the more unfavorable volume, which is the bend, of the farther BSE with respect to the inlet. The Figure 3.39 shows that the discharged water is almost total. The trend of the nitrogen flow rate is shown in Figure 3.40.

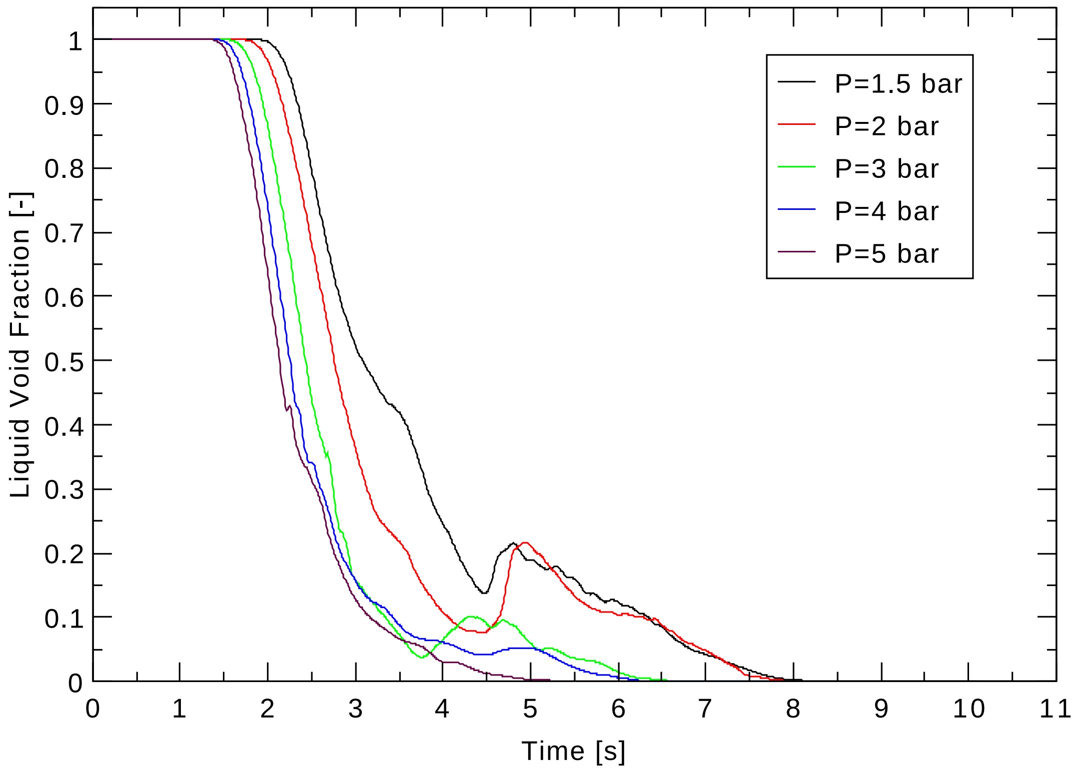


**Figure 3.39** *Time variation of the liquid void fraction of Panel 2 & Panel 4*

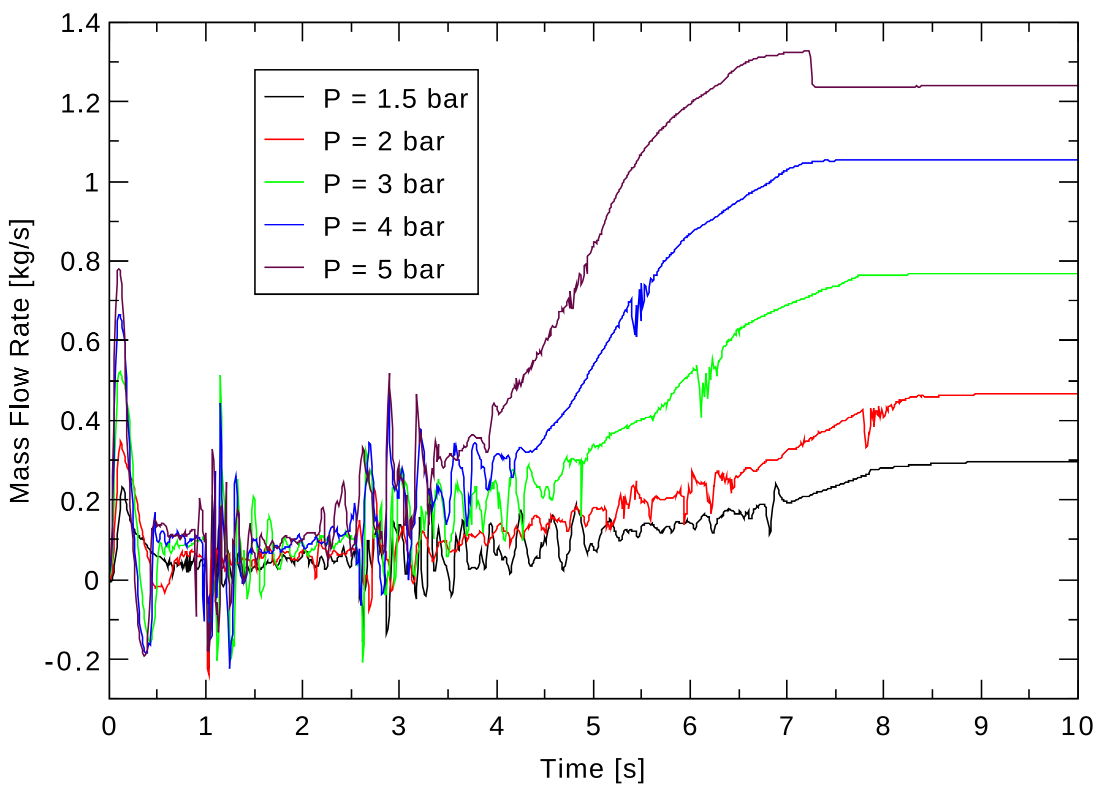


**Figure 3.40** *Time variation of inlet mass flow rate of Panel 2 & Panel 4*

The outlet mass flow rate is shown in Figure 3.41.

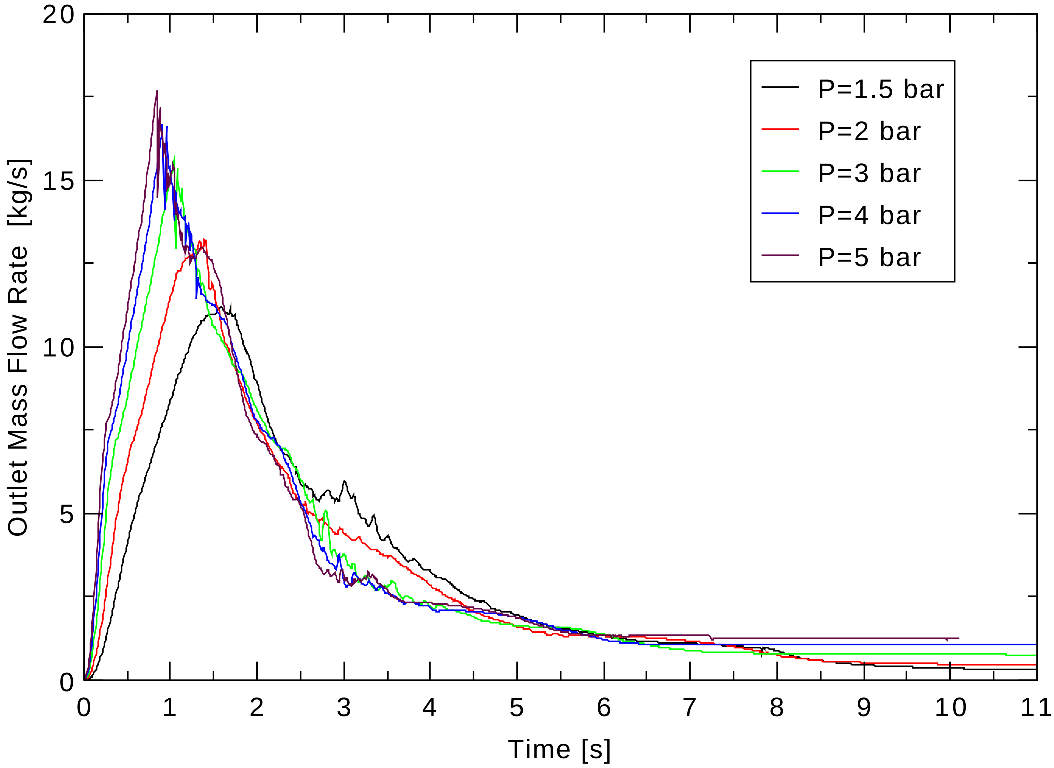


**Figure 3.41** *Time variation of outlet mass flow rate of Panel 2 & Panel 4*

The results are summarized in Table 3.22.

**Table 3.22** *Results for Panel 2 & Panel 4*

| $P$ [bar] | $t$ [s] | $\dot{m}_{N_2}$ [kg/s] |
|---|---|---|
| 1.5 | 10.3 | 0.2981 |
| 2 | 8.9 | 0.4671 |
| 3 | 7.6 | 0.7681 |
| 4 | 7.1 | 1.055 |
| 5 | 6.8 | 1.239 |

## 3.7 Headers

Headers (see Figure 3.42) connect all inputs and outputs of the Panels, and represent the last elements to perform the ERID simulation.
Inlet header is equal to the outlet header, so the RELAP model is exactly the same and it is represented in Figure 3.42.

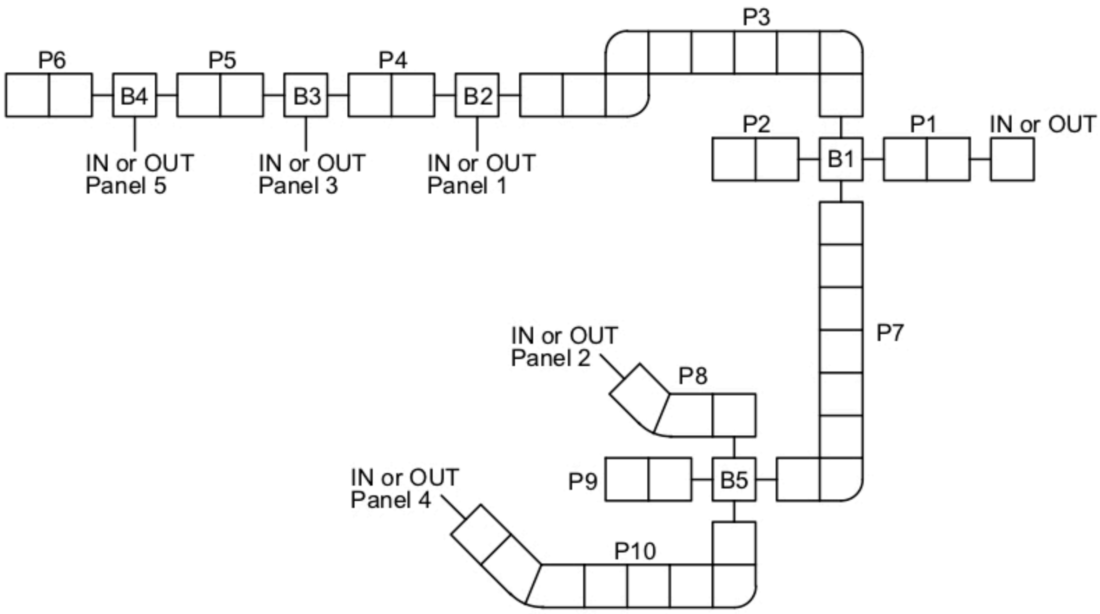


**Figure 3.42** *Header model*

It consists of 10 pipes with different number of volumes and 5 branches; the details are reported in Table 3.23.

**Table 3.23** *Data for the headers*

| Element | Volume number [-] | L [mm] | D [mm] | Incl. angle [°] |
|---|---|---|---|---|
| PIPE 1 | 1 | 66.68 | 193.7 | 0.0 |
| | 2 | 66.68 | 193.7 | 0.0 |
| BRANCH 1 | 1 | 70.65 | 193.7 | 0.0 |
| PIPE 2 | 1 | 25.18 | 193.7 | 0.0 |
| | 2 | 25.18 | 193.7 | 0.0 |
| PIPE 3 | 1 | 56.7 | 141.3 | 90.0 |
| | 2 | 56.7 | 141.3 | 90.0 |
| | 3 | 56.7 | 141.3 | 0.0 |
| | 4 | 60.0 | 141.3 | 0.0 |
| | 5 | 60.0 | 141.3 | 0.0 |
| | 6 | 245 | 141.3 | 0.0 |
| | 7 | 245 | 141.3 | 0.0 |
| | 8 | 69.0 | 141.3 | -90.0 |
| | 9 | 20.0 | 141.3 | 0.0 |
| | 10 | 117 | 141.3 | 0.0 |
| BRANCH 2 | 1 | 35.45 | 141.3 | 0.0 |
| PIPE 4 | 1 | 47.38 | 141.3 | 0.0 |
| | 2 | 47.38 | 141.3 | 0.0 |
| BRANCH 3 | 1 | 35.45 | 141.3 | 0.0 |
| PIPE 5 | 1 | 39.88 | 141.3 | 0.0 |
| | 2 | 39.88 | 141.3 | 0.0 |
| BRANCH 4 | 1 | 35.45 | 141.3 | 0.0 |
| PIPE 6 | 1 | 42.69 | 141.3 | 0.0 |
| | 2 | 42.69 | 141.3 | 0.0 |

| Element | Volume number [-] | L [mm] | D [mm] | Incl. angle [°] |
|---|---|---|---|---|
| PIPE 7 | 1 | 384 | 114.3 | -90.0 |
| | 2 | 384 | 114.3 | -90.0 |
| | 3 | 384 | 114.3 | -90.0 |
| | 4 | 384 | 114.3 | -90.0 |
| | 5 | 384 | 114.3 | -90.0 |
| | 6 | 384 | 114.3 | -90.0 |
| | 7 | 83.0 | 114.3 | -90.0 |
| | 8 | 100.8 | 114.3 | 0.0 |
| BRANCH 5 | 4 | 10.26 | 114.3 | 0.0 |
| PIPE 8 | 1 | 63.69 | 76.1 | 0.0 |
| | 2 | 63.69 | 76.1 | 0.0 |
| | 3 | 69.07 | 76.1 | 45.0 |
| PIPE 9 | 1 | 14.0 | 114.3 | 0.0 |
| | 2 | 14.0 | 114.3 | 0.0 |
| PIPE 10 | 1 | 63.69 | 76.1 | -90.0 |
| | 2 | 63.69 | 76.1 | -90.0 |
| | 3 | 104.5 | 76.1 | 0.0 |
| | 4 | 104.5 | 76.1 | 0.0 |
| | 5 | 104.5 | 76.1 | 0.0 |
| | 6 | 104.5 | 76.1 | 0.0 |
| | 7 | 69.07 | 76.1 | -45.0 |
| | 8 | 53.35 | 76.1 | -45.0 |

The total volume of an header is V=0.05589 m$^3$ and the water mass is $M_{l0}$=55.72 kg. These two elements are necessary to complete the simulation of the ERID. Due to the higher number of elements, RELAP was not able to process all elements and the simulation does not run. For this reason a simplification of the overall system has been studied to perform the simulation. This simplification is dealt with in next Chapter.

## 3.8 Analysis Results

Starting from the beam stopping elements simulations, the results show that increasing pressure, the time needed for the draining process decreases. The nitrogen flow rate needed increases when the nitrogen pressure increases. The beam stopping elements fed from the bottom take more time to draining water at low pressure, but when the nitrogen pressure increases the time is almost the same of the other BSEs. All BSEs respect the requirement of the draining efficiency parameter. The simulations of the panels show that Panel 1 and Panel 5 have the faster draining process if compared with the other two types of Panel, because of the more favorable position of the feed for the inlet and the outlet and the lower hydraulic resistance. The time needed for draining Panel 2 and Panel 4 is higher than that of Panel 3, even if the total amount of water is lower, because of the unfavorable feed position. Observing the trends of the curves some similar considerations can be done in order to understand some phenomena that take place during the draining process. The plot of the time needed to blow out water from the circuit shows some changes in the slope of the curves that is due to the flow regime transition [25]. Because of a complicated geometry of the cooling system the boundary between water and gas diffuses, as nitrogen moves inward the cooling circuit, and the two-phase two-component flow passes all stages of flow regimes starting with the bubble regime and ending with the dispersed one, as the gas content in the cooling channel volume is increased. So, at the beginning of the draining procedure, the water-nitrogen mixture is a two-phase bubble structure. Then, when the slope changes, a slug flow is developed and water discharge is defined mostly by droplets dragged away from the water film wetting the inner surface of the channels. The final draining phase of the cooling system is solely by water droplets in the dispersed regime of the two-phase flow (see Figure 3.43). In some graphs, the inlet mass flow rate shows an interval of negative values as some of the water flow downward in the opposite direction than the high pressure gas. This is due to the Rayleigh-Taylor instability, which is an instability of an interface between two fluids of different densities, which occurs when the light fluid is pushing the heavy fluid. There is a complex phenomenology associated with the evolution of a Taylor unstable interface. This includes the formation of spikes, curtains and bubbles. Also, as the system is initially full, any force on its inlet and outlet boundaries results in limited counter-current flow. Slug flow is developed due to Kelvin-Helmholtz instabilities in which immiscible, incompressible, and inviscid fluids are in relative and irrotational motion. The velocity and density profiles are uniform in each fluid layer, but they are discontinuous at the interface between the two fluids. This discontinuity in the velocity induces vorticity at the interface and temporary and locally increases the resistance and reduces the mass flow rate. Its signature in a form of the mass flow fluctuations can also be detected at the inlet. As seen from the figures of the outlet flow rates, the draining process of the cooling system might be conventionally divided into two stages [26]. At the initial stage, water is blown out of the cooling channels followed by a sharp increase of two-phase flow rate at the system outlet. At the second stage of the draining procedure, the two-phase flow becomes quasi-steady-state, the gas mass flow increases further and matches the outlet flow rate, so the flow rates are almost equal at the inlet and outlet of the panel cooling system (see Figure 3.44).

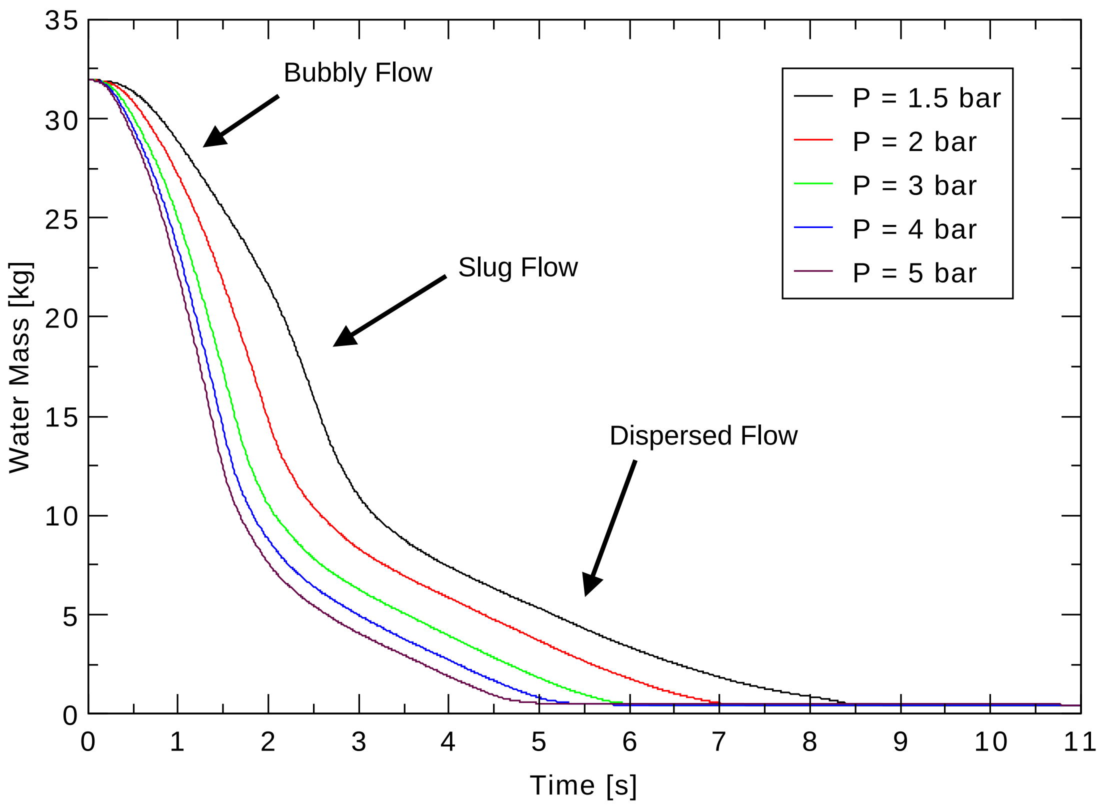


**Figure 3.43** *Flow regimes in the time variation of water mass of Panel 1*

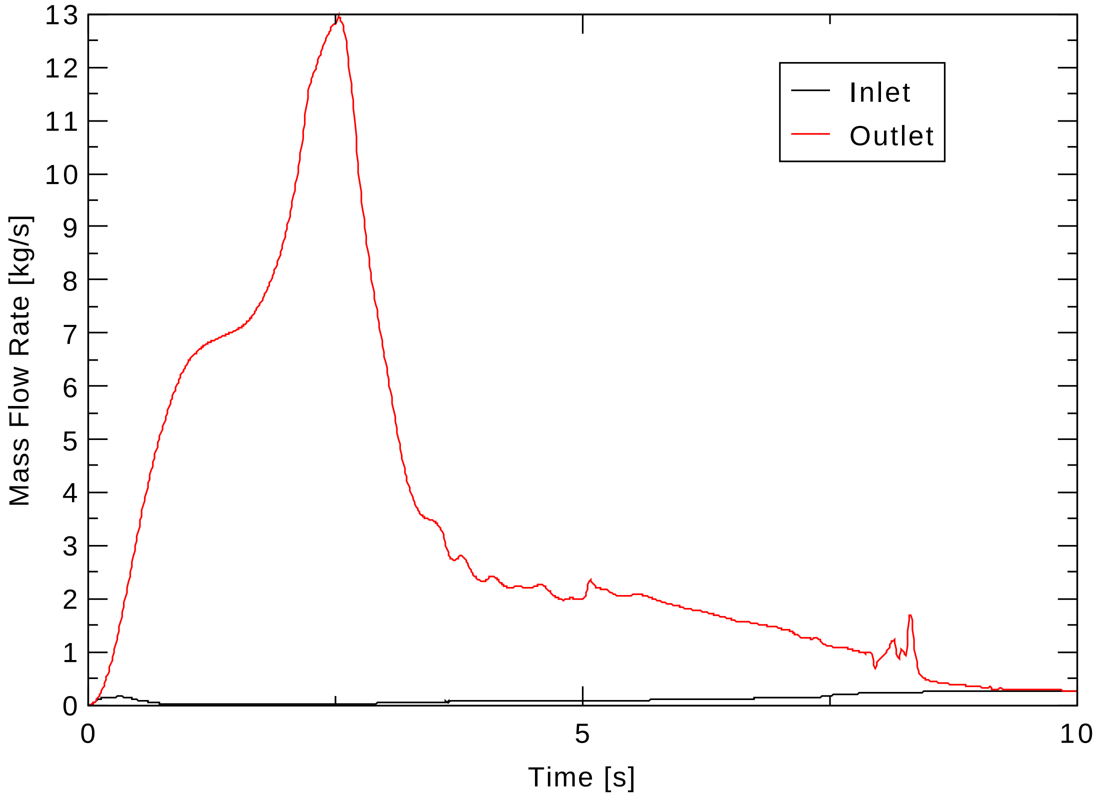


**Figure 3.44** *Time variation of intlet and outlet mass flow rate of Panel 1*

# Chapter 4
# One-dimensional ERID model

In the first part of this Chapter a simplification of the panels are described in order to find a good approximation with respect to the results obtained in the previous chapter. Then the simplifications are used to build the overall model of the Residual Ion Dump and find the characteristic parameters of the draining process.

## 4.1 Simplification of the panels

In order to find a simplification of the system that respects the same simulation results found in the previous chapter, some different configurations have been studied until the results of the simplified system are almost equal to the non-simplified system. From the hydraulic simulations the pressure drop of the BSEs , when water is flowing in the system (difference between outlet and inlet pressure), are found and the results are reported in Table 4.1.

**Table 4.1** *BSEs pressure drops*

| Feed position [-] | Tape thickness [m] | $\Delta p$ [Pa] |
|---|---|---|
| Top | 0.002 | 319041 |
| | 0.004 | 318799 |
| Bottom | 0.002 | 336026 |
| | 0.004 | 333865 |

The approach is to group in a single u-tube the BSEs with the same characteristics in terms of hydraulic diameter (considering the twisted tape thickness), calculate their geometry parameters and then calculate the loss coefficient thanks to the BSEs pressure drops and the water mass flow rate. The loss coefficient is inserted in each junction of the u-tube. Also the inlet pipe and the outlet pipe of each BSE are considered inside the simplification of the u-tube. For all panels the geometry of the manifolds is maintained, the only difference is the number of branches and pipes. Finally the time variation of the water mass of each panel is compared to the simplified one, to asses if the simplification can be acceptable. Each u-tube is made of 8 volumes: starting from the inlet, there are 3 vertical volumes with an inclination angle of -90°, 2 bends with an inclination angle of -45° and 45° respectively and 3 other volumes with an inclination angle of 90°. If water is flowing in the circuit, different boundary conditions are set. In fact, in that case, for water is necessary to insert its temperature, pressure and mass flow rate. The error introduced by the model simplification can be calculated at each time of the transient simulated process looking at the values of the simulated parameters (water, flow rate, liquid void fraction). Considering the quantification of the residual water mass as the main parameter investigated in the analyses, the maximum error can be identify as the maximum difference between the water mass simulated by the simplified model and the one calculated with the detailed model. Moreover, the minimisation of the residual water mass is recognised as the objective of the draining process, so the draining efficiency parameter is also monitored to quantify the different behaviour of the simplified model with respect to the detailed one.

### 4.1.1 Panel 1 & Panel 5 simplification

The simplified configuration for this type of panel is shown in Figure 4.1, where u-tube number 1 is equivalent to 6 BSEs, u-tube number 2 is equivalent to of 9 BSEs and u-tube number 3 is equivalent to 3 BSEs. In this case, all BSEs have 4 mm of tape thickness.

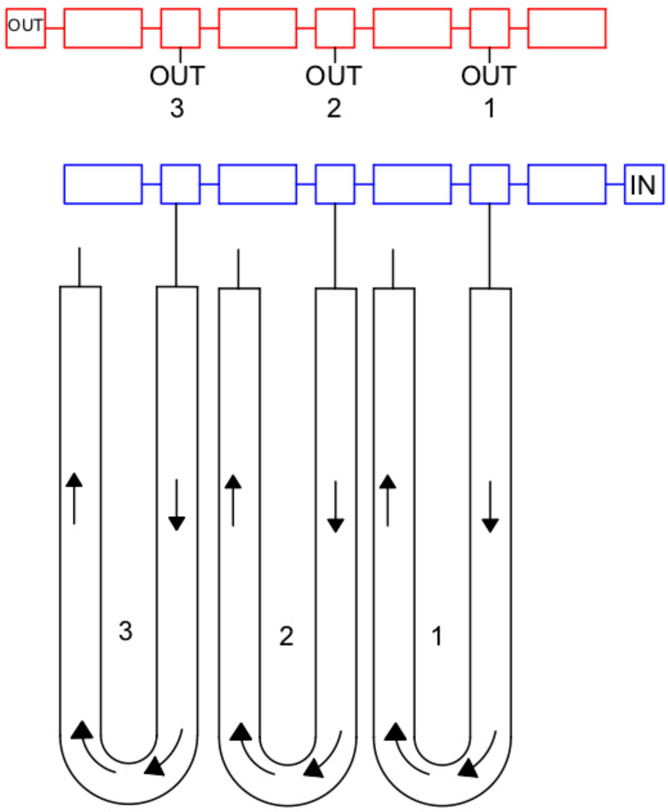


**Figure 4.1** *Panel 1 & Panel 5 simplification*

Each u-tube has a total length of 4 m and the simulation data are reported in Table 4.2.

**Table 4.2** *Panel 1 & Panel 5 data for the simplification*

| U-tube number [-] | V [m$^3$] | A [m$^2$] | $\dot{m}_w$ [kg/s] | $K$ [-] | $K_j$ [-] |
|---|---|---|---|---|---|
| 1 | 0.005922 | 0.0014805 | 6.06 | 37.94 | 5.42 |
| 2 | 0.00883 | 0.0017766 | 9.09 | 38.30 | 5.47 |
| 3 | 0.002961 | 0.0007403 | 3.03 | 37.95 | 5.42 |

After checking that the simulation can run, the boundary conditions are changed in order to have the draining process. The results of the time variation of water mass are shown in Figure 4.2.

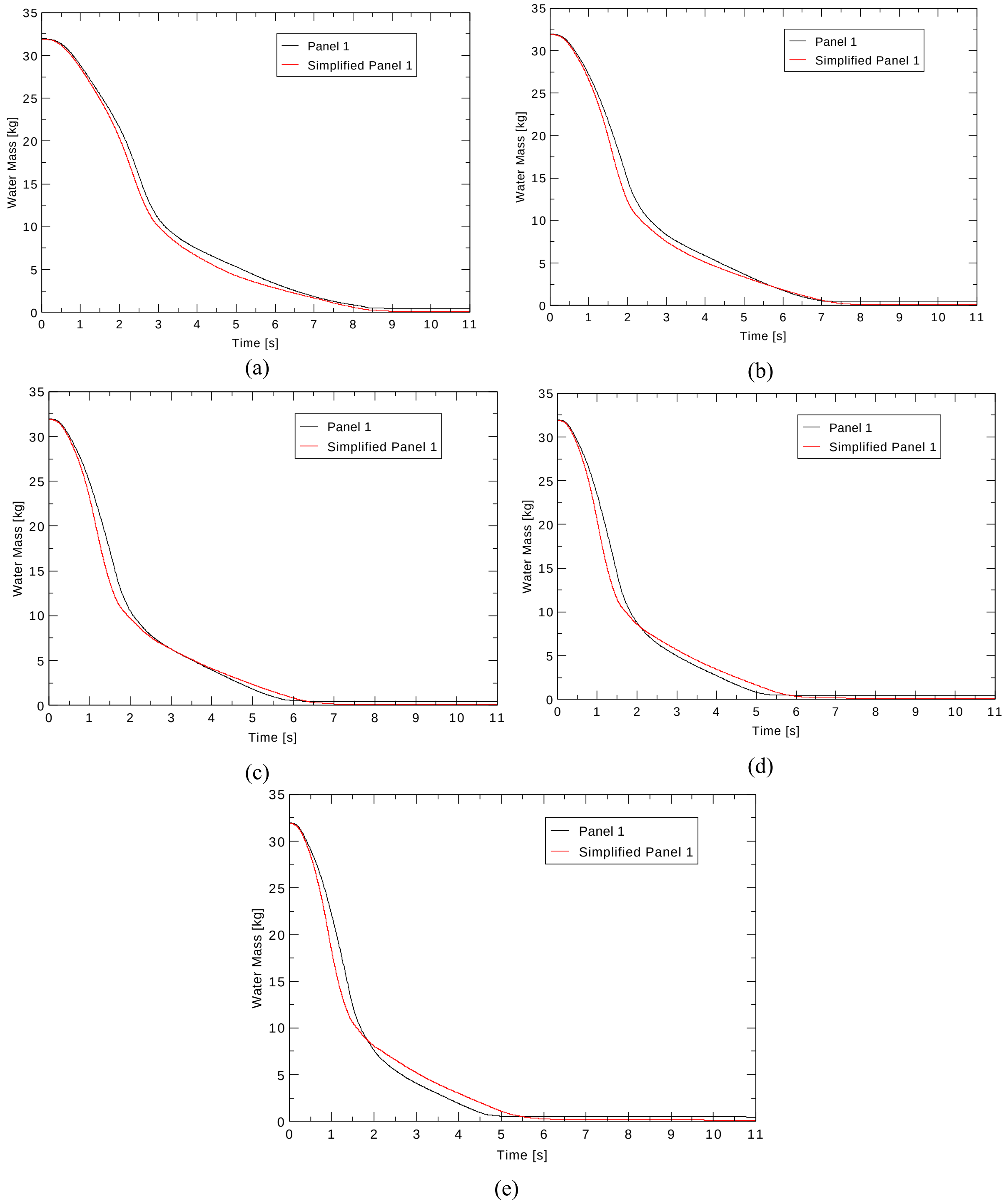


**Figure 4.2** *Comparison between the time variation of water mass for Panel 1 and its simplification: (a) P=1.5 bar; (b) P=2 bar; (c) P=3 bar; (d) P=4 bar; (e) P=5 bar*

Observing the figures, it is possible to see that the trends of the curves are qualitatively well represented by their approximation. The error introduced by the model simplification can be calculated at each time of the simulated process looking at the values of the simulated parameters (water mass, flow rate, void fraction). This error is quantified in the point where the curve of the simulated panel looks farther than the curve of the panel and it is calculated as:

$$E_{\%} = \frac{|M_s - M_r|}{M_r} * 100 \tag{4.1}$$

where, $M_s$ is the water mass of the simplified panel and $M_r$ is the real water mass of the panel for a given time. The results for Panel 1 and Panel 5 are reported in Table 4.3.

**Table 4.3** *Errors calculation for Panel 1 & Panel 5*

| P<br>[bar] | t<br>[s] | $M_r$<br>[kg] | $M_s$<br>[kg] | $E_{\%}$<br>[%] |
|---|---|---|---|---|
| 1 | 5.28 | 5.02 | 4.51 | 10.2 |
| 2 | 2.33 | 11.5 | 10.1 | 12.2 |
| 3 | 1.77 | 12.8 | 10.9 | 14.8 |
| 4 | 1.44 | 15.5 | 12.1 | 21.9 |
| 5 | 2.70 | 4.91 | 6.03 | 22.8 |

The maximum error in this type of Panel is of about 22.8%.

### *4.1.2 Panel 3 simplification*

The scheme of panel 3 simplification is the same as that of the panel 1, but the difference stays on u-tube 2 because in this case the BSEs have 2 mm of twisted tape thickness. The data for the hydraulic characterization are reported in Table 4.4. After changing the boundary conditions, the simulation can run in order to have the draining process. The results are shown in Figure 4.3.

**Table 4.4** *Panel 3 data for the simplification*

| U-tube number<br>[-] | V<br>[m$^3$] | A<br>[m$^2$] | $\dot{m}_w$<br>[kg/s] | $K$<br>[-] | $K_j$<br>[-] |
|---|---|---|---|---|---|
| 1 | 0.005922 | 0.0014805 | 6.06 | 37.94 | 5.42 |
| 2 | 0.010755 | 0.002689 | 12.15 | 31.14 | 4.45 |
| 3 | 0.002961 | 0.0007403 | 3.03 | 37.95 | 5.42 |

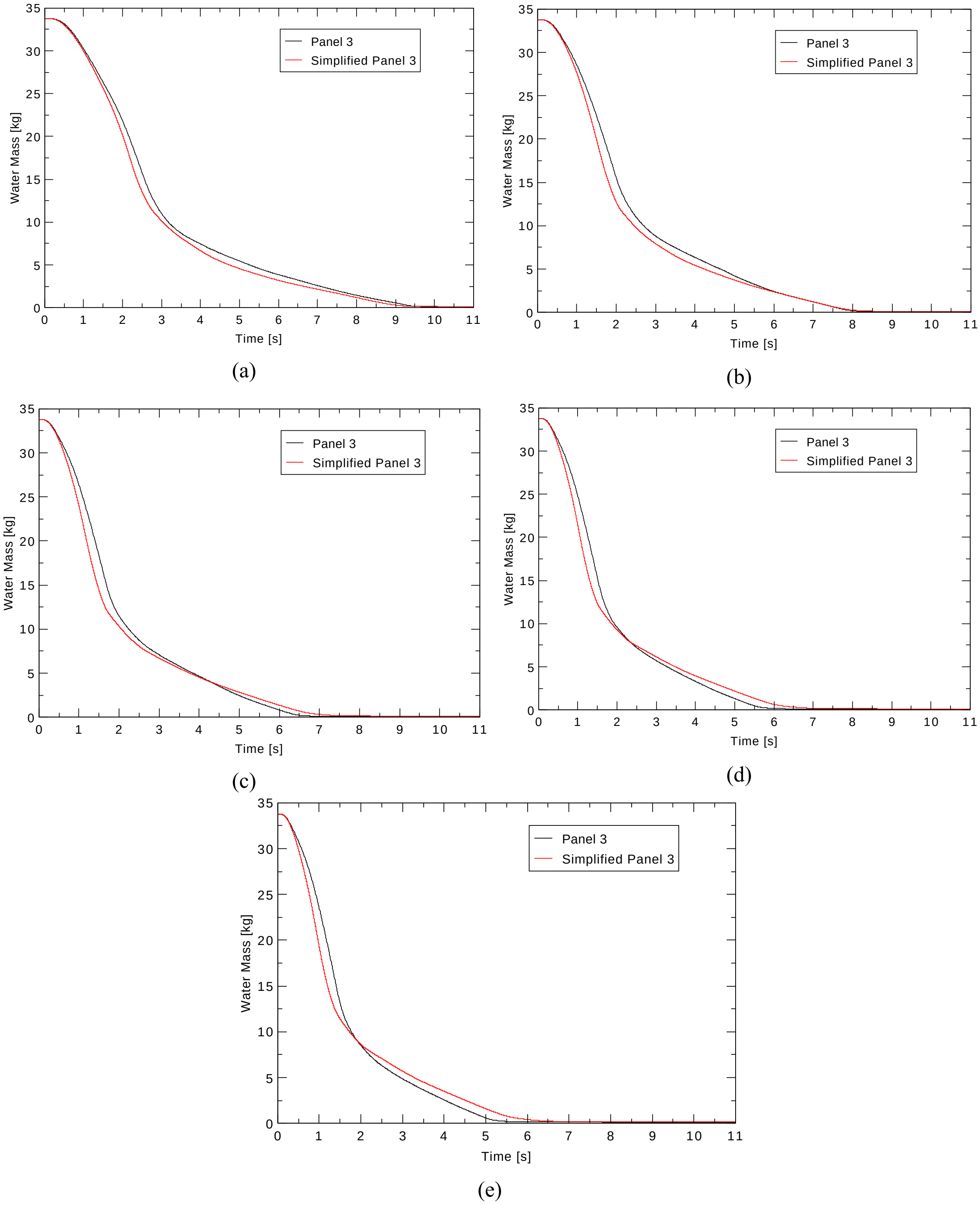


**Figure 4.3** *Comparison between the time variation of water mass for Panel 3 and its simplification: (a) P=1.5 bar; (b) P=2 bar; (c) P=3 bar; (d) P=4 bar; (e) P=5 bar*

Observing the figures, it is possible to see that the trends of the curves are qualitatively well represented by their approximation. It is possible to quantify the error, in the point where the curve of the simulated panel looks farther than the curve of the panel. The results for Panel 3 are reported in Table 4.5.

**Table 4.5** *Errors calculation for Panel 3*

| P [bar] | t [s] | $M_r$ [kg] | $M_s$ [kg] | $E_{\%}$ [%] |
|---|---|---|---|---|
| 1 | 4.88 | 5.67 | 4.76 | 16.0 |
| 2 | 4.03 | 6.28 | 5.37 | 14.5 |
| 3 | 1.90 | 12.3 | 10.9 | 11.4 |
| 4 | 1.48 | 15.7 | 12.5 | 20.3 |
| 5 | 1.41 | 14.9 | 12.1 | 18.9 |

The maximum error in this type of Panel is of about 20.3%.

### *4.1.3 Panel 2 & Panel 4 simplification*

The simplified configuration for this type of panel is shown in Figure 4.4. In this case the u-tubes have the same characteristics as that of panel 3, in terms of twisted tape thickness. The difference is the feed position and the pressure drops of the BSEs. Also the length of the u-tubes is maintained.

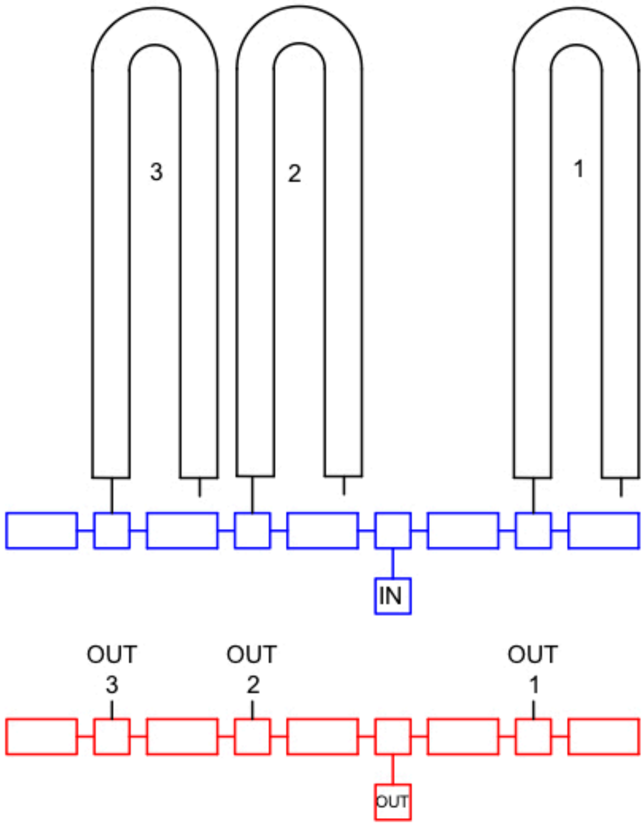


**Figure 4.4** *Panel 2 & Panel 4 simplification*

The data for the hydraulic characterization are reported in Table 4.6. The comparison between the panel and its simplification is shown in Figure 4.5.

**Table 4.6** *Panel 3 data for the simplification*

| U-tube number [-] | V [m$^3$] | A [m$^2$] | $\dot{m}_w$ [kg/s] | $K$ [-] | $K_j$ [-] |
|---|---|---|---|---|---|
| 1 | 0.004945 | 0.001236 | 6.06 | 27.70 | 3.96 |
| 2 | 0.009288 | 0.002322 | 12.15 | 24.46 | 3.49 |
| 3 | 0.002473 | 0.0006183 | 3.03 | 27.72 | 3.96 |

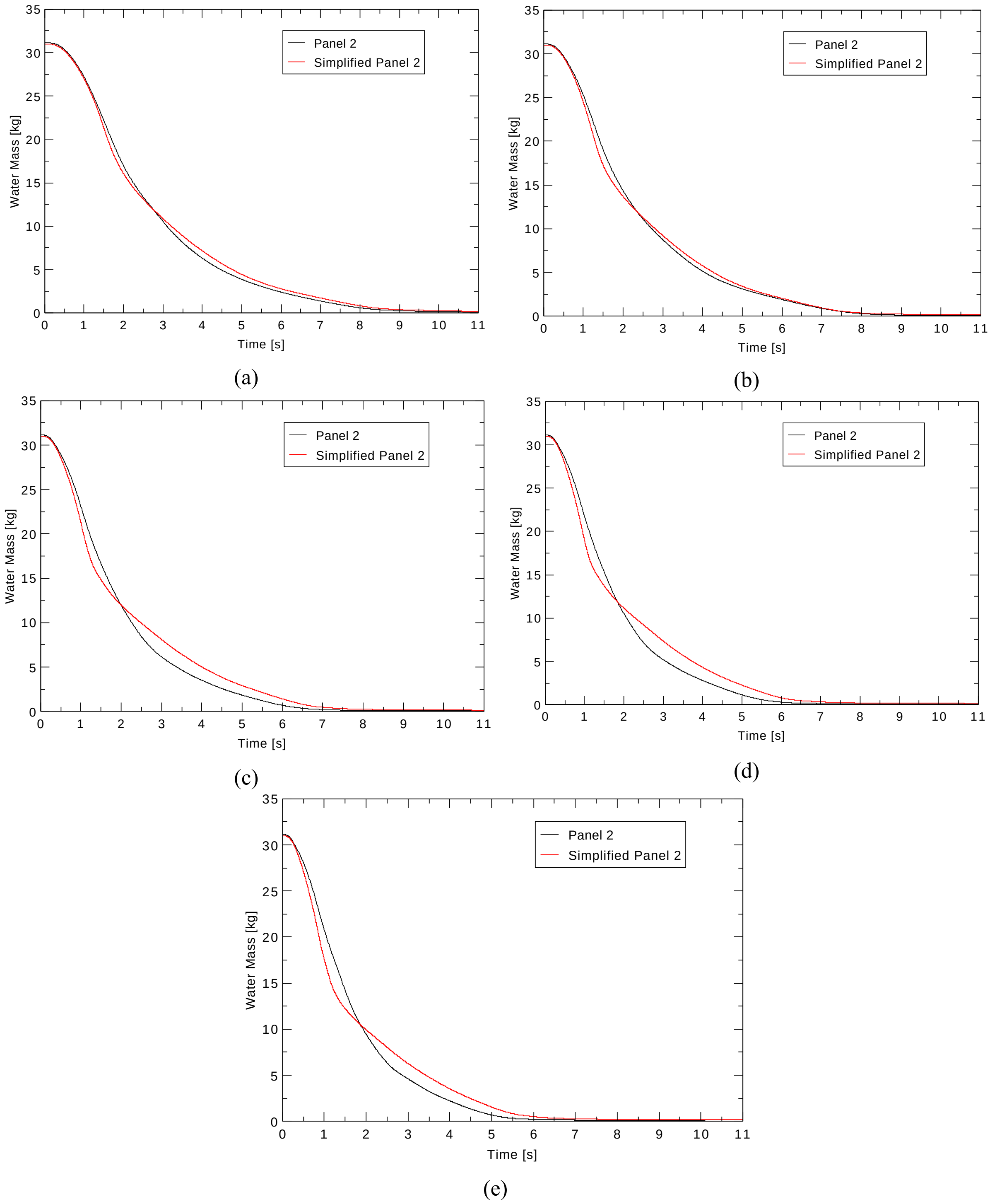


**Figure 4.5** *Comparison between the time variation of water mass for Panel 2 and its simplification: (a) P=1.5 bar; (b) P=2 bar; (c) P=3 bar; (d) P=4 bar; (e) P=5 bar*

Observing the figures, it is possible to see that the trends of the curves are qualitatively well represented by their approximation. It is possible to quantify the error, in the point where the curve of the simulated panel looks farther than the curve of the panel. The results for Panel 2 and Panel 4 are reported in Table 4.7.

**Table 4.7** *Errors calculation for Panel 2 & Panel 4*

| P [bar] | t [s] | $M_r$ [kg] | $M_s$ [kg] | $E_{\%}$ [%] |
|---|---|---|---|---|
| 1 | 4.35 | 5.29 | 6.10 | 15.3 |
| 2 | 1.64 | 17.5 | 16.0 | 8.57 |
| 3 | 3.60 | 4.97 | 6.11 | 22.9 |
| 4 | 3.47 | 4.59 | 5.78 | 25.9 |
| 5 | 3.01 | 5.06 | 6.23 | 23.1 |

The maximum error in this type of Panel is of about 25.9%.

## 4.2 Draining of the ERID

Errors introduced by the model simplification and discretisation as calculated in the previous paragraph can be compared with other approximations ascribed to one-dimensional modelling and uncertainty of boundary conditions.

The maximum difference in the water mass between the simplified model and the detailed one is 25.9% (see previous paragraph) as the simplified model is not able to simulate the dynamics with flow regime transitions produced by the specific features in the cooling circuits. Looking at the overall behaviour, the draining efficiency parameters of the two models are very similar considering a draining time of 6 s: 97.8% for the detailed model and 95.4% for the simplified model with a difference of 1.2% (p=3 bar, panel 2); moreover, the difference between the two models decreases up to negligible values (about 0.3%) by increasing the draining time up to 9 s. The details of these calculations for each panel considering a pressure of 3 bar is reported in Table 4.8.

Considering software convergence error of 0.1% for the balance equations (see section 3.1.2) and about 1% the measurement accuracy of the boundary conditions applied on the real system, then the error introduced by the model simplification can be considered acceptable and the simplified model can represent the draining behaviour of the overall ERID.

**Table 4.8** *Comparison between the draining efficiency parameter of the detailed panels and the simulated ones for P=3 bar*

| Panel<br>[-] | t<br>[s] | $\varepsilon_r$<br>[%] | $\varepsilon_s$<br>[%] | $\Delta\varepsilon$<br>[%] |
|---|---|---|---|---|
| Panel 1 | 6 | 98.4 | 97.2 | 1.2 |
| | 9 | 98.9 | 99.7 | 0.8 |
| Panel 3 | 6 | 97.6 | 96.0 | 1.6 |
| | 9 | 99.7 | 99.6 | 0.1 |
| Panel 2 | 6 | 97.8 | 95.4 | 2.4 |
| | 9 | 99.7 | 99.4 | 0.3 |

Then, the simplification of the panels represent the last step to build the overall model of the ERID and find the parameters for the draining process. The model of the two headers of the ERID is maintained and each of them connects the inlets and the outlets of the simplified panels. A summary of the volume of water and mass for each panel, and the one for the total ERID is reported in Table 4.9.

**Table 4.9** *Data of the ERID*

| Component | V<br>[$m^3$] | $M_{l0}$<br>[kg] |
|---|---|---|
| Panel 1 | 0.0319646 | 31.87 |
| Panel 2 | 0.031084 | 30.99 |
| Panel 3 | 0.0338896 | 33.79 |
| Panel 4 | 0.031084 | 30.99 |
| Panel 5 | 0.0319646 | 31.87 |
| Inlet header | 0.05589 | 55.72 |
| Outlet header | 0.05589 | 55.72 |
| **ERID** | **0.27177** | **270.95** |

The minimum nitrogen pressure used in the simulations is P=1.5 bar and, according to the PED, the maximum is set to P=3 bar, because of fluctuations that lead to considerable variation in pressure during the process (see Figure 4.6). In fact, if an inlet pressure of 3.5 bar is set, it is possible to see that a pick of pressure increases and goes over the maximum admissible pressure (see Figure 4.7).

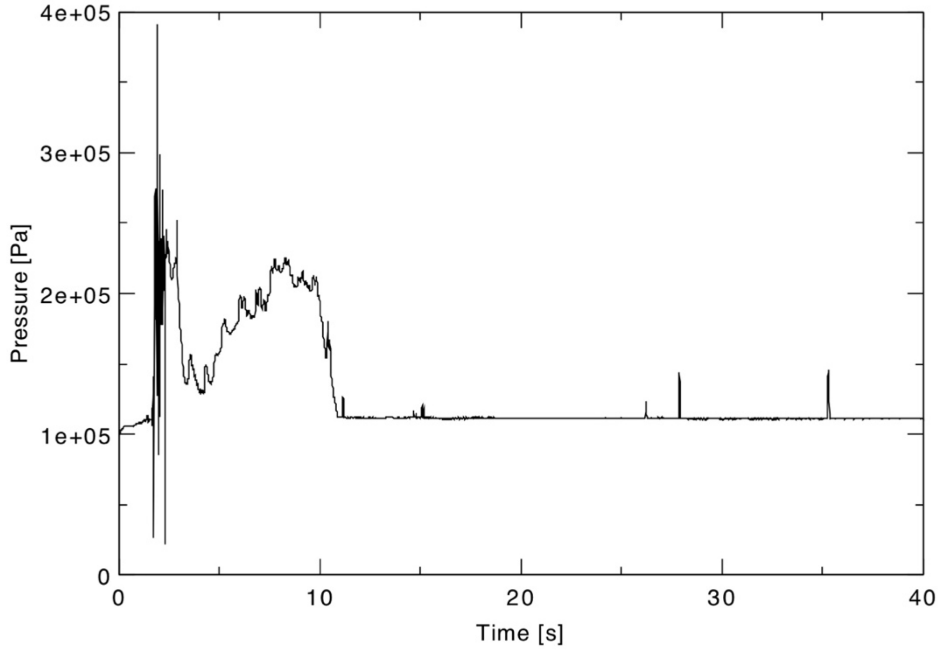


**Figure 4.6** *Pressure fluctuations in a point of the system for P=3 bar*

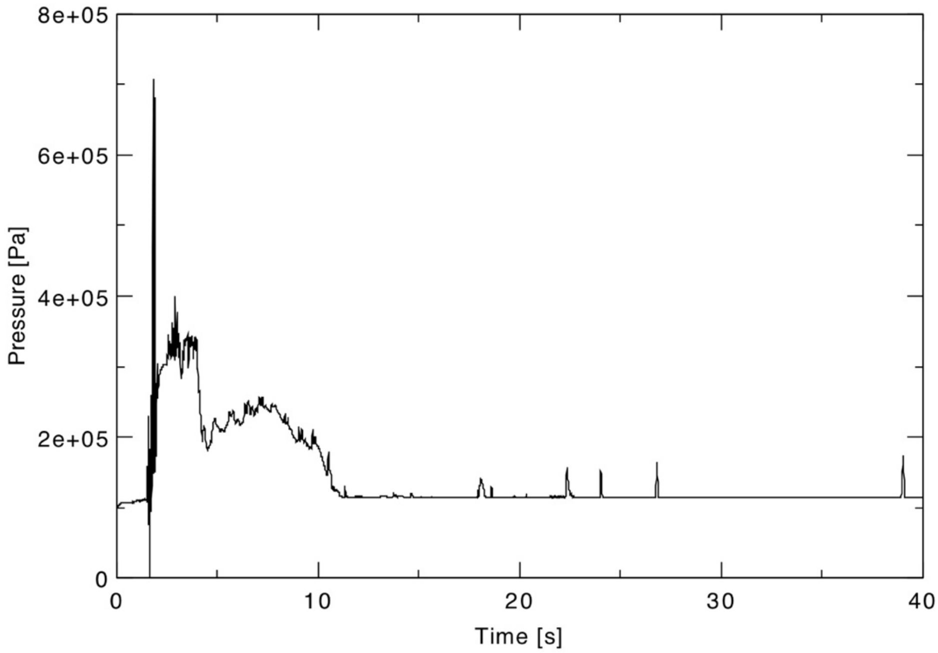


**Figure 4.7** *Pressure fluctuations in a point of the system for P=3.5 bar*

The time needed to blow out water from the circuit is shown in Figure 4.8.

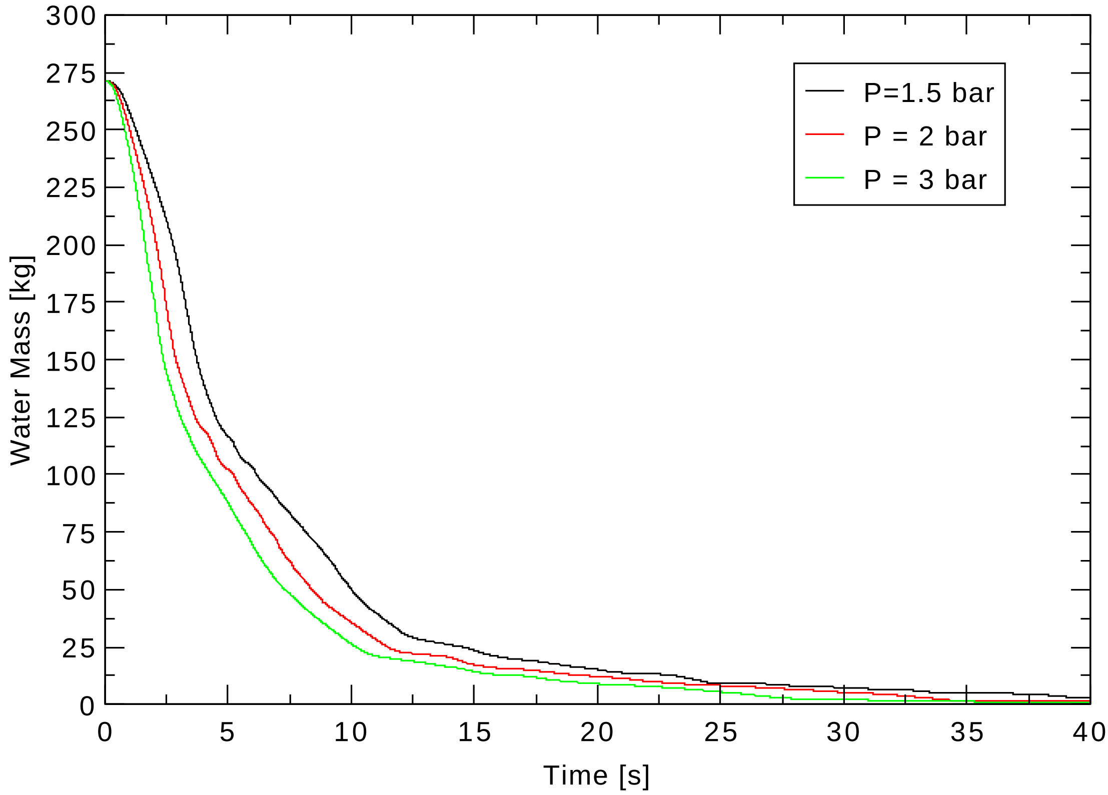


**Figure 4.8** *Time variation of water mass of the ERID*

It is possible to see that the draining process is successfully achieved because the residual water amount is low: 0.908 kg after 37 s for a pressure of 3 bar.
The liquid void fraction (see Figure 4.9) is evaluated in a bend of the u-tube of Panel 4. It is possible to see that as pressure increases, the water discharged increases. The nitrogen flow rate required to discharge water is shown in Figure 4.10.

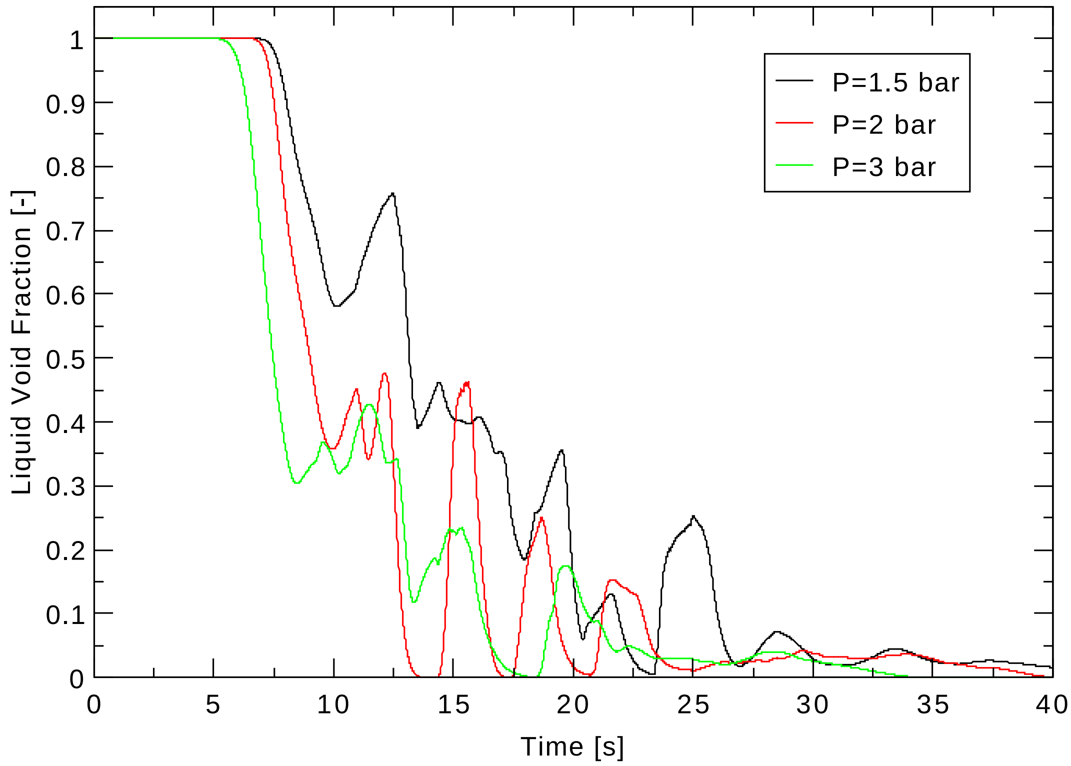


**Figure 4.9** *Time variation of the liquid void fraction of the ERID*

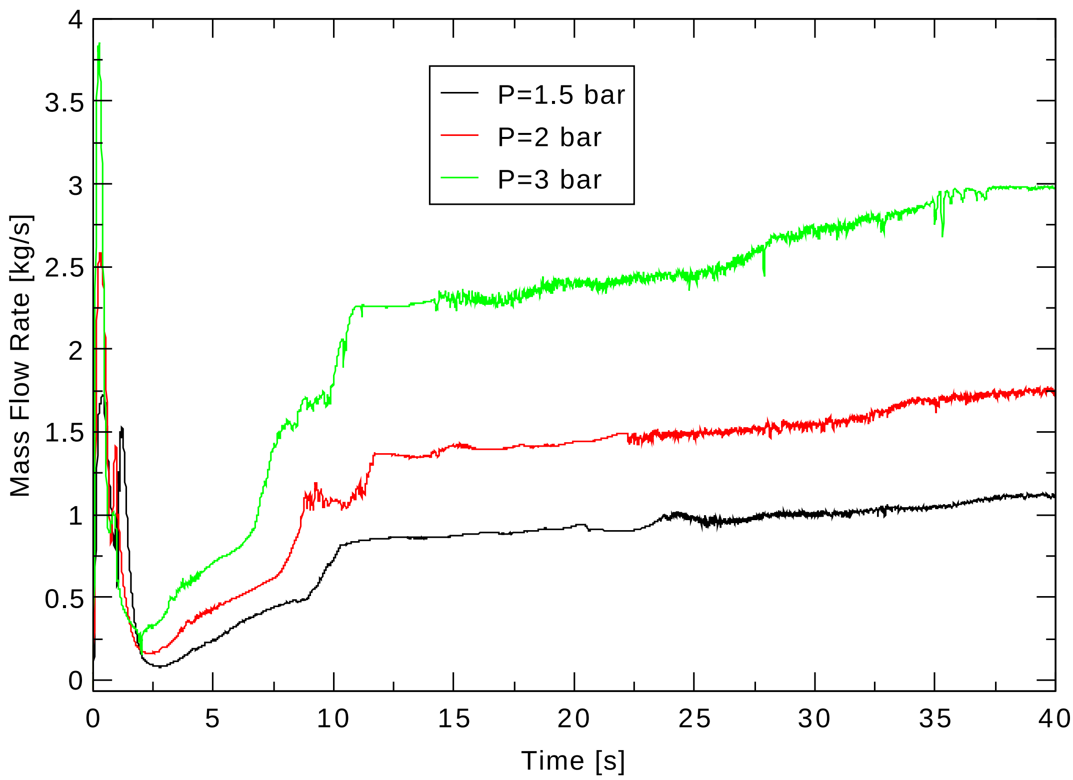


**Figure 4.10** *Time variation of inlet mass flow rate of the ERID*

Also in this case there are some fluctuations due to the flow regime transition. Considering that the draining process is achieved in 40 seconds, the nitrogen flow rate and the residual amount of water are reported in Table 4.10, where also the draining efficiency parameter is calculated.

**Table 4.10** *Results of the ERID*

| P [bar] | $\dot{m}_{N_2}$ [kg/s] | $M_l^{residual}$ [kg] | $\varepsilon$ [%] |
|---|---|---|---|
| 1 | 1.11 | 2.685 | 99.0 |
| 2 | 1.75 | 1.270 | 99.5 |
| 3 | 2.99 | 0.908 | 99.7 |

As pressure increases, the residual amount of water decreases. When the maximum pressure is applied the discharged water is almost total and the draining process can be considered done. Also in this case, it is possible to observe the two stages of the draining process: in the first stage the two-phase flow rate increases and then, in the second stage the inlet mass flow rate increases and matches the outlet flow rate (see Figure 4.11).

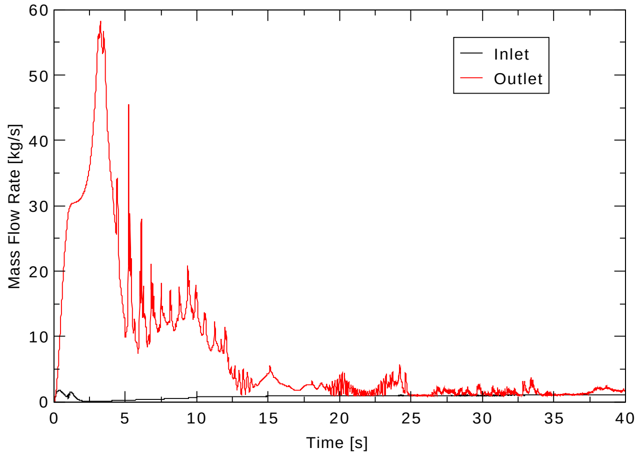


(a)

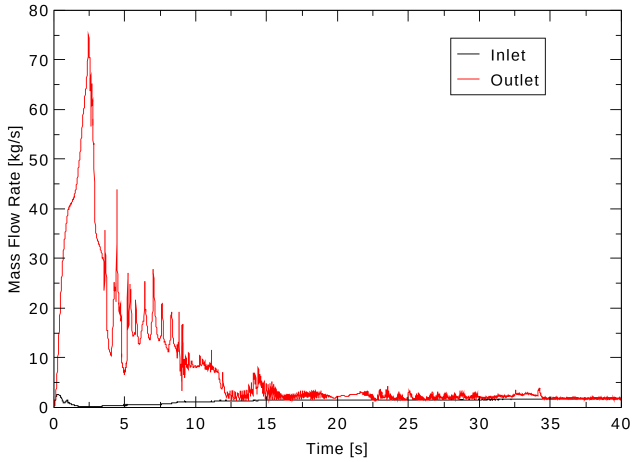


(b)

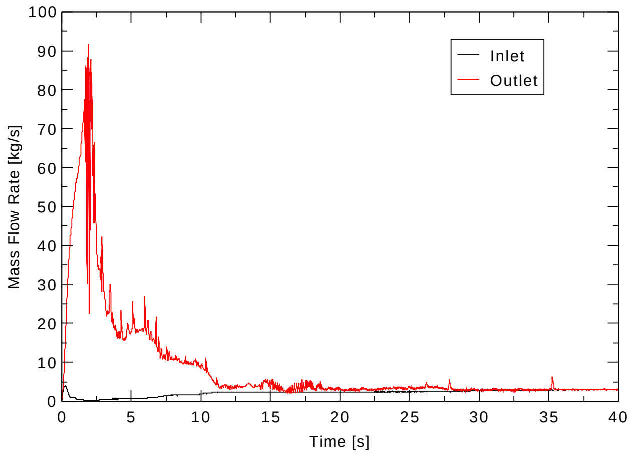


(c)

**Figure 4.11** *Time variation of inlet and outlet mass flow rate of the ERID: (a) P=1.5 bar; (b) P=2 bar; (c) P=3 bar*

Observing the results, the draining process for the ERID cooling system can be done by applying an inlet nitrogen pressure of P=3 bar, in order to have the total water discharged, in fact the residual amount of water is 0.908 kg. The nitrogen flow rate is of about 3 kg/s.
The residual water amount, that is the 0.3% with respect to the total water amount will be discharged using the drying process.

## 4.3 Implementation of the ERID draining

The time evolution of the gas mass flow rate can be integrated to get the total gas mass required to remove the water. The end of the draining process can be identified at the achievement of the full gas mass flow, e.g. at 37 s when applying 3 bar pressure. In this condition the total gas mass required is 111 kg. The gas flow from the bottle to the component through the throttling valve is an isenthalpic process that can be made of a first isothermal part and a second isentropic part. If the gas is assumed ideal, then the isenthalpic process corresponds to the isothermal. Simplifying, the expansion of nitrogen is assumed to be an isothermal process and the mass of nitrogen needed corresponds to the gas contained in 10 bottles of 50 litres each pressurised at 200 bar. Practically, the draining process will be realised by progressively increasing the gas pressure injected in the component to prevent excessive over pressures that have been identified in figures 4.6, 4.7 as described in section 4.2 thus avoiding vibrations that can damage the component. The scheme of the draining plant is shown in Figure 4.12.
As already discussed in Chapter 2, the water remaining in the cooling circuits after draining will be removed by drying; this further process is needed to evacuate tritium and to confine corrosion products in the component avoiding shedding of contaminants. Drying will be performed in two main step [27]:

I. Heating up of the component mass, including the residual water, up to a maximum temperature that can be set equal to the maximum coolant temperature expected during operation (for the ERID this maximum temperature is 100°C); this step can be executed with nitrogen at high pressure that exchanges heat through forced convection to the component.
II. Drying out through evaporation of the heated water in the drying gas; this step can be executed with nitrogen flowing through the component at the same temperature as for step I. Then, the maximum quantity of vapour in the mixture in thermodynamic equilibrium is obtained when the partial pressure of the condensable phase is equal to the saturation pressure at the given temperature.

Calculations are not proposed for drying as the actual behaviour cannot be easily modelled.

Measurements sections are required at the draining and drying facilities, in particular regarding the gas pressure, flow rate, humidity, in order to experimentally control and determine the end of these operations.

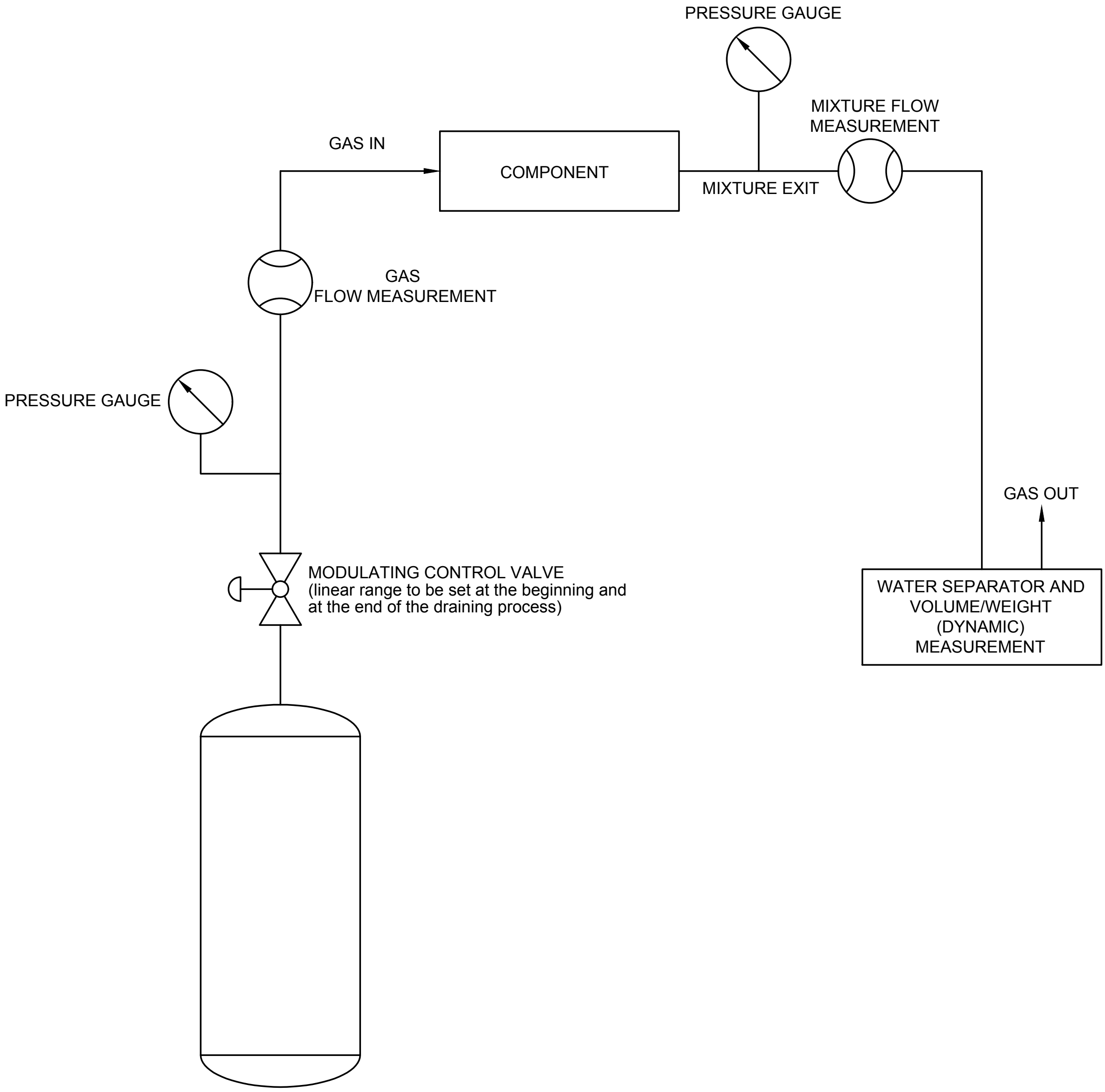


**Figure 4.12** *Scheme of the draining process*

# Conclusions and future works

This thesis work is placed in an international research framework aiming at obtaining energy from thermonuclear fusion. For this purpose, the two experiments for testing ITER neutral beam injectors have been realized at Consorzio RFX in Padova. The research activity is focused on a MITICA component, that is the Electrostatic Residual Ion Dump, whose cooling circuit must be drained before carrying out maintenance and inspection operations due to operating environment contamination caused by activated corrosion products. When coming in contact with the coolant, the internal surface of pipes tends to be corroded to form oxides and when these corrosion products are under neutron radiation, they will be activated to become Activated Corrosion Products (ACPs) that circulate along the loop continuously decaying and emitting gamma-rays. For this reason, a draining procedure based on blowing out water with high pressure nitrogen has been studied in this work. RELAP5 is the software used for this purpose, that is a highly generic code that, in addition to calculate the behaviour of a reactor coolant system during transients, can be used for simulation of a wide variety of hydraulic systems during transients in both nuclear and non-nuclear systems. Boundary conditions are set for the simulations: in particular, the maximum allowable pressure of nitrogen must be fixed. For this reason the Pressure Equipment Directive has been applied to the beam stopping elements and to the cooling pipes and headers to find the maximum admissible pressure in order to stay in the region where the sound engineering practice (SEP) category can be applied. The advantage to work in this region is that the components must not to bear the CE marking and purely requires the manufacturer to use common sense. Considering these reasons, for the ERID, the maximum admissible pressure is set to 5 bar(g). Other boundary conditions for the simulations are related to water pressure and temperature, nitrogen pressure and temperature and to the static quality, a condition to asses that the component is filled of water. At this point, all simulations, starting from the smaller element that is the BSE are developed. All different types, in terms of feed position and twisted tape thickness of BSEs are simulated. In fact, for a given twisted tape thickness, the BSE fed from the top has a different mass of water with respect to the BSE fed from the bottom because of the different length of the inlet and outlet pipes. The results of the draining simulations for the BSEs show that the process is completed in about 4 s with a nitrogen flow rate in a range between 0.01 kg/s and 0.07 kg/s. Thanks to the simulation of the BSEs, each panel model can be built, by adding also the two manifolds. Also in this case, due to the feed position, different types are analysed and the results are all reported. The draining process for panels is completed in about 10 s with a nitrogen flow rate in a range between 0.2 kg/s to 1.4 kg/s. The residual amount of water is almost zero. Observing the trend of the time variation of water mass, it is possible to see some changes in the slope of the curves. This is due to the flow regime transition, a phenomenon that occur when a two phase process occurs. In particular, at the beginning the water-nitrogen mixture is a two phase bubble structure, then, when the slope changes, a slug flow is developed and water discharge is defined mostly by droplets dragged away from the water film wetting the inner surface of the channels. The final draining phase is solely by water droplets in the dispersed regime of the two-phase flow.

Observing the graphs of the time variation of the inlet mass flow rate, it is possible to see that in many cases the inlet mass flow rate shows an interval of negative values that is associated to the Rayleigh-Taylor instability, that is an instability of an interface between two fluids of different densities. The graphs of the outlet flow rate enables to understand the two different stages of the draining process: in fact, at the beginning there is an increase of the outlet flow rate because of the water blowing out from the circuit, and then the two-phase flow becomes quasi-steady-state and the inlet mass flow is almost equal to the outlet mass flow rate. Also the graphs of the void fraction show that the water discharge is almost total.

To complete the model of the ERID, the two headers are modelled and their connections with the panels can be done. At this point, the software was not able to process all the parts included in the system because of a storage problem due to the greater number of elements. For this reason, a simplified system has been studied. Each panel has been built maintaining the two manifolds and by grouping the BSEs in terms of twisted tape thickness, by which each group can be considered as a u-tube.

The simulations of the draining process have been compared for each panel, in order to understand if the approximations produced by the simplification can be acceptable or not. Results show that the draining behaviour of all panels can be well represented by their simplification, in fact the error introduced by the model simplification can be calculated at each time of the transient process looking at the values of the simulated parameters. The maximum difference in the water mass between the simplified model and detailed one is 25.9%, as the simplified model is not able to simulate the dynamics with flow regime transitions produced by the specific features in the cooling circuits. Considering software convergence error and measurement accuracy of boundary conditions, the error introduced by the model simplification can be considered acceptable and the simplified model can represent the draining behaviour of the overall ERID. So, maintaining the two headers, the connections can be made and simulation can run. Results show the same characteristic of the trend of the curve, with a maximum increase of the draining time of 19%, as previously described and the draining process can be successfully achieved in about 40s. The residual amount of water is very low, as it can be possible to see from the plot of the void fraction. The calculation of the draining efficiency parameter, with a value greater than 90%, confirms that the discharged water is almost total and the target of this thesis is achieved.

The draining process can be applied by using an inlet nitrogen pressure of 3 bar, in order to minimize pressure fluctuations and to have a value of the draining efficiency parameter of 99.7%. In this condition the total gas mass required is 111 kg corresponding to the gas contained in 10 bottles of 50 litres each pressurised at 200 bar.

Future works could be related to the experimental validation of the parameters found in this work. In fact, the BSEs prototype are available at Consorzio RFX and it will possible to fill with water a BSE or a series of BSEs, and then blow out water from the system; then using some instruments, the gas pressure, the evacuation time, and the gas flow rate can be measured in order to compare the simulations results with the experimental ones. In the water-nitrogen mixture, water will be separated, collected in a tank, then its volume or weight could be measured. This experimental approach has important limitations as only the mass flow rate and pressure of the gas can be measured during the draining process, whereas the exhausted water can be quantified, e.g. by weighting, only at the end of the process. A plastic model of the system cannot be studied to represent the behaviour of the real system when stagnation regions and dead-ends are removed or simplified. Indeed, the draining condition of a tube with constant cross section will be very different from that one of a real part made with nozzles or composed of more vessels connected with pipes. Moreover, the flow regime and the dynamic behaviour of the gas-liquid interface can vary when changing the channel diameter.

Regarding the residual amount of water that remains in the circuit, a drying operation must be performed. During this operation, hot nitrogen gas (at reduced pressure if necessary) is circulated through the system for an extended time to remove residual water by evaporation. The water vapor is condensed out and sent to drain tanks. After the completion of the drying operations, the system is cooled down to the maintenance temperature.

# Nomenclature

**Roman symbols**

| | | |
|---|---|---|
| A | = | flow area [$m^2$] |
| $B_x$ | = | body force in x coordinate direction [$m/s^2$] |
| $C$ | = | Wallis constant [-] |
| $D_h$ | = | hydraulic diameter [m] |
| $D_i$ | = | inner diameter [m] |
| $E_{\%}$ | = | percentage error [%] |
| $f_{sw}$ | = | friction factor [-] |
| g | = | acceleration due to gravity [$m/s^2$] |
| $h_f^*$ | = | fluid enthalpy associated with bulk interface [J/kg] |
| $h_f'$ | = | fluid enthalpy associated with wall interface [J/kg] |
| $h_g^*$ | = | gas enthalpy associated with bulk interface [J/kg] |
| $h_g'$ | = | gas enthalpy associated with wall interface [J/kg] |
| $j_g$ | = | gas superficial velocity [m/s] |
| $j_g^*$ | = | dimensionless gas superficial velocity [-] |
| $j_l$ | = | liquid superficial velocity [m/s] |
| $j_l^*$ | = | dimensionless liquid superficial velocity [-] |
| K | = | loss coefficient [-] |
| $K_b$ | = | bend loss coefficient [-] |
| $K_j$ | = | junction loss coefficient [-] |
| $K_{sw}$ | = | twist ratio [-] |
| L | = | length [m] |
| $M_f$ | = | fluid mass [kg] |
| $M_g$ | = | gas mass [kg] |
| $M_{l0}$ | = | initial water amount [kg] |
| $M_l^{residual}$ | = | residual water amount [kg] |
| $MW_g$ | = | nitrogen molecular weight [g/mol] |
| $m$ | = | Wallis constant [-] |
| $\dot{m}_{N_2}$ | = | nitrogen mass flow rate [kg/s] |
| $\dot{m}_w$ | = | water mass flow rate [kg/s] |
| P | = | pressure [Pa] |

| | | |
|---|---|---|
| $P_w$ | = | wetted perimeter [m] |
| $\Delta p$ | = | pressure drop [Pa] |
| Q | = | volumetric heat rate [W/m$^3$] |
| $Q_{ig}$ | = | gas interface heat transfer rate [W/m$^3$] |
| $Q_{if}$ | = | fluid interface heat transfer rate [W/m$^3$] |
| $Q_{wf}$ | = | fluid wall heat transfer rate [W/m$^3$] |
| $Q_{wg}$ | = | gas wall heat transfer rate [W/m$^3$] |
| R | = | ideal gas constant [Pa m$^3$/mol K] |
| $Re_{sw}$ | = | Reynolds number referred to the swirl flow [-] |
| T | = | temperature [K] |
| t | = | time [s] |
| $U_f$ | = | fluid specific internal energy [J/kg] |
| $U_g$ | = | gas specific internal energy [J/kg] |
| V | = | volume [m$^3$] |
| $v_f$ | = | fluid velocity [m/s] |
| $v_g$ | = | mass velocity [m/s] |
| $w_g$ | = | minimum nitrogen mass flow rate [kg/s] |
| X | = | static quality [-] |

**Greek symbols**

| | | |
|---|---|---|
| $\alpha_f$ | = | fluid void fraction [-] |
| $\alpha_g$ | = | gas void fraction [-] |
| $\delta$ | = | twisted tape thicnkness [m] |
| $\varepsilon$ | = | draining efficiency parameter [-] |
| $\varepsilon_r$ | = | reduced roughness [-] |
| $\mu_b$ | = | bulk dynamic viscosity [Pa s] |
| $\rho_b$ | = | bulk density [kg/m$^3$] |
| $\rho_g$ | = | gas density [kg/m$^3$] |
| $\rho_l$ | = | liquid density [kg/m$^3$] |
| $\rho_m$ | = | mixture density [kg/m$^3$] |
| $\Gamma_f$ | = | fluid volumetric mass exchange rate [kg/m$^3$ s] |
| $\Gamma_g$ | = | gas volumetric mass exchange rate [kg/m$^3$ s] |
| $\Gamma_{ig}$ | = | interface condensation rate [kg/m$^3$ s ] |

$\Gamma_w$ = interface vaporization rate [kg/m$^3$ s]

**Acronyms**

FIF = liquid interphase drag coefficient [s$^{-1}$]

FIG = vapour interphase drag coefficient [s$^{-1}$]

FWF = liquid wall drag coefficient [s$^{-1}$]

FWG = vapour wall drag coefficient [s$^{-1}$]

$DISS_g$ = vapour energy dissipation function [W/m$^3$]

$DISS_f$ = liquid energy dissipation function [W/m$^3$]

# References


[1] www.iter.org

[2] B. Viswanathan, “Energy sources: Fundamentals of Chemical Conversion Processes and Applications”, Newnes, 2016

[3] M. Kovari et al., “Converting energy from fusion into useful forms”, Proceeding of the Institution of Mechanical Engineers, Part A: Journal of Power and Energy, 2014

[4] ITER EDA Final Design Report, ITER Technical Basis, Plant Description Document, G A0 FDR 1 01-07-13 R1.0, IAEA EDA Documentation No. 24, 2002.

[5] V. Toigo et al., “A substantial step forward in the realization of the ITER HNB system: The ITER NBI Test Facility”, Fusion Engineering and Design 123 (2017) 32-39

[6] P. Sonato et al., “Status of PRIMA, the test facility for ITER neutral beam injectors”, Third International Symposium on Negative Ions, Beams and Sources, Finland (2012)

[7] M. Zaupa, "Thermo-hydraulic model and analyses for design optimization of a cooling circuits and components of SPIDER and MITICA experiments”, PhD thesis, Padova, 2016.

[8] J. Zhang et al., “Calculation of radioactivity and dose rate of activated corrosion products in water-cooled fusion reactor”, Science and Technology of Nuclear Installations, (2016)

[9] J. Zhang et al., “CATE: A code for activated corrosion products evaluation of water-cooled fusion reaction”, Fusion Engineering and Design 100 (2015) 340-344

[10] G. B. Wallis, “One-dimensional Two-phase Flow”, McGraw-Hill, 1969

[11] S. Kim et al., “Draining and drying process development of the Tokamak Cooling Water System of ITER”, Fusion Engineering and Design 109-111 (2016) 272-277

[12] P.A. Di Maio et al., “Numerical simulation of the transient thermal-hydraulic behaviour of the ITER blanket cooling system under the draining operational procedure”, Fusion Engineering and Design 98-99 (2015) 1664-1667

[13] S. Mokhatab, W.A.Poe, “Handbook of Natural Gas Transmission and Processing,” Gulf professional publishing, 2012

[14] M.J. Da Silva, “Impedance sensors for fast multiphase flow measurement and imaging”, PhD thesis, 2008

[15] B. Rehm et al., “Underbalanced drilling: limits and extremes”, Elsevier, 2013

[16] RELAP5/MOD3.3 Code Manual, Vol. IV: Models and correlations, Information Systems Laboratories Inc, Rockville, MD, US

[17] RELAP5/MOD3.3 Code Manual, Vol. II: user’s guide and input requirements, Information Systems Laboratories Inc, Rockville, MD, US

[18] RELAP5/MOD3.3 Code Manual, Vol. I: code structure, system models, and solution methods, Information Systems Laboratories Inc, Rockville, MD, US

[19] Pressure Equipment Directive 2014/68/EU, Available at https://ec.europa.eu/growth/sectors/pressure-gas/pressure-equipment/directive_en

[20] PED conformity assessment and MD329/04 regulation for the MITICA Beam Line Components, RFX document ID: RFX_MITICA_TN_133, revision 3 of 20/01/2015

[21] C.F. Colebrook and C.M. White, "Fluid friction in roughened pipes", Proceeding of the Royal Society of London, 1937, 161A:367-381

[22] G. Maschio, Lecture notes of Impiantistica di Processo course, Università degli Studi di Padova, 2016

[23] https://webbook.nist.gov/chemistry/

[24] D.W. Green, R.H. Perry, "Perry's Chemical engineers' handbook", 8th edition, McGraw-Hill, 2007

[25] F. Geli, "Draining/Drying of HNB Duct Liner using IBED PHTS strategy", 01 August 2012

[26] V. Tanchuk et al., "Numerical simulation of draining and drying procedure for the ITER Generic Equatorial Port Plug cooling system", Fusion Engineering and Design 109-111 (2016) 207-212

[27] M. Dalla Palma et al., "Design of a cooling system for the ITER Ion Source and Neutral Beam test facilities", Fusion Engineering and Design, vol 84, number 7-11, (2009), 1460-1464

# Acknowledgments

Vorrei ringraziare il mio relatore, prof. Piergiorgio Sonato per avermi permesso di svolgere questa tesi presso il Consorzio RFX.
Ringrazio l'Ing. Mauro Dalla Palma per avermi accolta nel suo gruppo e per non avermi mai negato un consiglio durante questi mesi trascorsi in Consorzio.
Ringrazio in modo particolare l'Ing. Matteo Zaupa per avermi guidata fin dall'inizio, dall'apprendimento dell'utilizzo del software alla risoluzione dei problemi sorti durante il progetto.
Un ringraziamento particolare va alla mia famiglia: a mio papà Fausto, a mia mamma Donatella e a mio fratello Samuele per aver sempre supportato le mie scelte, essermi sempre vicini e per rappresentare il mio punto di riferimento.
Ringrazio Federico, per essere sempre al mio fianco, per sostenermi in qualsiasi situazione e per aiutarmi sempre nel momento del bisogno. Vorrei ringraziare anche Luciano e Michela.
Ringrazio i miei amici, in particolare Federica che sopporta le mie ansie. Grazie ai miei compagni di università per aver reso questi anni meno impegnativi.
Infine ringrazio il "gruppo cugini", in particolare Angela, per i bei momenti trascorsi insieme.